Lawrence Berkeley National Laboratory
Recent Work

Title
CROSSED MOLECULAR BEAM STUDIES OF SUBSTITUTION AND EXCHANGE REACTIONS

Permalink
https://escholarship.org/uc/item/3gt4h3nm

Author
Robinson, S.N.

Publication Date
1987-12-01

eScholarship.org Powered by the California Digital Library
University of California

LBL-24635

Lawrence Berkeley Laboratory
UNIVERSITY OF CALIFORNIA

Materials & Chemical Sciences Division

RECEIVED
LAWRENCE
BERKELEY LABORATORY
APR 19 1988
LIBRARY AND
DOCUMENTS SECTION

Crossed Molecular Beam Studies of Substitution and Exchange Reactions

G.N. Robinson
(Ph.D. Thesis)

December 1987

TWO-WEEK LOAN COPY

This is a Library Circulating Copy which may be borrowed for two weeks.

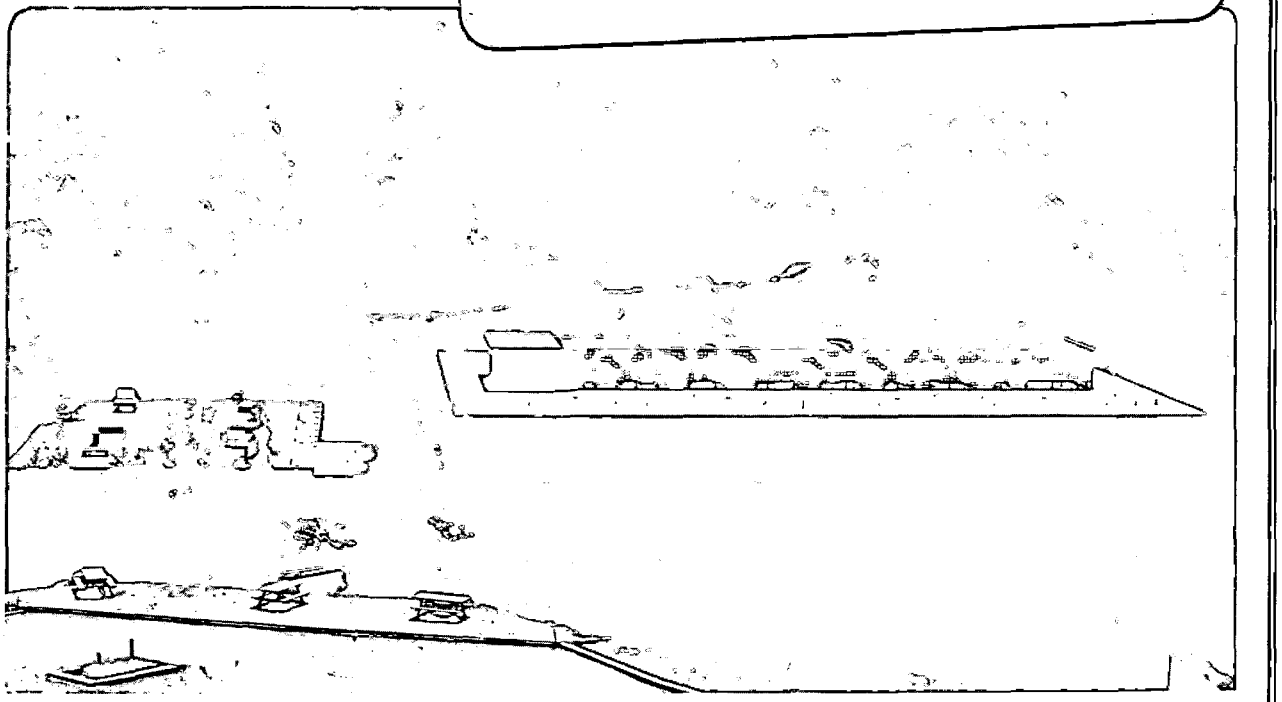

Prepared for the U.S. Department of Energy under Contract DE-AC03-76SF00098

LBL-24635

DISCLAIMER

This document was prepared as an account of work sponsored by the United States Government. While this document is believed to contain correct information, neither the United States Government nor any agency thereof, nor the Regents of the University of California, nor any of their employees, makes any warranty, express or implied, or assumes any legal responsibility for the accuracy, completeness, or usefulness of any information, apparatus, product, or process disclosed, or represents that its use would not infringe privately owned rights. Reference herein to any specific commercial product, process, or service by its trade name, trademark, manufacturer, or otherwise, does not necessarily constitute or imply its endorsement, recommendation, or favoring by the United States Government or any agency thereof, or the Regents of the University of California. The views and opinions of authors expressed herein do not necessarily state or reflect those of the United States Government or any agency thereof or the Regents of the University of California.

CROSSED MOLECULAR BEAM STUDIES OF SUBSTITUTION AND EXCHANGE REACTIONS

Gary N. Robinson

Ph.D. Thesis

Department of Chemistry
University of California, Berkeley

and

Materials and Chemical Sciences Division
Lawrence Berkeley Laboratory
University of California
Berkeley, California 94720

December 1987

CROSSED MOLECULAR BEAM STUDIES OF SUBSTITUTION AND EXCHANGE REACTIONS

Gary Neil Robinson

ABSTRACT

The dynamics of several atom + alkene/aromatic and radical + iodoalkane reactions have been studied using the crossed molecular beams method.

The reaction $F + C_2H_4 \rightarrow [C_2H_4F]^* \rightarrow H + C_2H_3F$ has been investigated at very low collision energies (E_c=0.8-2.5 kcal/mol) using a narrow velocity spread F atom beam (Chapter 1). The substitution cross section is found to decrease with increasing E_c suggesting that there is no potential energy barrier to the initial addition step and that long range attractive forces dominate the $F\text{-}C_2H_4$ interaction. The CM frame C_2H_3F angular distributions are qualitatively different from those previously obtained for this reaction and may reflect unusual angular momentum partitioning in the C_2H_4F collision complex.

Chapters 2 and 3 describe studies of endoergic substitution reactions, Br + R-Cl → R-Br + Cl, where R-Cl = o-, m-, and $p\text{-}CH_3C_6H_4Cl$, C_6X_5Cl (X=H,F), and 1,1- and trans-$C_2H_2Cl_2$ (ΔH°_0≃13-15 kcal/mol) carried out in the collision energy range 15-35 kcal/mol. In these reactions, Br adds to the

double bond to form a weakly bound (with respect to reactants) collision complex which subsequently decomposes through Cl elimination. Competition between intramolecular vibrational energy redistribution and Cl elimination in these complexes results in product translational energy distributions and excitation functions that can be modeled by assuming that a limited number of vibrational modes participate in energy sharing prior to bond fission. Substituents influence the orientation and probability of Br addition as well as the extent of energy redistribution in the complexes.

The first crossed beam studies of CH_3 radicals with polyatomic molecules are reported in Chapter 4. The CH_3I products from the approximately thermoneutral I atom exchange reactions $CH_3 + R\text{-}I \rightarrow CH_3I + R$ ($R=CF_3$, $(CH_3)_3C$) are found to be strongly backward scattered with respect to the incident radical beam indicating a preferred collinear $CH_3\text{-}I\text{-}R$ configuration. Most of the ≈15 kcal/mol of available energy is channeled into product translation (≈50% for $R=(CH_3)_3C$ and ≈70% for $R=CF_3$). This large repulsive energy release is rationalized in terms of the stabilities of the $CH_3\text{-}I\text{-}R$ transition structures.

TABLE OF CONTENTS

ACKNOWLEDGEMENTS

It is a pleasure to thank Yuan Lee for his guidance and support over these last few years. His keen scientific insight, deep commitment to teaching, and love of his work are truly inspiring.

Bob Continetti worked with me on all of the experiments described in this thesis (and many other aborted missions) and his creativity and hard work contributed enormously to their success. Gil Nathanson and I suffered the birth pangs of the methyl radical experiments described in Chapter 4. Gil's boundless enthusiasm in tackling difficult problems was crucial to our getting the results that we did. I have also learned a lot from him about angular momentum. Dan Neumark and Alec Wodtke taught me many of the basics of crossed beams research. Alec also proved to me that one can have hopelessly naive political views and still do good science. Tim Minton designed the electrode assembly used in the methyl radical experiments and offered good suggestions for improving the source's performance. Rick Buss, who wrote the bulk of the forward-convolution program used to analyze the data presented here, was a helpful source of information during my first year. Anne Williamson's assistance in many of the daily chores during the Br atom experiments is also appreciated.

Other members of the group have taught me much about

science and life. Anne-Marie Schmoltner has been a good and caring friend; I am greatly indebted to her for her heroic efforts in preparing most of the figures for this thesis. Eric Hintsa and Barbara Balko, both kind-hearted and tolerant office mates, always lifted my spirits. I have also learned from and enjoyed conversations with Lisa Yeh, Marion Helfand, Xinsheng Zhao, Paul Weiss (yes Paul, yours is still the longest thesis out of this group), Rick Brudzynski, and Howard Nathel. Pam Chu's efforts in getting the group computational facility up and running are much appreciated.

Ann Weightman, the group czar, deserves special recognition for her no b.s. allowed approach to life. I am just one of many that have benefitted from her legendary ability to get things done. The excellent technical support staffs on campus and at LBL helped to make all of these experiments possible. Most noteworthy are the department machinists (headed by Fred Wolff, Andy Anderson, and George Weber), and Tony Moscarelli, Fred Vogelsberg, Ed Arnold, and Bill Wilkie.

Most deserving of thanks are my parents, my first and foremost teachers. They have supported me in everything that I have done and I love them for that.

This work was supported by the Director, Office of Energy Research, Office of Basic Energy Sciences, Chemical Sciences Division of the U. S. Department of Energy under Contract No. DE-AC03-76SF00098.

Chapter 1: The Translational Energy Dependence of the $F + C_2H_4 \rightarrow H + C_2H_3F$ Reaction Cross Section near Threshold

I. INTRODUCTION

An understanding of potential energy barriers is central to the field of chemical kinetics. Although activation energies can be extracted from the temperature dependence of reaction rates, these are phenomenological quantities that cannot always be directly correlated with the mechanical barrier on the potential energy surface (PES). The most direct way to probe such a barrier is to measure the translational energy dependence of the reaction cross section, or the excitation function. In an effort to learn more about the potential energy surfaces for atom-molecule addition reactions, we have studied the excitation function of the reaction $F + C_2H_4 \rightarrow H + C_2H_3F$ at six collision energies in the range 0.8 - 2.5 kcal/mol using the crossed molecular

beams method. The energetics of this reaction are outlined in Fig. 1.

There have been few kinetic studies of F + alkene substitution reactions owing largely to the high reactivity of fluorine atoms. Notable, however, are experiments by Wolfgang on $^{18}F + C_2H_4$ [1] and more recent work by Rowland and coworkers on the relative reactivity of ^{18}F with various substrates [2]. Pukhal'skaya et al. [3] have measured the rate of reaction of $F + C_2H_4$ to give both substitution (C_2H_3F) and abstraction (HF) products by monitoring the quenching of HF chemiluminescence from the reaction $F + H_2$ caused by the reaction $F + C_2H_4$.

Earlier crossed molecular beam studies of the title reaction [4] yielded center-of-mass (CM) frame C_2H_3F angular distributions that were forward-backward symmetric, indicating that the reaction proceeds through a collision complex which decomposes on a time scale longer than its rotational period. In addition, the CM angular distributions peaked slightly at θ=90°, suggesting that the F atom adds roughly perpendicular to the plane of the C_2H_4 double bond and that the H atom is ejected parallel to the total angular momentum vector (see Section III). The product translational energy distribution, P(E'), could not be reproduced by a statistical model that assumes that energy is completely randomized in the intermediate complex and that the P(E') reflects the distribution of vibration-rotation states along the reaction

coordinate at the exit-channel transition state (TS). From chemiluminescence experiments, McDonald and co-workers [5] likewise concluded that the internal state distribution of the C_2H_3F product reflects a non-statistical partitioning of energy in the collision complex. Marcus [6,7] has pointed out that for a "tight" transition state such as $H-C_2H_3F$, where there are no free internal rotations, exit channel interactions between the departing fragments will tend to shift the product translational energy distribution to higher energies, complicating any comparison of the experimental and RRKM P(E') distributions. Classical trajectory calculations by Hase and Bhalla [8] on a semi-empirical $F + C_2H_4$ PES indicate that the relative product translational energy distribution is indeed statistical at the exit channel saddle point but that it becomes skewed to higher energies as the products descend the 5.5 kcal/mol barrier. Ref. 4c shows, however, that the form of the P(E') changes little when the excess energy at the exit transition state is ≈5 times larger than this barrier, suggesting that the P(E') really does reflect non-statistical energy redistribution in the collision complex.

The reaction $F + C_2H_4 \rightarrow [C_2H_4F]^*$ is representative of a broad class of radical-alkene addition reactions. The activation energies for these reactions are typically low (0 - 10 kcal/mol) [9,10,11]. There has, however, been considerable discussion in the literature about the factors that

determine the magnitudes of these activation energies. Using a three-electron, three-center valence bond model, Salem [12] concludes that the degree of ionic character in the incipient radical-alkene bond determines the magnitude of the activation energy. Essentially, including polar resonance structures of the adduct radical lowers the activation energy to addition. Thus halogen atom addition to ethylene is expected to have a lower activation energy than methyl radical or hydrogen atom addition and this is indeed the case (Cl: 0 kcal/mol; H: 2.8 kcal/mol; CH_3: 7.7 kcal/mol) [10]. Alternatively, for many reactions the activation energy is roughly proportional to the difference between the ionization potential of the alkene and the electron affinity of the incoming atom [13]. Here again, the more polar the new bond, the lower the activation energy. From a series of experiments on radical addition reactions, Tedder and Walton [14] likewise find an inverse correlation between the polarity of the incipient bond and the activation energy. These activation energies also correlate well with Huckel localization energies [14,15], the π-electron energy that is lost upon forming the adduct, although when comparing the reactivities of different radicals with the same substrate the localization energy is not a useful quantity.

Ab initio quantum chemical calculations offer more detailed insights into the potential energy surfaces for addition reactions. Kato and Morokuma [16] have found that

the largest contribution to the 5 - 6 kcal/mol barrier to H atom addition to C_2H_3F (the reverse of the reaction here under study) comes from the deformation energy, or the energy required to distort the ethylene to its transition state configuration. Schlegel et al. [17] have calculated the barrier to F atom addition to ethylene to be 3 kcal/mol using an optimized transition structure in which the C-F bond length is 2.0 Å, the F-C-C angle is 94°, and the ethylene moiety is essentially undistorted [18]. The C-C-F bending frequencies that they calculate for this structure (242 and 405 cm^{-1}) suggest a "tight" transition state. Including electron correlation reduces the barrier to less than 2 kcal/mol and causes the $F-C_2H_4$ transition structure to become more reactant-like. Clark et al. [19] find that, although the computed saddle point geometry of the adduct corresponds to an early, or reactant-like, TS, the electron density is characteristic of a more product-like TS. They calculate an activation energy of 3.1 kcal/mol for addition. By eliminating spin contamination in their unrestricted Hartree-Fock wave functions, Schlegel and Sosa [20] have recently obtained a barrier height of -0.9 ± 0.3 kcal/mol for $OH + C_2H_4 \rightarrow C_2H_4OH$, which yields an activation energy that is in close agreement with experiment. They conclude [21] that F atom addition to C_2H_4 will have no barrier, in agreement with the results presented here.

II. EXPERIMENTAL

The experimental apparatus has been described elsewhere [22,23]. Ref. 23 contains a detailed description of the F atom source and of the pumping configuration for both sources and for the detector. Briefly, a doubly differentially pumped, velocity selected F atom beam was crossed with a singly differentially pumped, supersonic ethylene beam at 90° in a reaction chamber held at about 10^{-7} torr. Product C_2H_3F signal, m/e=46, was measured with a mass spectrometric detector that rotates in the plane of the two beams.

The primary beam was produced by velocity selecting an effusive F atom beam formed by thermally dissociating pure F_2 (Matheson) in a resistively heated nickel oven. The oven temperature was approximately 650°C. The six disk velocity selector gave a fwhm velocity spread of 11% which was independent of the wheel frequency. The angular divergence of the F beam was ≈2°.

The supersonic ethylene beam was produced by expanding 500 torr of ultra-high purity ethylene (Matheson) or 20% ethylene in helium through a 0.21 mm diameter nozzle. The source consisted of a platinum electron microscope aperture brazed onto a copper tube. The nozzle was held at a distance of 1.0 cm from a 0.81 mm aperture stainless steel skimmer. A coaxial heater and a liquid nitrogen contact allowed us to raise or lower the temperature of the source.

Table 1 lists the experimental beam conditions. Changing the velocity selector frequency and/or seeding or cooling the ethylene beam enabled us to vary the collision energy, E_c. Experiments were carried out at six nominal collision energies: 0.8, 1.1, 1.4, 1.9, 2.0, and 2.5 kcal/mol. The fwhm spread in collision energy was ≈20%.

Product angular distributions were obtained by modulating the F atom beam with a 150 Hz tuning fork chopper. Counting times ranged from 2-17 minutes per angle. Time-of-flight (TOF) spectra of the reactive product were measured using the cross-correlation method [22b] near the center-of-mass angle for four of the six collision energies. A 255-channel multi-channel scaler connected to a LSI/11 minicomputer controlled the data acquisition. A Cu-Be wheel, photoetched with a 255 element pseudo-random sequence of open and closed slots, was spun at 436 Hz giving 9 μsec/ channel resolution in the TOF spectra. The flight path from the chopping wheel to the ionizer was 30.4 cm. Counting times were from 1-4 hours per angle. The velocity distributions of both reactant beams were measured by spinning a stainless steel wheel with four equally spaced slots at 300 Hz.

III. RESULTS AND ANALYSIS

The product angular distributions are plotted in Figs. 3 - 8; low level elastic scattering background from impuri-

ties has been subtracted. More structure is evident in these distributions than in those of the earlier studies as a result of the improved product velocity and angular resolution of the present apparatus and the narrower velocity spread of the fluorine beam. The bimodality of the TOF spectra (Fig. 9) indicates that the product recoil energy distribution peaks away from zero (Fig. 2).

The product angular distributions and TOF spectra were fit using a forward convolution program that starts with a separable form for the CM frame product flux distribution [24], $I_{CM}(\theta,E') = T(\theta)P(E')$, and generates LAB frame angular distributions and TOF spectra averaged over the spread in relative velocities. $T(\theta)$, the CM frame product angular distribution, was initially taken to be a sum of Legendre polynomials whose coefficients were varied to optimize the fit. A point-form was used for the CM frame product translational energy distribution, P(E'). The fits were refined by altering sections of $T(\theta)$ and P(E').

The $T(\theta)$ distributions (Fig. 10) are largely symmetric about θ=90° confirming the earlier findings [4] that the reaction proceeds via a long-lived collision complex. However, unlike the earlier studies, in which the CM angular distributions rise monotonically from 0° to 90° (with $T(0°)/T(90°) \simeq 0.7$ at E_c=2.0 kcal/mol), we observe forward-backward as well as a sideways peaking at some energies. Presented in Figs. 3 - 8 are fits to the LAB angular distri-

butions using different CM frame angular distributions. The E_c=1.9, 2.0, and 2.5 kcal/mol LAB distributions are fit adequately by $T(\theta)$ distributions having a single maximum at θ=90°, but the fits to the E_c=1.9 and 2.0 kcal/mol data are improved a bit by including smaller peaks at 0° and 180° (Fig. 10; a,b). A slight excess of forward scattering improves the fit to the E_c=1.9 kcal/mol distribution.

The LAB angular distribution at E_c=1.4 kcal/mol has a pronounced dip at $\theta \approx 65°$. This dip can be fit only if $T(\theta)$ has a local minimum at $\theta \approx 150°$. For instance, the LAB data can be fit by a $T(\theta)$ that is level from 0° to 120°, dips at 150°, and has a maximum at 180° (Fig. 10; c(i)). Forcing $T(\theta)$ to be approximately forward-backward symmetric gives distributions d(i) and d(ii), which have maxima at 0° and 180° and a broad peak ≈90°. These distributions are still slightly asymmetric, the valley at 150° being wider, and in the case of d(ii), deeper than the valley at 30°. In deriving distribution d(ii), an effort was made to keep the ratio $T(0°)/T(90°)$ a small as possible. The backward portion of the angular distribution is not fit well by a $T(\theta)$ having a single maximum at 90° (c(iii)). Distributions b(i) and b(ii) also yield poor fits, giving too much intensity near θ_{CM}.

Although the signal-to-noise ratio is worse at E_c=1.1 kcal/mol, the LAB angular distribution at this energy also shows a backward dip. The data can be fit with CM distri-

butions d(i) and d(ii), or with distribution c(ii) which rises gradually from 0° to 90°, dips at 150°, and peaks at 180°. Again, the fit to the forward part of the LAB angular distribution is insensitive to the form of $T(\theta)$ from 0°-90° and the sideways peaked c(iii) distribution does not fit the backward part of the LAB distribution. The E_c=0.8 kcal/mol data is too noisy to be fit with certainty; an adequate fit is obtained with an isotropic $T(\theta)$ although their is a hint of a peak near θ_{CM}.

Changing $T(\theta)$ at E_c=1.4 and 1.1 kcal/mol as described above barely changed the calculated TOF spectra. In retrospect, it would have been wise to measure product TOF spectra at more than one angle but at the time of these experiments we did not suspect that the CM angular distributions would be different from those obtained earlier.

Two different models have been proposed to explain the sideways peaked angular distributions observed in the earlier crossed beam studies of this reaction. Lee and co-workers have argued [4] that if the F atom adds roughly perpendicular to the plane of C_2H_4 molecule and if the rotational angular momentum of the C_2H_4 reagent is small, then the heavy atoms (C-C-F) will rotate in a plane containing the relative velocity vector, **v**, and perpendicular to the orbital angular momentum vector, **L**. Since the H atom will be perpendicular to the C-C-F plane (and hence to **v**) in the exit channel transition state, the products will scatter sideways and

parallel or anti-parallel to **L**. However, this sort of scattering occurs only because **L'** << **L**, which is to say that the rotational angular momentum vector of the C_2H_3F product, **j'**, is polarized parallel to **L**.

McClelland and Herschbach [25] have maintained that, being a nearly prolate top [26], the fluoroethyl radical will rotate predominantly about its A-axis (the axis corresponding to it smallest moment of inertia) while this axis precesses about the total angular momentum vector, **J**. Averaging over the relative orientations of **A**, **J**, **v**, and **v'**, they arrived at a CM angular distribution that is sideways peaked. In calculating these cylindrical averages, however, they assume that there is a steric preference for F atom attack perpendicular to the double bond and that the H atom is ejected perpendicular to the C-C-F plane.

Scattering at 0° and 180° occurs when some fraction of the C_2H_4F complexes decompose with their C_β-H^* bond (the bond that is breaking) lying in the <u>initial</u> C-C-F plane. If the C_β-H^* bond is perpendicular to the C-C-F framework, it can lie in the initial C-C-F plane only if the radical rotates about its **A**-axis. Our data might, therefore, reflect prolate motion of the fluoroethyl complex. In particular, at low collision energies when long range attractive forces between the atom and molecule become dominant (see next section), collisions involving an F atom striking off of the C=C axis may lead to complex formation. Such off-axis collisions will

cause the complex to tumble in a prolate manner. If the period of this motion is comparable to the period of the oblate C-C-F rotational motion (which is responsible for the sideways scattering), we may observe peaks in the CM angular distribution at 0°, 90°, and 180°.

The rotational angular momentum, **j**, of the ethylene molecule will also contribute to the total angular momentum of the C_2H_4F complex and therefore affect the symmetry of $T(\theta)$. However, it will constitute only a small fraction of **J**. Taking the rotational temperature of the ethylene molecules in the beam to be ≈30 K, we calculate the peak of the rotational state distribution to be $j = 3\hbar$. From their classical trajectory calculations, Hase and Bhalla concluded that the maximum impact parameter for the F + C_2H_4 addition reaction is 2.5 Å [8], but, not knowing the opacity function for this reaction, it is not possible to calculate **L** accurately. Assuming an average impact parameter of 2.0 Å, $L \approx 50\hbar$ at E_c=2.5 kcal/mol and $30\hbar$ at 0.8 kcal/mol. So, at most, $j \approx (0.1)J$. Molecular rotations might be more relaxed in the seeded C_2H_4 beam (E_c=2.5 and 2.0 kcal/mol) but the best fit CM angular distributions for the 1.9 kcal/mol data, obtained with a neat C_2H_4 beam, are rather similar to those at the two highest energies. In any case, the rotational angular momentum of the ethylene molecule would be expected to make $T(\theta)$ more, rather than less, isotropic.

It should be noted that the C_2H_3F product scatters over

a wider range of LAB angles at the lower collision energies as a result of the different kinematics. For instance, the distances between the peaks of the forward and backward lobes of the angular distributions are about 24°, 25°, 18°, and 16° at E_c=1.1, 1.4, 2.0, and 2.5 kcal/mol respectively. Thus, the lower energy angular distributions might actually afford a more detailed insight into the dynamics of this reaction. However, it is not entirely clear at this time why the CM angular distributions at E_c=1.4 and 1.1 kcal/mol are so different from those at the higher collision energies. Hase [27] is currently carrying out classical trajectory calculations on this reaction at low collision energies to see what effect angular momentum partitioning has on the differential cross section.

The calculated P(E') distributions (Fig. 11) are in general agreement with those of ref. 4 in that approximately 50% of the available energy is channeled into translation (Table 2). The data at different collision energies could be fit using P(E') distributions having similar forms. The fits are most sensitive to the peak values and thresholds of the translational energy distributions. The threshold of the E_c=2.5 kcal/mol P(E') is uncharacteristically high. This is undoubtedly due to the lack of TOF data at this energy; the TOF intensity at the center-of-mass flight time always constrained the threshold of the P(E') to be lower than what it would have been based on the angular data alone.

Although it was found in the earlier scattering studies that an exoergicity of 13 kcal/mol was necessary to fit the data, the present fits are not very sensitive to the cutoff energies of the P(E'). Accordingly, we take $\Delta H^\circ = -11$ kcal/mol, which is the difference between the product and reactant heats of formation at 300 K [13]. Adding a tail of up to 2 kcal/mol additional energy to the P(E') did not affect the calculated angular and TOF distributions.

Since the ethylene beam was cooled to -100°C in order to reach the two lowest collision energies, small amounts of clusters of various sizes were present in the beam. Fluorine atoms condense on these clusters and the resulting complexes have the velocities of the centers-of-mass [28]. Since the center-of-mass angle moves progressively closer to the ethylene beam as the cluster size increases, fragmentation of these complexes in the electron bombardment ionizer will give rise to a large unreactive m/e=46 signal near the ethylene beam. This spurious signal was neglected in the fits of the E_c=0.8 and 1.2 kcal/mol product angular distributions. Also, in order to minimize detector background, no data was ever collected at angles closer than 7° to the ethylene beam.

Relative cross sections, S_r, were obtained by integrating the CM frame product flux (Table 2; Fig. 12):

$$S_r = 2\pi \int_0^\infty \int_0^\pi P(E')T(\theta) \sin\theta \, dE'd\theta \ .$$

Since the product angular distributions were measured over a period of several weeks, fluctuations in the F oven

temperature and consequently in the F beam intensity unavoidably occurred. Also, because the collision energy was varied by lowering the velocity selector frequency and cooling or seeding the ethylene beam, the intensities of both beams varied considerably over the energy range studied. For example, at a velocity selector frequency of 500 Hz the most probable F atom velocity is 8.7×10^4 cm/sec. This velocity is near the peak of the Maxwell-Boltzmann velocity distribution at 650°C. From 500 Hz to 250 Hz ($8.7\text{-}4.3 \times 10^4$ cm/sec) the F atom number density drops by a factor of 21. Likewise, on cooling the ethylene beam to -100°C the observed m/e=28 number density drops as a result of cluster formation. Seeding 20% ethylene in helium leads to a slight increase in the monomer number density. Thus, in order to compare the integrated product flux at different collision energies, one day was spent measuring beam intensities and product signal at two laboratory angles at each collision energy for which a complete product angular distribution was already measured. The signals at both angles were divided by the corresponding signals from the complete angular distributions giving two normalization factors. The computed relative cross sections were scaled using the average of these two normalization factors. To account for changes in reactant flux, the cross sections were further scaled by a reactant flux factor, $n_F n_{C_2H_4} v_{rel}$, where n_i is the number density of the i-th beam and v_{rel} is the relative velocity.

Relative reactant number densities were determined by directly measuring reactant count rates. Since the F/F_2 ratio changes with velocity (because the two species have different Maxwell-Boltzmann velocity distributions), one needs to know the percentage of F_2 that fragments in the ionizer to give m/e=19. We had hoped to determine the extent of fragmentation of F_2 by comparing the experimental velocity distributions for F and F_2 with the Maxwell-Boltzmann distributions. However, with $\Delta v/v \approx 30\%$ (fwhm), the F atom beam was not truly effusive and no such comparison was possible.

Earlier measurements in our laboratory on the dissociative ionization of F_2 from a 650°C supersonic nozzle yielded $F^+/F_2^+ = 0.47$ [29]. However, it can be seen in Fig. 13 that this value for F^+/F_2^+ causes the excitation function to behave non-monotonically. A more reasonable value is $F^+/F_2^+ = 0.20$ since it causes the slope of the excitation function between E_c=1.9 and 2.0 kcal/mol to have a value less than that between 1.4 and 1.9 kcal/mol and greater than that between 2.0 and 2.5 kcal/mol (Fig. 13). Setting $F^+/F_2^+ = 0.27$ makes $S_r(1.9) = S_r(2.0)$.

The uncertainties associated with the reactant flux scaling factors are neglected since the statistical errors in the n_i values are very small and the relative cross section does not change considerably over the spread in v_{rel}. The largest uncertainty in the relative cross section, represented by the error bars in Fig. 12, arises from the first

scaling factor and reflects the statistical noise in the data. It should also be noted that weighting the relative velocities used in the analysis by the experimental excitation function (Fig. 12) had no effect on the E_c=1.4 kcal/mol fit. This is to be expected since the spread in collision energy is a small fraction of the total energy available to the products.

The decrease in the relative substitution cross section with increasing collision energy indicates that the barrier to F atom addition is likely nil, but in any case must be less than 0.8 kcal/mol. Since $T(\theta)$ is weighted by $\sin\theta$ in calculating S_r, S_r will be most sensitive to the form of $T(\theta)$ near θ=90°. For the E_c=1.9 kcal/mol data, however, a 10% change in $T(\theta)$ at θ=90° caused less than a 1% deviation in S_r. At E_c=0.8 kcal/mol, an isotropic $T(\theta)$ yields a value of S_r that is only 2% larger than the value obtained using distribution d(i). Likewise, changing the position of the threshold or the peak of P(E') enough to perceptibly worsen the fit changes S_r by only 3%. However, the lack of data at $\theta > 82°$ for four of the six collision energies (and especially at E_c=0.8 kcal/mol) necessarily introduces some error in S_r.

Raising the ethylene beam nozzle temperature from -100° to 30°C changes the fraction of molecules that are in their ground vibrational states negligibly. The largest change (≈2%) will occur in the population of ν_{10}, the CH_2 rocking

mode (843 cm^{-1} [30]). Hase et al. have run classical trajectories on semi-empirical potential energy surfaces to study the effect of vibrational excitation of C_2H_4 on the H + C_2H_4 → C_2H_5 reaction cross section [31]. They find that placing up to 2 quanta in ν_2 (1655 cm^{-1}; C-C stretch), ν_7 (969 cm^{-1}; CH_2 wag), or ν_8 (959 cm^{-1}; CH_2 wag) has little effect on the addition cross section.

IV. DISCUSSION

The decrease of S_r with increasing collision energy might perhaps be understood within the context of RRKM theory. Assuming that the probability of adduct formation is independent of collision energy in the range studied, the observed excitation function will reflect the probability of unimolecular decay of the energized fluoroethyl radical to products relative to reactants or to other energetically accessible products. Rate constants for these decay pathways, k_i, can be calculated as a function of energy from RRKM theory and the branching ratio,

$$S^p_{RRKM} = k_p / \sum_i k_i,$$

where p represents the H atom elimination channel, can then be compared to the observed excitation function. Each rate constant reflects the state density at the transition state for a given pathway so, for an exoergic reaction, the above ratio is expected to decrease on increasing the collision

energy since the state density at the reactant ($F\text{-}C_2H_4$) transition state increases more rapidly with energy in the threshold region than the state density at the product ($H\text{-}C_2H_3F$) transition state.

In addition to atomic elimination, we must, however, consider the possibility of exothermic 3- and 4-center HF elimination:

$$F + C_2H_4 \rightarrow C_2H_3 + HF\ (v=0\text{-}2), \quad \Delta H^\circ = -27\ \text{kcal/mol}.$$

In the crossed beam study of the reaction $F + C_2D_4 \rightarrow DF + C_2D_3$ [4a], only DF (v=4) was observed and the authors concluded that the reaction occured through the direct abstraction of D by F. The DF angular distribution from that experiment, however, shows a marked forward-backward symmetry, indicating that the reaction very likely proceeds through formation of a long lived intermediate followed by DF elimination. The fact that DF in lower vibrational states was not observed could be attributed to the poorer detection efficiency for these faster products. In a related experiment, Moehlmann and McDonald [32] found that the HF vibrational state distribution from the reaction, $F + C_2H_4 \rightarrow HF + C_2H_3$, peaks at v=1. Radiative decay of HF in higher vibrational states is, however, a possibility in that experiment. Donaldson et al. [33] observed an inverted HF vibrational distribution for the same reaction, in support of a direct abstraction mechanism.

In halogenated ethanes and ethylenes, 3- and 4-center

elimination reactions are known to have activation energies in the range of 60-80 kcal/mol [34-36]. The activation energy for elimination of HF from C_2H_3F is 80 kcal/mol; from C_2H_5F it is 60 kcal/mol [34a-c]. Ab initio calculations by Kato and Morokuma [36] indicate that the barrier to 3-center HF elimination from C_2H_3F is about 1 kcal/mol lower than the 4-center barrier. However, the magnitudes of the barriers to HX elimination from haloethyl radicals are unknown. The 4-center barrier in fluoroethyl radical might be expected to be closer in magnitude to that for C_2H_5F since the C-C and C-F stretching and C-C-F bending frequencies are predicted to be similar in the two species [16,35]. Chemical activation experiments suggest that the activation energies for 3-center HX elimination from haloethanes are slightly higher than those for 4-center elimination [34d,e]. In particular, 3-center elimination of HX from haloethanes is thought to be improbable in the absence of a second halogen atom on the primary carbon to stabilize the carbene product [34d,37]. However, the possibility of partial double bond formation during 3-center elimination of HF from fluoroethyl radical might lower the barrier to this process below 50 kcal/mol. The maximum energy available to the radicals in our experiment is $\approx$49 kcal/mol (E_c=2.5 kcal/mol).

In calculating the ratio of the RRKM constants, vibrational frequencies and moments of inertia for the radical and for the H-C_2H_3F transition state were obtained from Kato and

Morokuma [16]; frequencies for the F-C_2H_4 TS, the depth of the radical well relative to reactants (46 kcal/mol), and the barrier to H elimination (41 kcal/mol) were obtained from Schlegel et al. [17]. The moments of inertia for the radical and for the H elimination TS were taken from ref. 16; those for the F-C_2H_4 TS state were calculated using the optimized transition state geometry of Schlegel [18]. Frequencies and moments of inertia for a 3-center HF-C_2H_3 TS were derived from the calculations of Kato and Morokuma on $C_2H_3F \rightarrow HF + C_2H_2$ [36]. Three additional frequencies corresponding to C-H stretching and bending were added (3400, 1400, 950 cm^{-1}) and the C-C stretching frequency in the H atom elimination TS state was used. The F-C_2H_4 TS was assumed to be at the same energy as reactants (i.e. no barrier to addition) and the barrier to 3-center elimination was initially taken to be 45 kcal/mol.

Microcanonical RRKM rate constants were calculated for all three processes using the program of Hase and Bunker [38]. The calculated excitation function is scaled to the experimental points ($F^+/F_2^+ = 0.20$) using a weighted least-squares fit and is plotted in Fig. 12. It is obvious that the calculated curve barely declines with increasing energy. This is because the rate constant for H elimination is much larger than those for the other pathways. Lowering the barrier to HF elimination increases the rate constant for this process proportionately at both the low and high

energies and so does not change the slope of the calculated curve. Raising the barrier to, say, 47 kcal/mol so that radicals formed at the lowest experimental collision energy could not eliminate HF also does not appreciably affect the curve. Neither does excluding high frequency C-H stretching vibrations from the calculation. We conclude that, with the assumption that the cross section for complex formation is independent of collision energy, the observed excitation function cannot be modeled using statistical theory.

Since the fraction of energy in the fluoroethyl complex that is tied up in rotation, and thus unavailable to break bonds, increases very little in the collision energy range studied ($E_{rot}/E_{tot} \approx 1\%$ at E_c=0.8 kcal/mol and ≈4% at E_c=2.5 kcal/mol, using values for L calculated above and a moment of inertia of 58 amu·Å^2 [16]) the only alternative explanation for the decline in S_r with increasing collision energy is that the probability of forming the initial adduct decreases with increasing energy. In their classical trajectory calculations on H + C_2H_4 → C_2H_5, Hase *et al.* [31] find that the addition cross section rises steadily from E_c=4-20 kcal/mol, levels off around 30 kcal/mol and drops only when E_c > 60 kcal/mol. They do not study collision energies below 4 kcal/mol. The initial rise in cross section occurs because wider approach angles become energetically accessible at higher energies. For E_c < 20 kcal/mol, the addition cross section is lower on the PES with the more restricted range of

approach geometries. The decrease in the excitation function at higher energies results from an increase in the fraction of unproductive collisions in which the incipient C-H bond either never reaches its equilibrium length or, having reached its equilibrium length, ruptures in less than one vibrational period.

Although the F + C_2H_4 potential energy surface probably allows for a wider range of reagent approach geometries than the H + C_2H_4 PES, we might still expect the addition cross section to display a positive energy dependence. However, at lower relative energies, the collision partners may have more time to orient into the optimum reaction geometry. Assuming that the reactants interact over a range of 2 Å, the mean collision time increases from 0.15 to 0.26 ps on lowering the collision energy from 2.5 to 0.8 kcal/mol. Also, as the collision energy is raised, more energy will remain in the incipient C-F bond and this bond may break before the fully energized radical is formed. Of course, if only a few vibrational modes in the region of the F attack are involved in the dynamics then complete energy redistribution may never take place and C-F bond rupture will always compete with C-H rupture. The earlier crossed beam studies [4] support the latter view. The H + C_2H_4 classical trajectory study suggests, however, that there would not be a significant increase in the number of non-reactive F + C_2H_4 collisions in the collision energy range of our experiments.

A more convincing explanation for the drop in S_r with increasing collision energy is that the F-C_2H_4 interaction is dominated by a barrier-less, long range attractive potential. Such an interaction, characteristic of radical association reactions, gives rise to a loose transition state [13]. Now, the cross sections (rate constants) for many radical association reactions have been found to display a negative energy (temperature) dependence [13,39]. For example, a classical trajectory study of the H + CH_3 → CH_4 reaction indicates that the reaction cross section decreases by a factor of ≈1.7 from 0 - 2 kcal/mol [40]. Recent measurements on the kinetics of methyl radical recombination [41] suggest a drop of ≈25% in the high pressure rate constant for this reaction over the temperature range 296 - 577 K. This trend is explained by modern transition state theory which locates the transition state for reactions without a potential energy barrier at the intermolecular distance at which the density of states along the reaction coordinate is a minimum, $r^\dagger$ [39,42]. As the collision energy (or temperature) is raised, $r^\dagger$ decreases, causing the transition structure to become tighter, i.e., the relative motion of the collision partners at the critical configuration becomes more hindered. Alternatively, if the transition state is located at the centrifugal barrier to the reaction (the intermolecular distance at which the attraction between the reacting species is exactly balanced their centrifugal repulsion), $r^\dagger$ will decrease with increasing energy

[13,43]. In either case, a drop in the reaction cross section (rate constant) will accompany the decrease in $r^{\dagger}$. Our results are therefore consistent with an early, reactant like transition state for the F + C_2H_4 addition reaction. It is noteworthy that higher level ab initio calculations on this and related systems (see Section I) yield transition state properties that are consistent with our findings [17,21].

V. CONCLUSIONS

Our results show that the barrier to F atom addition to ethylene must be less than 0.8 kcal/mol, in agreement with evidence that halogen atom addition to alkenes proceeds with little or no activation energy and with recent ab initio calculations. The observed decline in the relative cross section with increasing collision energy indicates that formation of fluoroethyl radical is not independent of collision energy and suggests that long range attractive forces give rise to a loose adduct transition state. The CM C_2H_3F product angular distributions that fit our data at E_c=1.4 and 1.1 kcal/mol are not consistent with those previously found for this reaction at E_c=2.0 kcal/mol and might reflect unusual angular momentum partitioning in the C_2H_3F collision complex.

REFERENCES

1. N. Colebourne and R. J. Wolfgang, J. Chem. Phys. 38, 2782 (1963).
2. T. S. Smail, R. S. Iyer, and F. S. Rowland, J. Phys. Chem. 94, 1041 (1972).
3. G. V. Pukals'kaya, N. F. Chebotarev, V. B. Kolovskii, and S. Ya. Pashezhetskii, Kinet. Katal. 21, 1063 (1980).
4. (a) J. M. Parson and Y. T. Lee, J. Chem. Phys. 56, 4658 (1972); (b) J. M. Parson, K. Shobatake, Y. T. Lee, and S. A. Rice, Faraday Discuss. Chem. Soc. 55, 344 (1973); (c) J. M. Farrar and Y. T. Lee, J. Chem. Phys. 65, 1414 (1976).
5. J. G. Moehlmann, J. T. Gleaves, J. W. Hudgens, and J. D. McDonald, J. Chem. Phys. 60, 4790 (1974).
6. R. A. Marcus, Faraday Discuss. Chem. Soc. 55, 379, 381 (1973).
7. R. A. Marcus, J. Chem. Phys. 62, 1372 (1975); G. Worry and R. A. Marcus, J. Chem. Phys. 67, 1636 (1977).
8. W. L. Hase and K. C. Bhalla, J. Chem. Phys. 75, 2807 (1981).
9. S. W. Benson and H. E. O'Neal, Kinetic Data on Gas Phase Unimolecular Reactions (NSRDS-NBS 21, US Dept. of Commerce, Washington, D. C., 1970).
10. J. A. Kerr and Parsonage, Evaluated Kinetic Data on Gas Phase Addition Reactions (CRC, Cleveland, 1972).

11. J. A. Kerr and A. C. Lloyd, Quart. Rev. 22, 549 (1968).

12. V. Bonacic-Koutecky, J. Koutecky, and L. Salem, J. Am. Chem. Soc. 99, 842 (1977) .

13. S. W. Benson, Thermochemical Kinetics (Wiley, New York, 2nd ed., 1976).

14. J. M. Tedder and J. C. Walton, Accts. Chem. Res. 9, 183 (1976); J. M. Tedder and J. C. Walton, in Fluorine Containing Free Radicals, ACS Symposium Series 66, J. W. Root, Editor (ACS, Washington, D. C., 1978) p. 107; D. C. Nonhebel and J. C. Walton, Free Radical Chemistry (Cambridge University Press, Cambridge, 1974).

15. J. M. Tedder and J. C. Walton, Trans. Faraday Soc. 62, 1859 (1966).

16. S. Kato and K. Morokuma, J. Chem. Phys. 72, 206 (1980).

17. H. B. Schlegel, K. C. Bhalla, and W. L. Hase, J. Phys. Chem. 86, 4883 (1980).

18. H. B. Schlegel, J. Phys. Chem. 86, 4878 (1982).

19. D. T. Clark, I. W. Scanlan, J. C. Walton, Chem. Phys. Lett. 55, 102 (1978).

20. C. Sosa and H. B. Schlegel, J. Am. Chem. Soc. 109, 4193 (1987).

21. H. B. Schlegel (private communication).

22. (a) Y. T. Lee, J. D. McDonald, P. R. LeBreton, and D. R. Herschbach, Rev. Sci. Inst. 40, 1402 (1969); (b) R. K. Sparks, Ph. D. Thesis, University of California, Berkeley, 1979.

23. D. M. Neumark, A. M. Wodtke, G. N. Robinson, C. C. Hayden, and Y. T. Lee, J. Chem. Phys. 82, 3045 (1985); D. M. Neumark, Ph. D. Thesis, University of California, Berkeley, 1984.

24. R. J. Buss, Ph. D. Thesis, University of California, Berkeley, 1979.

25. G. M. McClelland and D. R. Herschbach, Faraday Discuss. Chem. Soc. 67, 251 (1979).

26. The moments of inertia of the C_2H_3F complex are given in ref. 16 as 13.2, 51.4, and 58.0 amu$\cdot$Å^2.

27. W. L. Hase (private communication).

28. R. Behrens, Jr., A. Freedman, R. R. Herm, and T. P. Parr, J. Chem. Phys. 63, 4622 (1975).

29. P. Casavecchia, C. Becker, and Y. T. Lee (unpublished results).

30. C. W. Bock, P. George, and M. Trachtman, J. Mol. Spectrosc. 76, 191 (1979).

31. W. L. Hase, D. M. Ludlow, R. J. Wolf, and T. Schlick, J. Phys. Chem. 85, 958 (1981).

32. J. G. Moehlmann and J. D. McDonald, J. Chem. Phys. 62, 3061 (1975).

33. D. J. Donaldson, D. G. Watson, and J. J. Sloan, Chem. Phys. 68, 95 (1982).

34. (a) J. M. Simmie, W. J. Quiring, and E. Tschuikow-Roux, J. Phys. Chem. 74, 992 (1970); (b) P. Cadman, M. Day, A. W. Kirk, and A. F. Trotman Dickenson, J. Chem. Soc.

Chem. Commun. 203 (1970); (c) P. Cadman, M. Day, A. F. Trotman-Dickenson, J. Chem. Soc. (A) 2498 (1970); (d) K. C. Kim, D. W. Setser, and B. E. Holmes, J. Phys. Chem. 77, 725 (1973); (e) K. C. Kim and D. W. Setser, J. Phys. Chem. 78, 2166 (1974).

35. S. Kato and K. Morokuma, J. Chem. Phys. 73, 3900 (1980).

36. S. Kato and K. Morokuma, J. Chem. Phys. 74, 6285 (1981).

37. (a) M. J. Perona, J. T. Bryant, and G. O. Pritchard, J. Am. Chem. Soc. 90, 4782 (1968); (b) K. C. Kim and D. W. Setser, J. Phys. Chem. 76, 283 (1972).

38. W. L. Hase and D. L. Bunker, Quantum Chemistry Program Exchange, University of Indiana, Bloomington, Indiana.

39. M. Quack and J. Troe, Ber. Bunseges. Phys. Chem. 81, 329 (1977).

40. R. J. Duchovic and W. L. Hase, J. Chem. Phys. 82, 3599 (1985).

41. M. T. Macpherson, M. J. Pilling, and M. J. C. Smith, J. Phys. Chem. 89, 2268 (1985).

42. (a) D. M. Wardlaw and R. A. Marcus, J. Phys. Chem. 90, 5383 (1986); (b) W. L. Hase, J. Chem. Phys. 64, 2442 (1976); (c) W. L. Hase, Chem. Phys. Lett. 139, 389 (1987).

43. S. W. Benson, Can. J. Chem. 61, 881 (1983).

Table 1. Experimental beam conditions.

E_c (kcal/mol)	C_2H_4 source temp. (°C)	C_2H_4 beam Speed ratio	v_{pk}[a] (x10^4 cm/s) F	v_{pk}[a] (x10^4 cm/s) C_2H_4	$n_1n_2v_{rel}$ (arb. units)
0.8	-100 (neat)	5.7	4.3	6.5	0.011
1.1	-100 (neat)	*	6.1	6.5	0.086
1.4	30 (neat)	7.9	6.1	8.2	0.17
1.9	30 (neat)	*	8.7	8.2	0.77
2.0	30 (20% in He)	12.3	6.1	10.5	0.26
2.5	30 (20% in He)	*	8.7	10.5	1.00

(a): Peak laboratory velocity.

Table 2. Fraction of available energy in product translation energies and relative cross sections.

E_c (kcal/mol)	$\langle E'/E_{avl} \rangle$	S_r[a] (arb. units)
0.8	0.52	1.00 (.09)[b]
1.1	0.52	0.75 (.02)
1.4	0.51	0.72 (.01)
1.9	0.50	0.55
2.0	0.51	0.53 (.01)
2.5	0.51	0.45

(a): For $F^+/F_2^+ = 0.20$; numbers in parentheses are $\pm 1\sigma$ error bars arising from the uncertainty in the mean value of the normalization factor described in the text.

(b): $S_r(0.8)$ is an average of the relative cross sections obtained with an isotropic $T(\theta)$ and b(i) in Fig. 10; it is normalized to 1. The uncertainty in $S_r(0.8)$ arises, in part, from the uncertainty in $T(\theta)$.

FIGURE CAPTIONS

Fig. 1: Generalized reaction coordinate diagram for F + C_2H_4 → H + C_2H_3F. Hatched region represents collision energy range.

Fig. 2: Kinematic ("Newton") diagram for F + C_2H_4 → H + C_2H_3F at E_c = 1.9 kcal/mol. v_{CM}: Velocity of center-of-mass; θ_{CM}: Center-of-mass angle for the collision in LAB frame; u_{C2H3F}: Maximum velocity of C_2H_3F product in center-of-mass frame; v_{L1} and v_{L2}: slow and fast components of C_2H_3F velocity at angle θ in LAB frame. For a P(E') that peaks away from zero, these components will give rise to a bimodal TOF spectrum.

Fig. 3: C_2H_3F (m/e=46) laboratory angular distribution at E_c=2.5 kcal/mol; all of the data are shown. Fit obtained with T(θ) a(ii) in Fig. 10. Arrow indicates center-of-mass angle.

Fig. 4: C_2H_3F (m/e=46) laboratory angular distribution at E_c=2.0 kcal/mol; all of the data are shown. ——— fit obtained with T(θ) a(i); ---- fit obtained with T(θ) a(ii).

Fig. 5: C_2H_3F (m/e=46) laboratory angular distribution at E_c=1.9 kcal/mol; all of the data are shown. ——— fit obtained with T(θ) b(i); ---- fit obtained with T(θ) b(ii).

Fig. 6: C_2H_3F (m/e=46) laboratory angular distribution at E_c=1.4 kcal/mol; all of the data are shown. upper panel: ——— fit obtained with T(θ) d(i); ---- fit obtained with T(θ) d(ii). lower panel: — – — fit obtained with T(θ) c(i); — – – – — fit obtained with T(θ) c(iii).

Fig. 7: C_2H_3F (m/e=46) laboratory angular distribution at E_c=1.1 kcal/mol. upper panel: same as Fig. 6(a). lower panel: — — fit obtained with T(θ) c(ii); — – – – — obtained with T(θ) c(iii). Error bars represent 90% confidence limits.

Fig. 8: C_2H_3F (m/e=46) laboratory angular distribution at E_c=0.8 kcal/mol. – – – obtained with an isotropic T(θ); ---- obtained with T(θ) d(ii); ——— obtained with T(θ) b(i). See Fig. 7.

Fig. 9: C_2H_3F (m/e=46) time-of-flight spectra at four collision energies. Solid lines are fits to data using P(E') distributions in Fig. 11. The following $T(\theta)$ distributions were used (see text): E_c=1.9, b(i); E_c=1.4 and 1.1, d(ii); E_c=0.8, isotropic.

Fig. 10: Center-of-mass frame C_2H_3F angular distributions used to fit laboratory angular distributions.
(a), (b), and (d): [i] ——— ; [ii] -----.
(c) [i] —— - —— ; [ii] — — ; [iii] — - - - —

Fig. 11: Center-of-mass frame product translational energy distributions used to fit the data at the six collision energies.

Fig. 12: Experimental excitation function for $F + C_2H_4 \rightarrow H + C_2H_3F$. Points are relative cross sections assuming $F^+/F_2^+ = 0.20$; see Table 2. Solid line is a RRKM calculation of the energy dependent branching ratio for this reaction (see text).

Fig. 13: Experimental excitation functions assuming different values for F^+/F_2^+.
□: F^+/F_2^+=0.0; ○: F^+/F_2^+=0.20; ○: F^+/F_2^+=0.47.

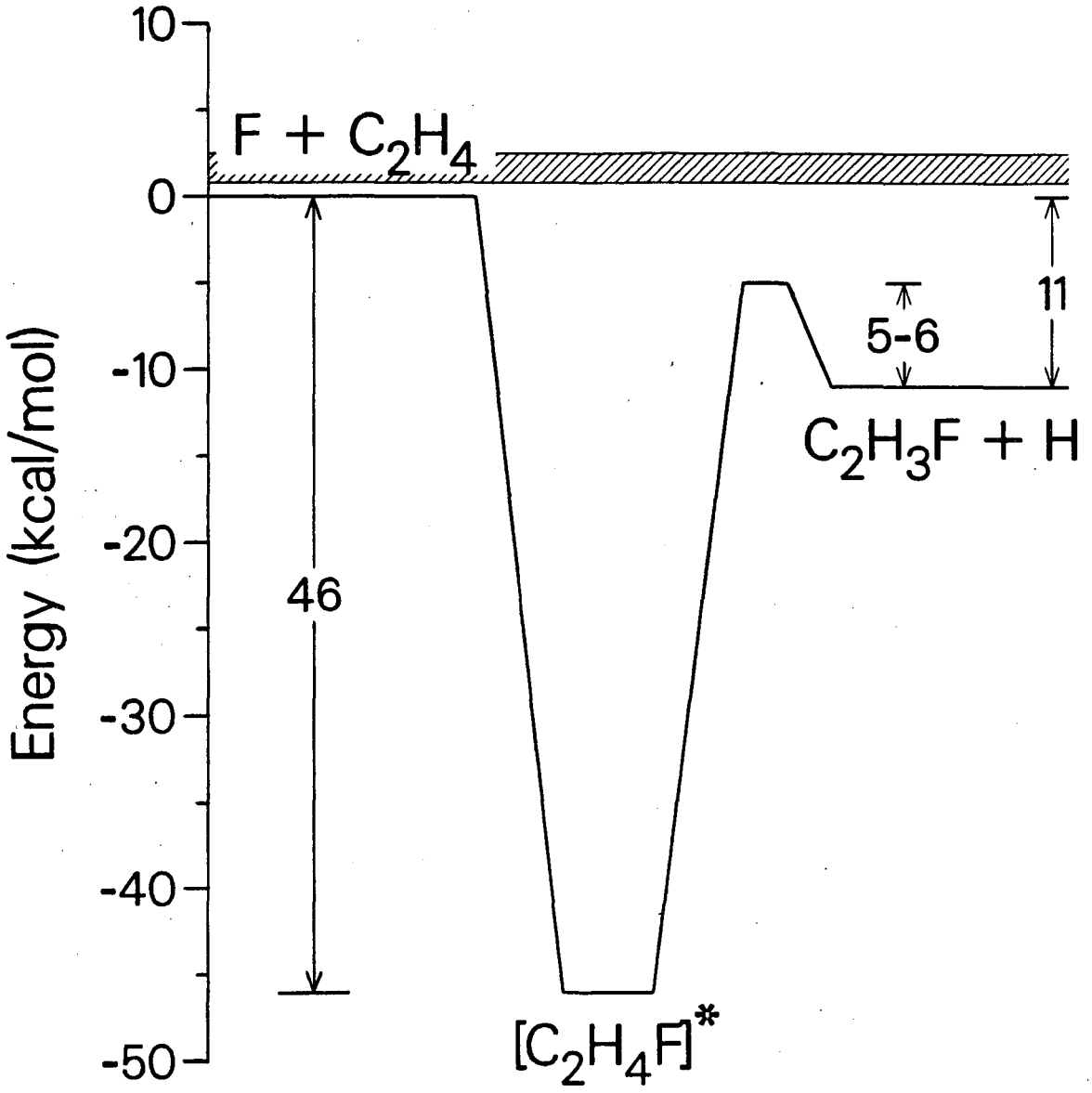

XBL 8712-5285

Figure 1

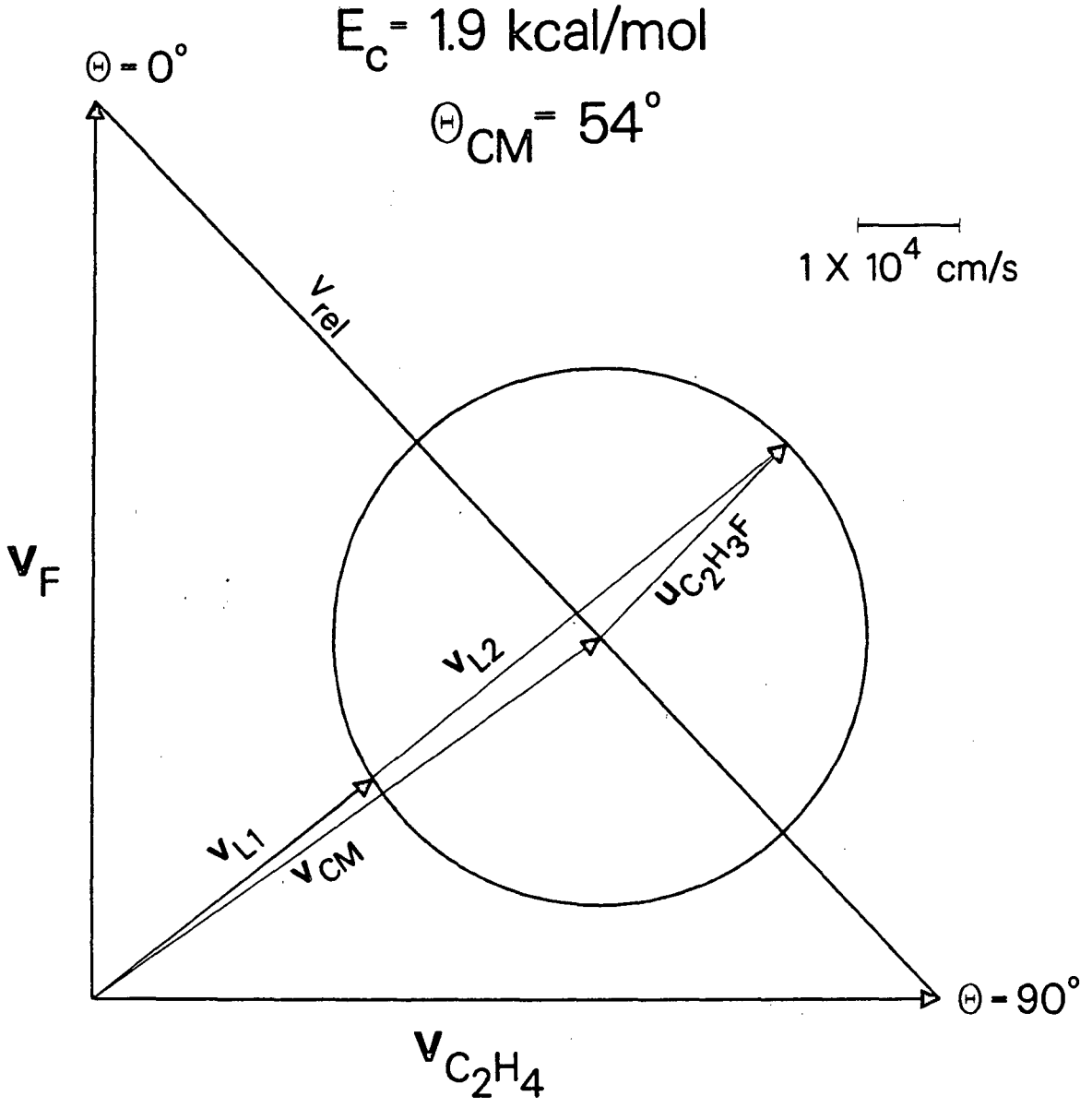

XBL 8712-5281

Figure 2

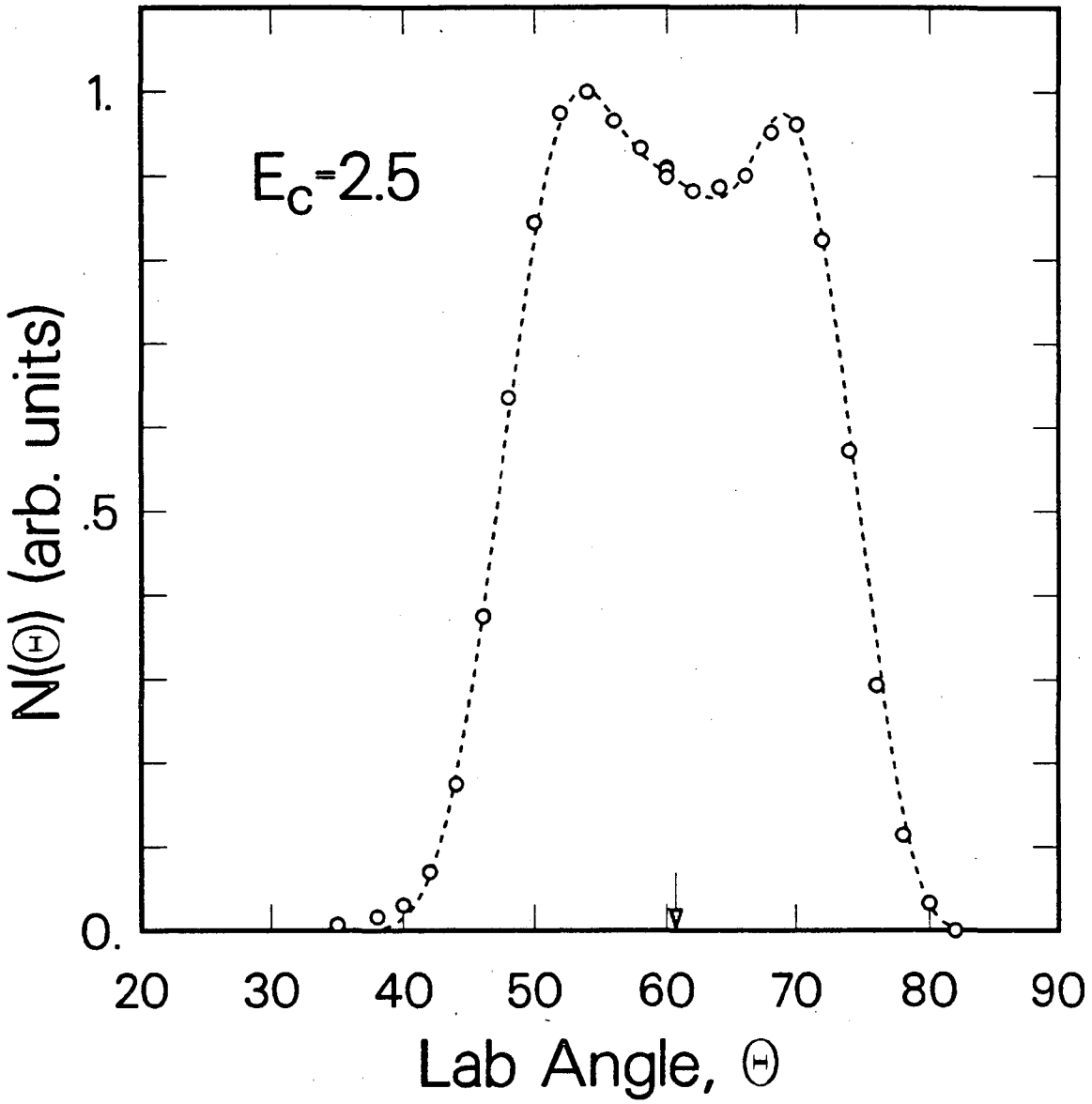

XBL 8712-5329

Figure 3

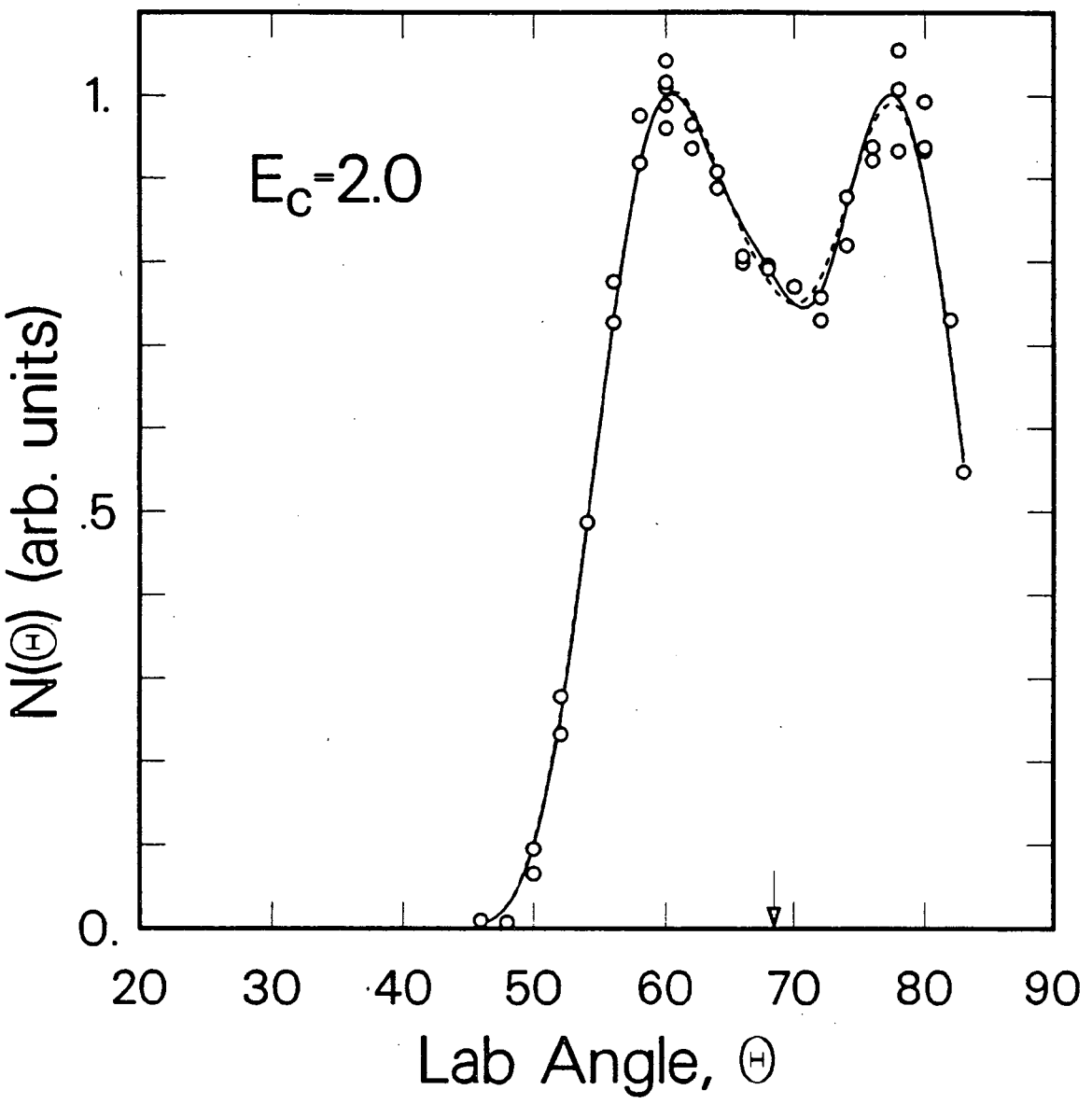

XBL 8712-5330

Figure 4

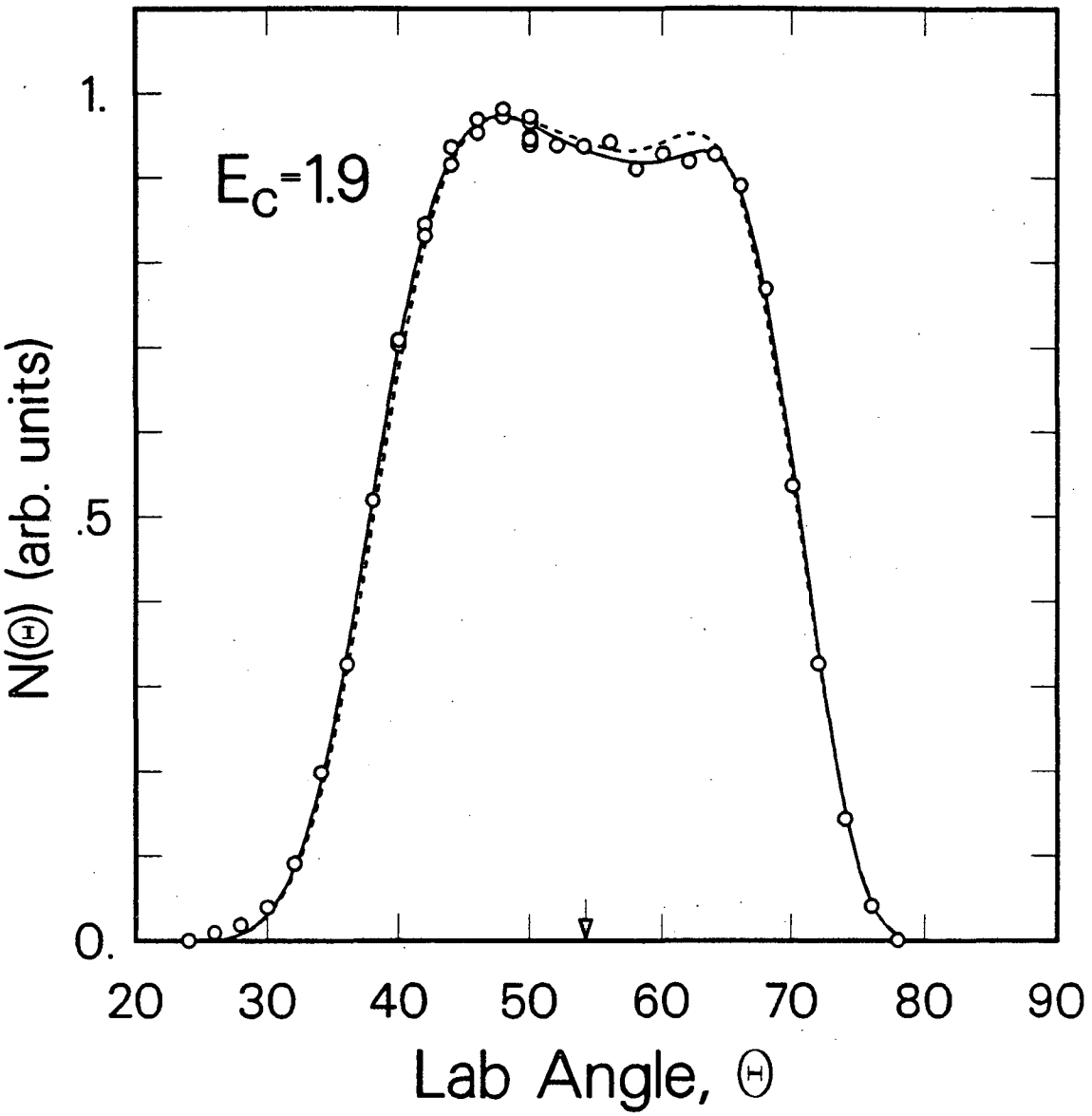

XBL 8712-5324

Figure 5

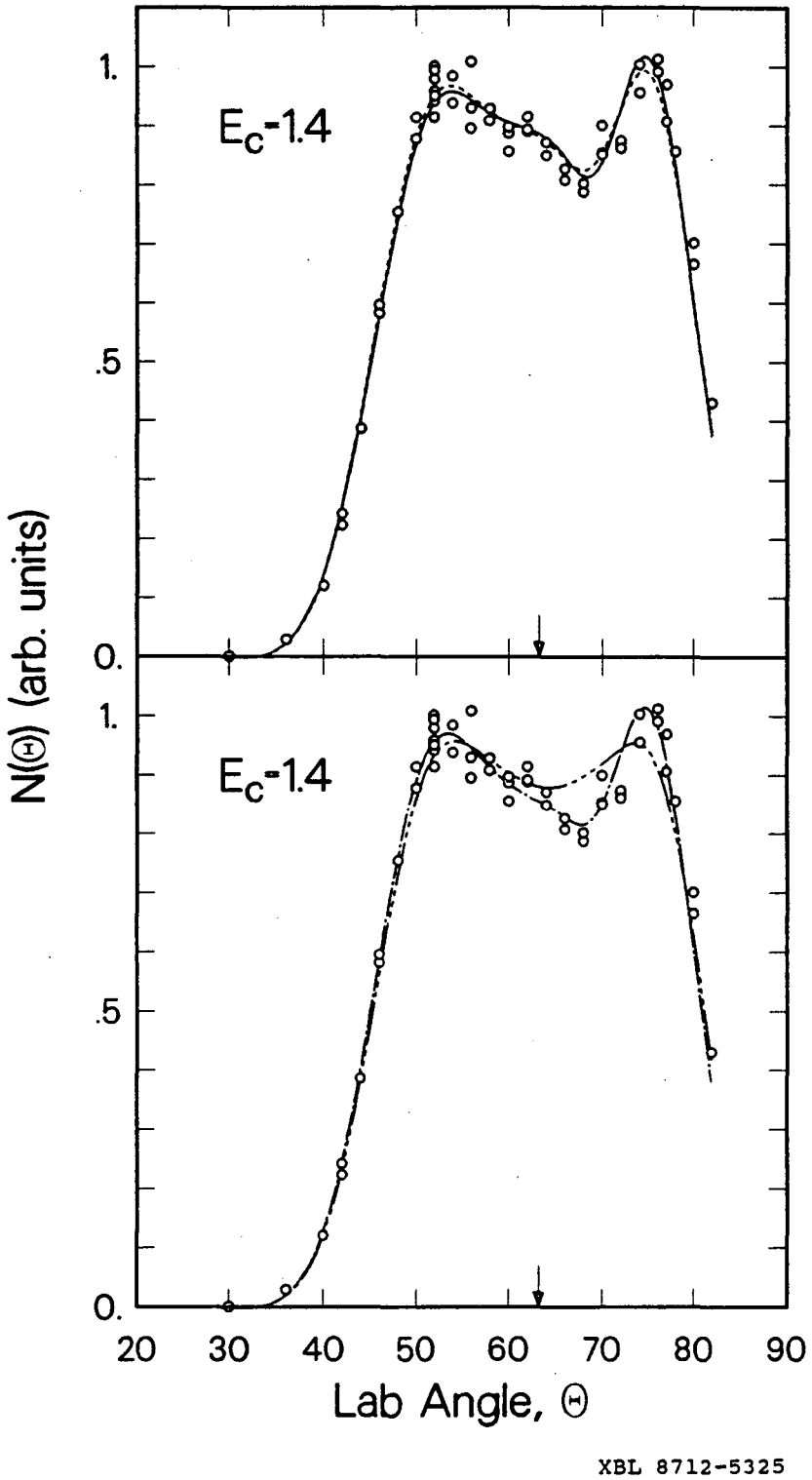
1.
.5
0.
E_c-1.4
1.
.5
0.
E_c-1.4
N(Θ) (arb. units)
20
30
40
50
60
70
80
90
Lab Angle, Θ
XBL 8712-5325

Figure 6

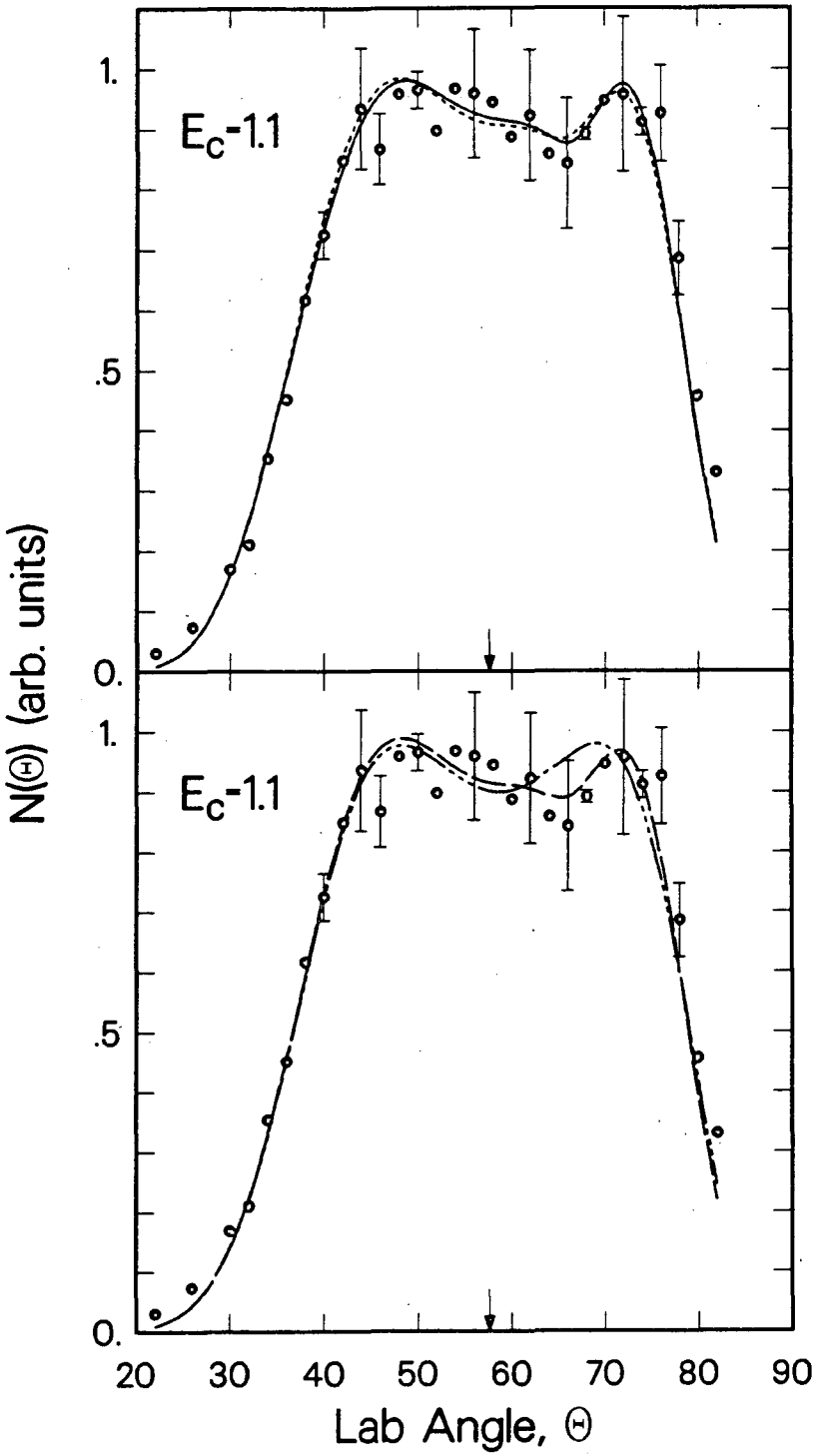

XBL 8712-5328

Figure 7

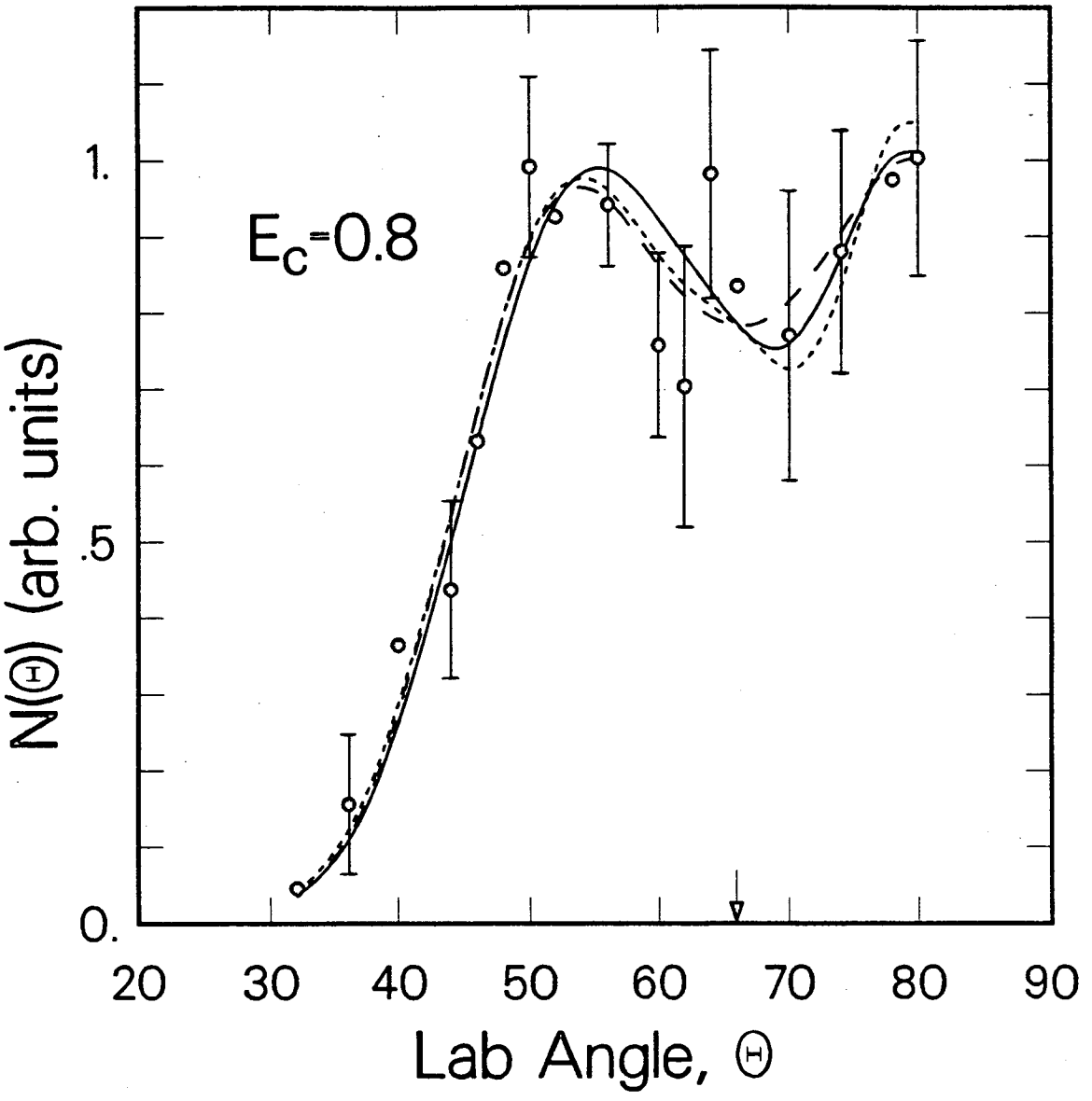

XBL 8712-5331

Figure 8

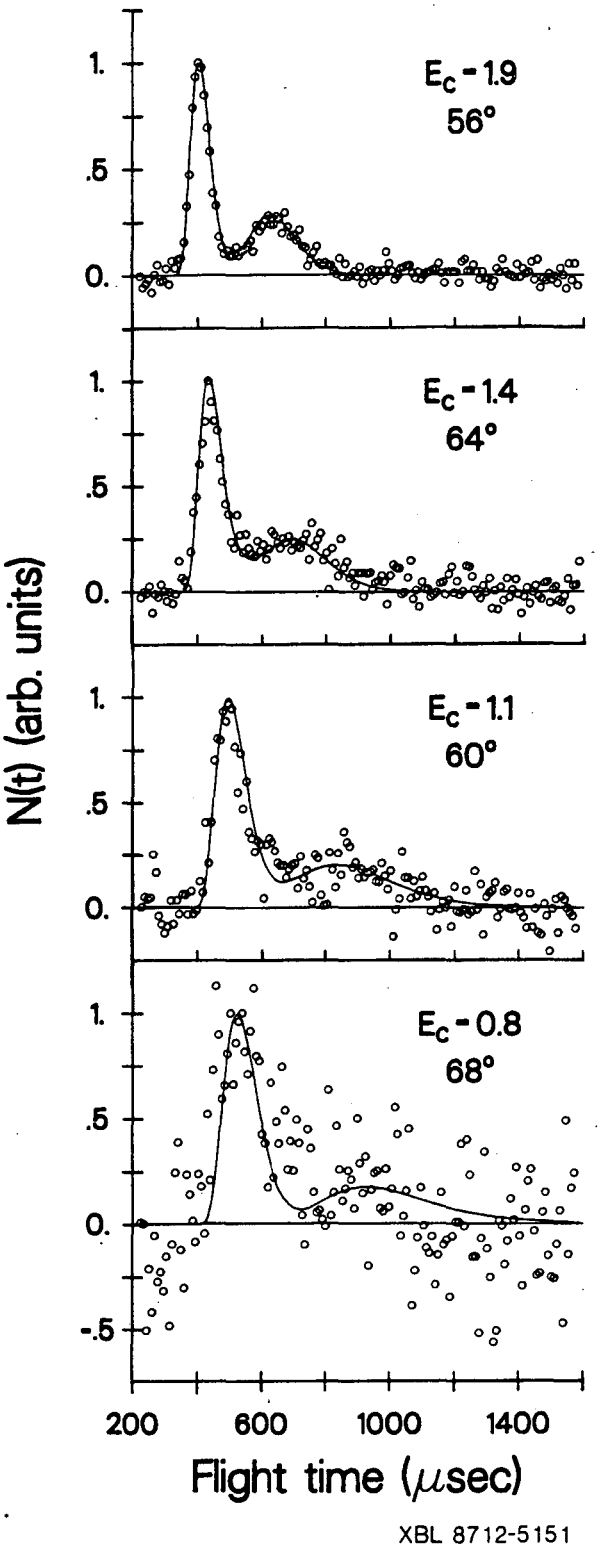
E_c - 1.9
56°
E_c - 1.4
64°
E_c - 1.1
60°
E_c - 0.8
68°
N(t) (arb. units)
1.
.5
0.
-.5
200
600
1000
1400
Flight time (μsec)
XBL 8712-5151

Figure 9

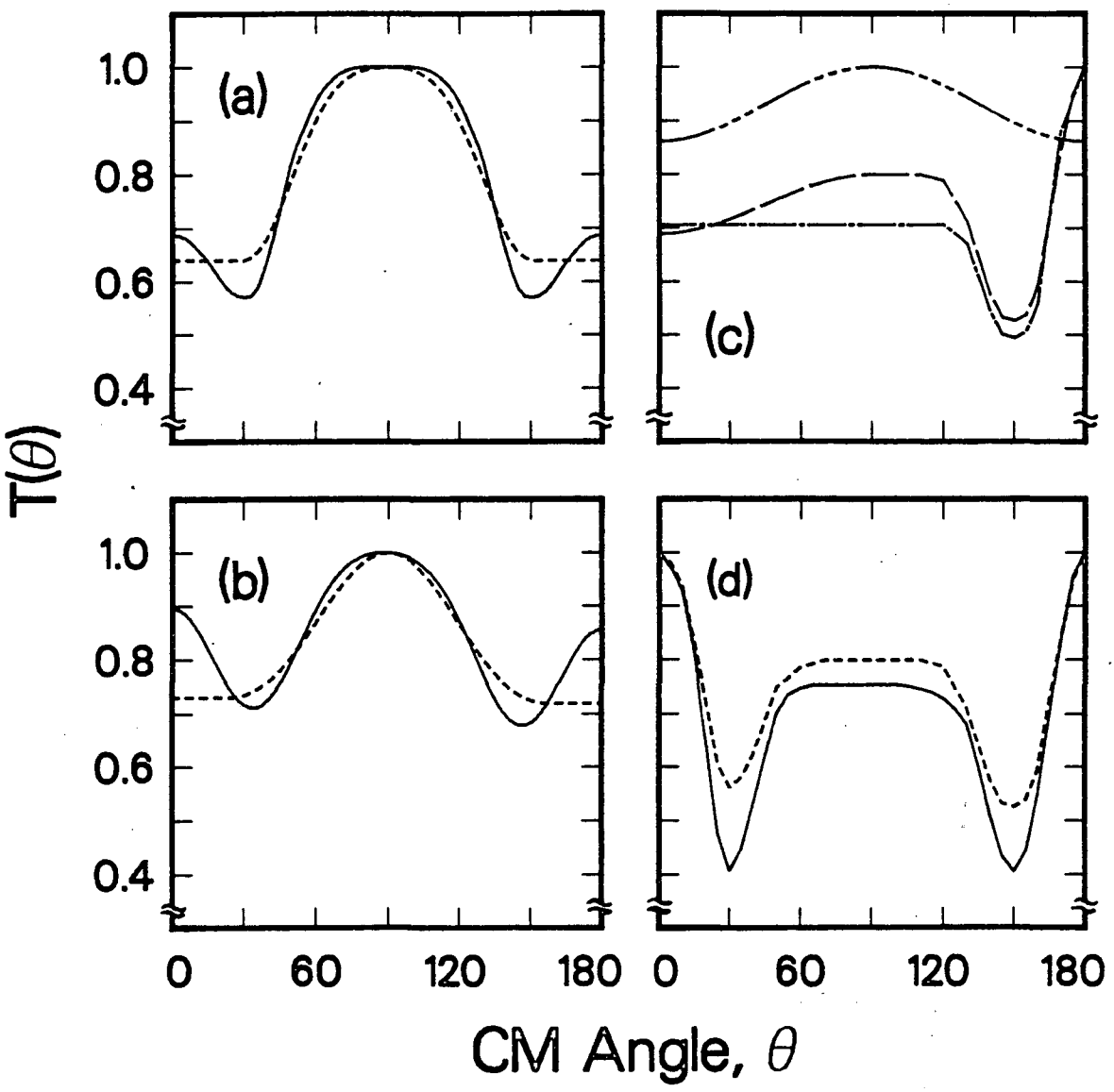

XBL 8712-5296

Figure 10

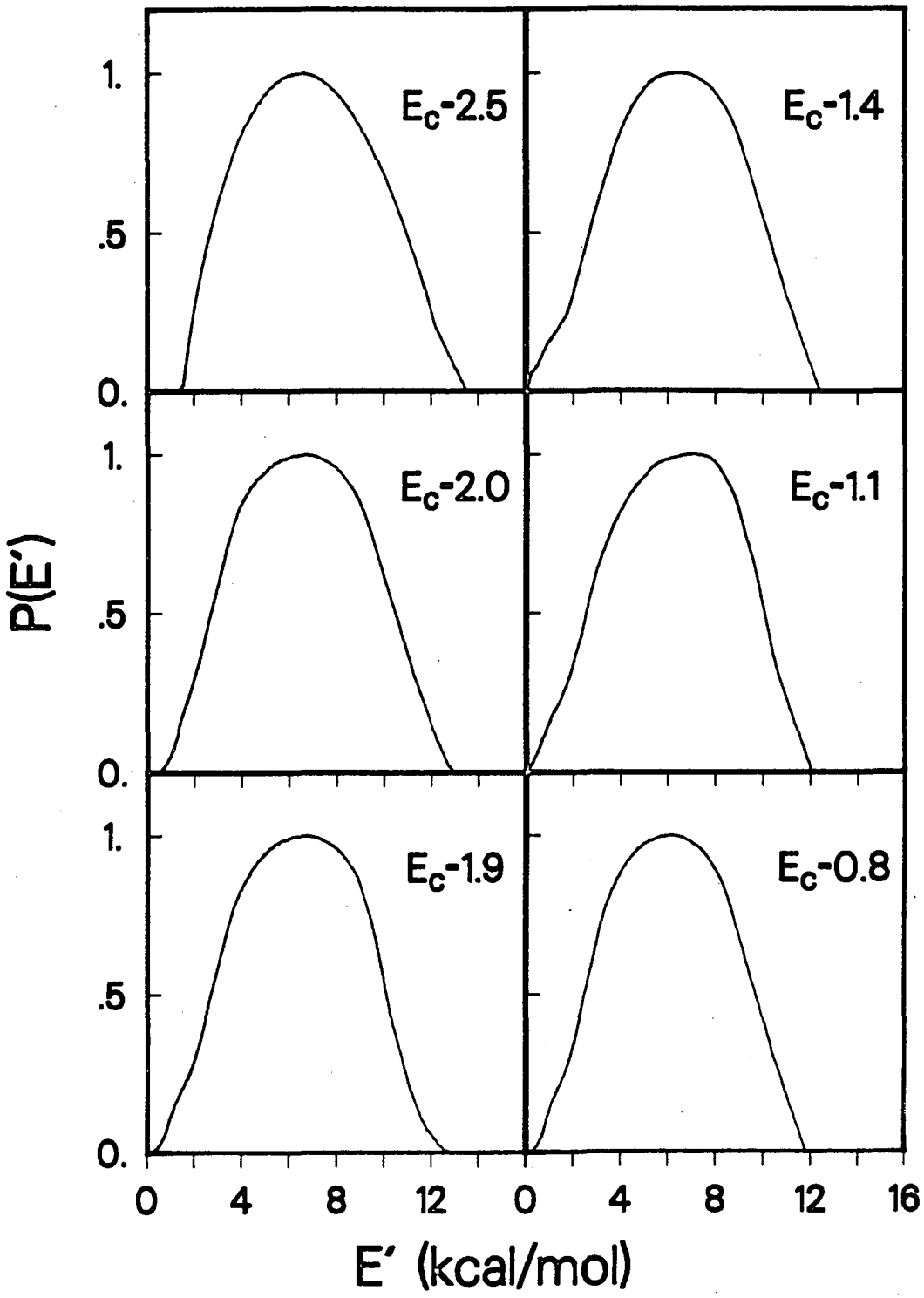

XBL 8712-5293

Figure 11

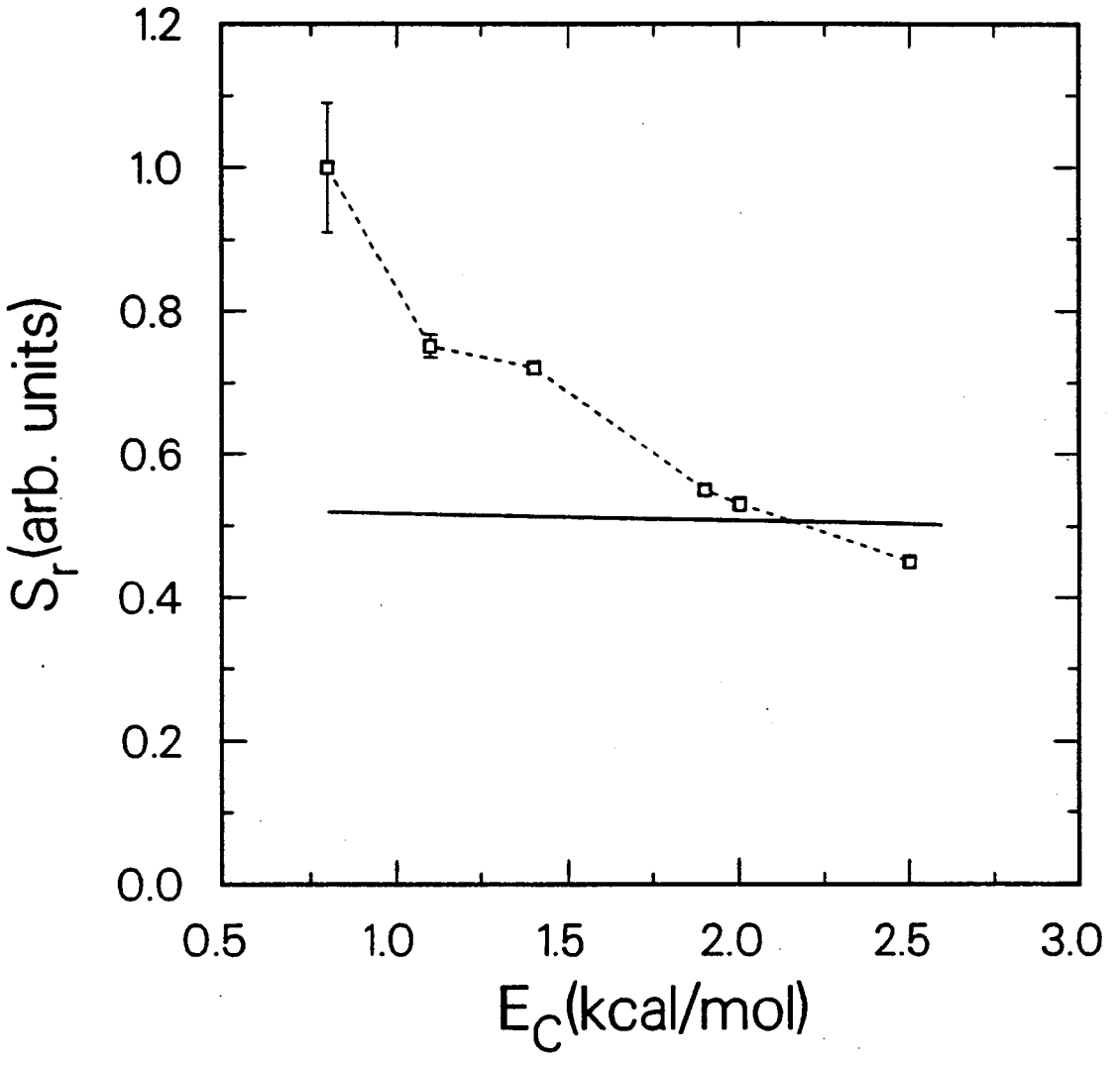

XBL 8712-5327

Figure 12

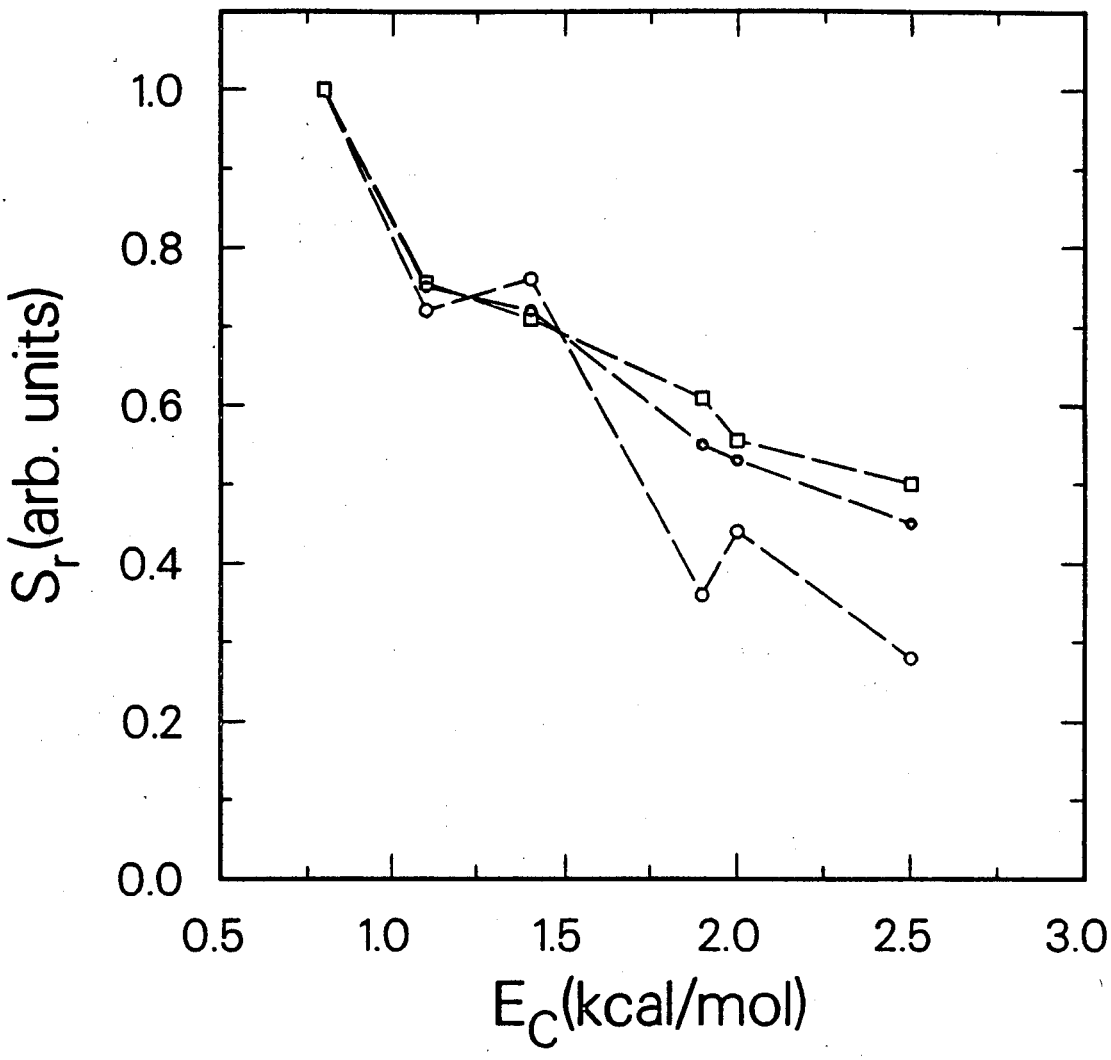

XBL 8712-5326

Figure 13

Chapter 2: Dynamics of Endoergic Substitution Reactions. I. Reactions of Br Atoms with Chlorinated Aromatic Compounds

I. INTRODUCTION

Although homolytic, or free-radical, aromatic substitution reactions have been the subject of many kinetic studies [1], their detailed dynamics in both the liquid and gas phases are only partially understood. In the gas phase, they proceed by addition of an atom or radical to an aromatic ring to form an activated cyclohexadienyl radical (collision complex) which subsequently decomposes through emission of another atom/radical. Previous crossed molecular beam studies of aromatic substitution reactions in this laboratory were directed towards determining (1) the extent of intramolecular vibrational energy redistribution in collision complexes of F atoms and substituted benzene molecules [2], (2) the primary products of the reactions of O atoms with benzene and toluene [3], and (3) the energetics of halogen

atom elimination from chemically activated halo-oxy-cyclohexadienyl radicals [4]. All of the reactions studied were exoergic.

We have focused our attention on endoergic aromatic substitution reactions since elimination of the more strongly bound substituent is not the statistically favored mode of decay of a chemically activated radical. In addition, the cross sections for endoergic reactions typically display a strong positive dependence on collision energy. Thus, by studying the translational energy dependence of the reaction cross section as well as the product angular and translational energy distributions for the endoergic channel, we may gain some insight into dynamical factors governing the formation and decomposition of chemically activated aromatic radicals. In this respect, the effect of ring substituents on both the probability of atomic addition and the degree of vibrational energy redistribution prior to bond fission are of particular interest. With bromine as the atomic reagent, site-selective substituent effects might manifest themselves since they are related to the energetics of adduct formation and should be most pronounced in those reactions in which the reagent atom bonds weakly to the aromatic ring.

We have carried out crossed molecular beam studies of the substitution reactions,

$$Br + \left\{ \begin{matrix} o- \\ m- \\ p- \end{matrix} \right\} CH_3C_6H_4Cl \rightarrow Cl + \left\{ \begin{matrix} o- \\ m- \\ p- \end{matrix} \right\} CH_3C_6H_4Br \qquad \begin{matrix} (1) \\ (2) \\ (3) \end{matrix}$$

in the collision energy, E_c, range 20 - 30 kcal/mol and,

$$Br + \left\{ \begin{array}{l} C_6H_5Cl \\ C_6F_5Cl \end{array} \right\} \rightarrow Cl + \left\{ \begin{array}{l} C_6H_5Br \\ C_6F_5Br \end{array} \right\} \quad (4) \quad (5)$$

in the range 20 - 35 kcal/mol (Fig. 1). The results of these experiments shed new light on the way in which substituents influence the orientation and dynamics of aromatic substitution reactions. We have previously reported results for reactions 1 - 3 [5]; as discussed in Section III, our analysis in this paper differs somewhat from that in ref. 5.

II. EXPERIMENTAL

The crossed beam apparatus used in these experiments has been described previously [6,7]. Two seeded, differentially pumped reagent beams were crossed at 90° in a vacuum chamber held at approximately 10^{-7} Torr. The products are detected with a triply differentially pumped mass spectrometric detector that rotates in the plane of the two beams.

The bromine atom beam was generated by passing a mixture of Br_2 in rare gas through a resistively heated high density graphite oven designed in this laboratory by Valentini et al. [8]. The Br_2/rare gas mixture is created by bubbling approximately 700 torr of He, Ne, or Ar through liquid bromine (reagent grade Fischer or Mallinkcrodt) at 0°C (vapor pressure, v.p.=60 torr). The oven had a nozzle diameter of 0.14 mm and was run at approximately 1400°C. A conical

graphite skimmer having an orifice diameter of 0.10 cm was positioned 0.76 cm from the nozzle. Ninety percent of the Br_2 dissociated into Br atoms, as determined from a direct measurement of Br/Br_2 in the beam.

The chlorinated aromatic (R-Cl) molecular beam was formed by bubbling He through the liquid reagent held at a constant temperature in a bath and expanding the resulting mixture through a 0.21 mm diameter nozzle. Conditions were as follows: 450 torr of He with o-, m-, or p-chlorotoluene (o-, m-, p-CT) at 60°C (v.p.≃22 torr); 450 torr He with pentafluorochlorobenzene (PFCB) at 19°C (v.p.≃11 torr [9]); 350 torr of He with chlorobenzene (CB) at 19°C (v.p.=9 torr [10]). A stainless steel skimmer with an orifice diameter of 0.66 mm was positioned 0.9 cm from the nozzle. The source and feed line were heated with coaxial heating wire to a temperature of 200°C for the CT experiments; the source temperature for the PFCB and CB experiments was 40°. o- and p-CT were purchased from MCB, m-CT from Aldrich, PFCB from Fairfield, and CB from Burdick and Johnson. All of the compounds were used without further purification, except for the p-CT which was distilled on a spinning band column.

A liquid nitrogen cooled copper cold finger was placed against the differential wall inside of the scattering chamber so that the detector would always face a cold surface during the angular scans thereby reducing the detector background at the product mass. Product angular distribu-

tions were measured by modulating the R-Cl beam with a 150 Hz tuning fork chopper and collecting data with the beam on and off using a dual channel scaler. Data were collected for 6 - 12 minutes per angle.

In order to compute relative cross sections for a given reaction at different collision energies, we scaled the product number density by the reactant flux, which is proportional to $n_{Br}n_{RCl}v_{rel}$, where n_i = number density of beam i and v_{rel} = relative velocity. Since the wide angle Br elastic scattering cross section does not change drastically as a function of energy, measuring Br on R-Cl elastic scattering allows us to measure changes in this quantity. During each scan, the m/e=79 signal was monitored at three different LAB angles. The angles were all beyond the cutoff angle for elastic scattering of Br on He so the Br^+ signal observed was from Br scattering on R-Cl. The contribution of undissociated Br_2 to the m/e=79 signal was very small and was neglected. Relative values for $n_{Br}n_{RCl}v_{rel}$ derived from the Br elastic number density at angle of 16° are given in Table 1.

The velocities of the reactant beams were measured using the time-of-flight (TOF) technique. A 256 channel scaler interfaced with an LSI-11 computer accumulated the data. No TOF measurement was made for the m-CT beam, but its velocity should be identical to that of o-CT since both have the same vapor pressure (22 torr; v.p.(p-CT)=21 torr [10]) at 60°C. The velocity of the CB beam was not measured under the exact

conditions of the scattering experiment but was inferred from measurements at a slightly different nozzle and bath temperature. The peak laboratory beam velocities (in units of 10^5 cm/s), v_{pk}, and speed-ratios, S, were: Br/He: v_{pk}=1.85-1.90, S=6.1; Br/Ne: v_{pk}=1.55, S=6.9; Br/Ar: v_{pk}=1.29, S=8.4; o-CT/He: v_{pk}=1.33, S=11.3; p-CT/He: v_{pk}=1.35, S=11.8; PFCB/He: v_{pk}=1.06, S=14.8; CB/He: $v_{pk}\simeq 1.4$, $S\simeq 15$. Product TOF spectra were measured using the cross-correlation method [7]. A Cu-Be alloy wheel photoetched with a pseudorandom sequence of 255 open and closed slots was spun at 392 Hz giving 10 μs/channel resolution in the TOF spectra. The flight path from wheel to ionizer was 30.0 cm. Counting times were approximately 1 hr per angle for the Br + CT experiments and 2 hr per angle for the Br + PFCB experiment.

III. RESULTS AND ANALYSIS

The product angular distributions and TOF spectra were fit using a forward convolution program [11] that starts with a separable form for the center-of-mass (CM) reference frame product flux distribution, $I_{CM}(\theta,E',E_c) = T(\theta)P(E',E_c)S_r(E_c)$, and generates a LAB frame angular distribution and TOF spectra averaged over the spread in relative velocity. $T(\theta)$, the CM frame angular distribution, is taken to be a sum of three Legendre polynomials whose coefficients are varied to opti-

mize the fit. $T(\theta)$ was adjusted for reactions 1 and 3, E_c=31 kcal/mol, to improve the fits to the data. A RRK functional form is used for P(E'), the CM frame product translational energy distribution: $P(E') = (E'-B)^p(E_{avl}-E')^q$, where B is related to any barrier in the exit channel and E_{avl} is the total energy available to the products ($E_c-\Delta H_0^\circ$). ΔH_0° was taken to be 15 kcal/mol for all of the reactions studied (see Section IV). The parameters p, q, and B were optimized to give the best fit to the data (see Tables 1 and 2).

$S_r(E_c)$ represents the collision energy dependence of the relative reaction cross section, i.e., the excitation function. For a given experiment, the spread in beam velocities and intersection angles gives rise to a spread in relative velocities and hence in collision energies. $\Delta E_c/E_c$(FWHM) ≈ 30% for the reactions with Br seeded in He and ≈25% for the reactions with Br seeded in Ne and Ar. Each beam velocity and intersection angle permutation corresponds to a different kinematic configuration (Newton diagram) over which the calculated angular distribution and TOF fits must be averaged. The collision energies corresponding to the most probable kinematic configurations are listed in Table 1. Since the cross section is found to depend on collision energy, each kinematic configuration was weighted according to E_c using a function $S_r(E_c)$. Our method of weighting the Newton diagrams differs from that used in ref. 5. Rather than using the calculated relative CM cross sections (which

represent a convolution over the spread in relative velocity) and interpolating linearly between these values, the Newton diagrams were weighted with a multiple-point excitation function which was modified to fit the relative ratios of the LAB angular distributions at the different nominal collision energies. The original form of $S_r(E_c)$ was derived from a statistical calculation of the product branching ratio as a function of energy (see Section IV). At each most-probable collision energy, the laboratory angular distribution calculated from the input $I(\theta,E',E_c)$, $N_{calc}(\theta)$, is scaled to the experimental angular distribution, $N_{exp}(\theta)$, using a least-squares fit, i.e.,

$$\frac{d}{dz} \sum_i [N_{exp}(\theta_i) - z\, N_{calc}(\theta_i)]^2 = 0.$$

The input $S_r(E_c)$ is then modified so that the least-squares scaling parameters, z, agree to within 1.5% indicating that the derived excitation function fits the experimental data. For reactions 1 and 3 the z parameters at the six most-probable collision energies (3 for each reaction) agree with each other.

Since, for an endoergic reaction, the maximum translational energy of the products will depend strongly on E_c, a P(E') with a unique value of E_{avl} was used for each Newton diagram in the analysis. Our present analysis procedure differs again from that used in ref. 5 in that each P(E') is normalized to its own area, as opposed to being normalized to the area of the most-probable P(E'). This has the effect of

enhancing the contribution of slow recoil velocity products to the calculated angular distributions and TOF spectra. The best-fit CM angular and energy distributions for the CT experiments are consequently somewhat different from those reported earlier, the main difference being that the $T(\theta)$ distributions here are more forward peaked.

A. Br + o-, m-, p-CT

The ortho- and para-bromotoluene (BT) substitution products were detected at m/e=170 (^{79}Br), however the quadrupole mass spectrometer resolution was set sufficiently low to allow some of the ^{81}Br product to be detected as well. The product angular distributions are shown in Figs. 2 and 3. Elastic and inelastic scattering of impurity in the p-CT beam contributed to background at m/e=170 near that beam. This was most problematic at E_c=21 kcal/mol where the product signal level was lowest. At this energy the in/elastic scattering background was measured by substituting a properly diluted beam of Kr in Ar for the Br in Ar beam. It was then scaled to the product angular distribution at 74° and subtracted from it. At the peak of the E_c=31 kcal/mol o-BT angular distribution, the product count rate was 20 Hz. The angular distributions reveal that, at all energies, the o- and p- products are mostly forward scattered with respect to the center-of-mass angle. Remarkably, no BT product was detected from Br + m-CT at a collision energy as high as 29

kcal/mol. TOF spectra of p-BT and of o-BT are presented in Figs. 4 - 6. At each collision energy, the peak product velocities are close to the center-of-mass velocity (v_{cm}, Fig. 9), indicating that little energy is channeled into product translation.

The best fits to the data were obtained with $T(\theta)$ distributions that peak at 0° and 180° with maxima at 0° (Fig. 7). There is a range of acceptable values for the P(E') parameters (as there is for the coefficients of the Legendre polynomials that constitute $T(\theta)$) yet the average fraction of energy that goes into product translation, $\langle E'/E_{avl} \rangle$ (Table 1), does not vary much within this range. Since the fits were relatively insensitive to the q parameter, which governs the curvature of the tail of the P(E'), this parameter was fixed for all the fits and the other parameters optimized. A value of 1.85 was chosen for q; it was possible, however, to fit the data by setting q=3.2 and varying p and B. The q=3.2 distributions fall more steeply, and consequently peak at higher energies, than the q=1.85 distributions. The q=1.85 distributions (Fig. 8) peak between 0.0 - 2.0 kcal/mol, with the o-BT distributions peaking at lower energies and having slightly lower values of $\langle E'/E_{avl} \rangle$ than those for p-BT. For both reactions, $\langle E'/E_{avl} \rangle \approx 0.3$ at all collision energies. The following changes in the best-fit P(E') for reaction 3, E_c=31 kcal/mol, while not significantly affecting the fit, produced the indicated changes in $\langle E' \rangle$: ±13% in p parameter

(equivalent to a change of ±9% in peak position), ±2% in <E'>; ±1 kcal/mol in ΔH_0°, ±6% in <E'>. A CM frame product flux contour diagram for Br + p-CT → Cl + p-BT, E_c=31 kcal/mol, is given in Fig. 9. The overall quality of the fits justifies our use of a separable form for the CM flux distribution.

Since we have data at only three nominal collision energies for reactions 1 and 3, it is difficult to determine the exact form of the excitation functions. Excitation functions which reproduced the relative intensities of the laboratory angular distributions for reactions 1 and 3 are plotted in Fig. 10. We obtained equally good fits from excitation functions with thresholds at 18 and 17 kcal/mol for reactions 1 and 3 respectively. However, these functions change slope abruptly near E_c=20 kcal/mol and are unlikely to be accurate representations of the true S_r. Because the collision energies for the Br/He, Br/Ne, and Br/Ar experiments overlap, the data constrain the curvature of S_r most strongly in the range $20 \leq E_c \leq 30$ kcal/mol. The curves extend to the maximum collision energy of the E_c=31 kcal/mol experiments (≈44 kcal/mol); the shaded regions represent the uncertainty in S_r above 32 kcal/mol. Curves going through these regions yield values of z at E_c=31 kcal/mol that are within 1.5% of $\bar{z}$ for reactions 1 and 3 (where $\bar{z}$ is determined from the fits based on the curves in Fig. 10). A ±13% change in the p parameter of the P(E') for reaction 3, E_c=31

kcal/mol, changes z by ±3%. These excitation functions will be discussed more in the next section.

The asymmetric CM angular distributions that we obtain indicate that the majority of 6-bromo-6-chloro-(3 or 5)-methylcyclohexadienyl (BCMC) complexes decompose in a time less than one rotational period [12b]. The p-BT CM angular distributions show more forward-backward symmetry at lower collision energies, suggesting that the lifetime of the p-BCMC [13] complex increases relative to its rotational period as E_c decreases. We can estimate the rotational period of the p-BCMC complex by assuming, for the sake of simplicity, that the Br atom collides perpendicular to the ring with an impact parameter of 0.9 Å (the distance from the center of mass of p-CT to the chlorinated carbon) and that the rotational angular momentum of the reagent is negligible. For the collision of Br with p-CT, E_c=31 kcal/mol, the orbital angular momentum, **L**, will be ≈160 $\hbar$. The moment of inertia about the rotation axis of the complex is ≈880 amu·Å^2, assuming that the halogenated carbon is tetrahedral, that the C-Br and C-Cl bond lengths are 2.0 and 1.7 Å respectively, and that the ring is undistorted. The rotational period, given by $\tau_{rot} = 2\pi I/L$, will therefore be ≈5 ps in the present example. At a collision energy of 21 kcal/mol, τ_{rot}≈7 ps.

The approximate product orbital angular momentum, **L'**, for reaction 3 at E_c=31 kcal/mol, using a relative velocity

corresponding to <E'> = 5 kcal/mol and an impact parameter of 0.1 Å (the distance between the chlorinated carbon and the center of mass of the complex, with the C-Cl bond perpendicular to the ring and the C-Br bond in the plane of the ring), is ≈6 $\hbar$, far lower than the initial 160 $\hbar$. It would take an average exit impact parameter of ≈2.7 Å for the total angular momentum of the complex to be carried away as product orbital angular momentum. However, even if most of the angular momentum of the collision were carried away in rotation of the BT product, the rotational energy of the product would be small (only ≈1.5 kcal/mol for p-BT in the present example) because of its large moment of inertia ($I \approx 770$ amu·Å^2).

The lack of a strong correlation between **L** and **L'** is the reason for the CM angular distributions not peaking more strongly in the forward and backward directions [12a]. The larger amount of sideways scattering for o-BT at 31.0 kcal/mol could indicate an even weaker **L** to **L'** correlation in reaction 1 at high collision energies. This may be due to the more complicated rotational motion of the o-BCMC complex that results from both the asymmetry of the complex and, perhaps, a decreased steric barrier for Br addition to o-CT at higher collision energies.

A fraction of the translational energy of BT will come from rotation of the complex at its exit transition state (TS). In the absence of extensive vibration-rotation coupling in the complex, the rotational energy at this TS will

be ≈1.2 kcal/mol for p-BCMC (E_c=31 kcal/mol, C-Cl bond perpendicular to the ring with a bond length of 2.6 Å [14]). The rotational motion of o-BCMC will, as noted above, be more complex. But the fact that the o-BT P(E') distributions peak at slightly lower energies than those for p-BT could indicate that the ortho complex has a lower rotational energy at its exit TS than the para complex.

B. Br + CB, PFCB

As for the CT reactions, the substitution product from Br + PFCB, pentafluorobromobenzene (PFBB), m/e=246, is mostly forward scattered with respect to the incident Br beam (Fig. 11). Elastic and inelastic scattering of impurities in the PFCB beam contributed significantly to the m/e=246 signal near that beam at all three collision energies studied. As noted above, this background was measured by substituting a beam of Kr for the Br beam. The in/elastic angular distributions were then scaled and subtracted from the reactive angular distributions. Uncertainties associated with this scaling and subtraction lead to the error bars in the angular distributions. At E_c=20 kcal/mol, no reactive signal could be discerned above the in/elastic background.

PFBB product TOF spectra are presented in Fig. 12. At E_c=35 kcal/mol, TOF spectra were measured at 52° and 62°. The signal-to-noise level at 62° was poor, making it difficult to distinguish the reactive and non-reactive components

of the TOF spectrum. Th narrowness of the angular distributions along with the relatively low m/e=246 signal level (≈4 Hz at 52° at E_c=35 kcal/mol) made it unprofitable to measure product TOF at several angles.

No bromobenzene (m/e=156) substitution signal was observed from Br + CB at a collision energy of 30 kcal/mol. At a mass spectrometer resolution equal to that at which the PFCB experiments were conducted, there was a contribution from in/elastically scattered $^{79}Br_2$ to the m/e=156 signal (≈9 Hz at θ=50°). At a higher resolution, no mass leakage occurred but at neither setting was any reactive signal observed. Our ability to observe PFBB product over BB is enhanced, however, by the larger mass of the former product which, assuming similar energy partitioning in reactions 4 and 5, causes its recoil velocity to be smaller. Since the transmission of the mass spectrometer changes with mass setting and the cracking patterns of the BB and PFBB products in the ionizer are not known, a quantitative comparison of the signal levels for the Br + CB and Br + PFCB reactions will not be attempted.

The uncertainties in the angular distribution data, especially at E_c=25 kcal/mol, make it difficult to determine accurately the forms of the CM product distributions. An asymmetric, forward peaked $T(\theta)$ distribution is found to fit the E_c=35 kcal/mol data (Fig. 13). At E_c=25 kcal/mol, there is evidence of more backward scattered product. Again, this

indicates that the lifetime of the adduct increases more than its rotational period as the collision energy is lowered. The P(E') distributions (Fig. 14) are very narrow (q=3.2), peaking slightly away from 0 kcal/mol. The data at both collision energies could also be fit with P(E') distributions which sloped more gradually (q=1.8) although the fits were not as good. $\langle E'/E_{avl} \rangle \simeq 0.19$ for both of the q=3.2 distributions (Table 2) and 0.23 for the q=1.8, E_c=35 kcal/mol, distribution.

In the absence of a product angular distribution at E_c= 20 kcal/mol, it was possible to reproduce the ratio of the E_c= 25 and 35 kcal/mol angular distribution intensities with two different excitation functions, one of which has a threshold of 20 kcal/mol (Fig. 15). The average ratio of the relative cross sections at the two nominal collision energies, $\bar{S}_r(35)/\bar{S}_r(25)$, is 3.4 for the two excitation functions. The fits to the data that are presented were generated with the higher threshold curve. As for the CT reactions, the shaded region indicates the uncertainty in S_r above the highest nominal collision energy.

IV. DISCUSSION

A. Br + o-, m-, p-CT

The endoergicities of the isomeric CT reactions under study should not differ markedly from one another. The heats

of formation of o-, m-, and p-CT ($\Delta H^\circ_{f298}(g)$) are 3.8, 4.1, and 5.3 kcal/mol respectively [10,15]. We were able to find heat of formation data for the para isomer of bromotoluene (BT) only ($\Delta H^\circ_{f298}(g)$ = 13.0 kcal/mol [10,16]), but Szwarc's work [17] indicates that the C-Br bond dissociation energies in o-, m-, and p-BT differ by only 0.6 kcal/mol. Using the known values for ΔH°_{f298} of Br, Cl [18], p-CT, and p-BT, we calculate ΔH°_{298} = 10.1 kcal/mol for the reaction, Br + p-CT → p-BT + Cl. This number strikes one as being too low considering that ΔH°_{298} = 15 kcal/mol for the reaction, Br + $C_6H_5Cl \rightarrow C_6H_5Br$ + Cl [19]. In the absence of firm values for the heats of formation of the CT and BT isomers, we have used an endoergicity of 15 kcal/mol for the present reactions.

The energetics of Br addition to CT are, as far as we can tell, unknown. Ref. 20 gives ΔH°_{298} = -8.8 kcal/mol for Br + C2H4 → C2H4Br. The exothermicity of Br addition to benzene (ΔH_{add}) will reflect the loss in resonance stabilization energy (RSE) that results from the disruption of the π electron framework of the ring. In the case of H atom addition to benzene the loss in RSE will be approximately 11 kcal/mol [21]. We conclude, therefore, that the BCMC radical will be unbound by ≈2 kcal/mol relative to reactants! Rodgers et al. [22] arrive at a similar value for the endothermicity of Br addition to benzotrifluoride. As a result, we do not expect there to be a potential minimum along the reaction coordinate corresponding to the BCMC complex.

Based on the energetics for Br addition to CT, it is not surprising that substitution occurs in less than one rotational period. We have calculated RRKM lifetimes, τ_{RRKM}, for the BCMC complex [23], using modified normal mode frequencies for toluene, and frequencies corresponding to C-Cl and C-Br stretching and Br-C-Cl, C-C-Br, and C-C-Cl bending modes [24]. Including all 42 frequencies, τ_{RRKM} at E_c=30 kcal/mol ($E^* = E_c + \Delta H_{add}$ = 28 kcal/mol) is 0.02 ps, much lower than the estimated rotational period. This unrealistic value for the lifetime results from the very large rate constant for decay of the complex through loss of Br. τ_{RRKM} changes little as the collision energy is lowered, indicating that a quantitative comparison of the angular distribution data with the lifetime and rotational period calculations is not possible.

Remarkably, very little of the energy available to the products ends up in translation. Apparently the vibrational modes of the aromatic ring act as a strong energy sink with Cl elimination occurring only when sufficient energy has accumulated in the C-Cl bond. The time scale of intramolecular vibrational energy relaxation (IVR) in highly excited aromatic molecules is a subject of continuing investigation. Reddy, Heller, and Berry [25] have studied the C-H overtone absorption spectra of benzene and several substituted benzene compounds. They conclude from linewidth measurements that the lifetime of the 5ν ortho aryl C-H overtone state in

toluene is 70 fs and that the lifetimes of the 3ν (8786 cm^{-1}) and 5ν (14072 cm^{-1}) C-H overtone states of benzene are 230 fs and >51 fs respectively. However, recent experiments on benzene by Page et al. [26] indicate that the lifetime of the 3ν state is greater than 0.5 ps. From $S_1 \rightarrow S_0$ fluorescence spectra, Parmenter and Stone [27] extract IVR lifetimes of less than 10 ps for the 3^2 S_1 level (2382 cm^{-1}) of p-fluorotoluene (p-FT) and 25-33 ps for the 5^3 state (2455 cm^{-1}) of p-difluorobenzene. Coupling of the internal rotation of the methyl group to the ring vibrations is believed to be responsible for the accelerated relaxation in p-FT [28]. If that is indeed the case, IVR may occur even more rapidly on the S_0 surface of p-FT since the barrier to methyl torsion is lower in the ground state [28,29].

Chemical activation is an inherently less precise way of preparing vibrationally excited molecules than either overtone or electronic excitation. A number of vibrational modes are excited by the impact of the atom and the release of chemical energy upon bond formation. Although studies of Br addition to unsaturated molecules indicate that 1,2-Br migration is possible [30], the short BCMC lifetimes that we infer from our angular distributions, the relatively small number of modes involved in energy redistribution (see below), and our ability to correlate features of the o-, m-, and p-BT excitation functions with the position of the methyl group relative to the chlorinated carbon atom (see below)

suggest that most of the reactive collisions in the present systems involve Br attacking the chlorinated carbon. Therefore, most of the energy of the collision will be deposited directly into the reactive site and C-Cl bond rupture might compete with rapid vibrational energy redistribution.

Although roughly 70% of the total available energy finds its way into BT product vibration, it does not seem that Cl elimination from BCMC is a statistical process involving energy sharing among a large number of vibrational degrees of freedom. We have calculated RRKM-AM P(E') distributions [31] for BT, E_c=31 kcal/mol, assuming different numbers of "effective" vibrational modes. The maximum centrifugal barrier, B_m', is treated as a parameter. Since the activation energies for Cl addition reactions are known to be very near zero [32], we have no reason to expect that there will be a barrier above the threshold for Cl elimination. Although a definitive comparison between the experimental and RRKM-AM P(E') distributions is not possible given the uncertainties in the fits, we obtain reasonable agreement between the experimental o-BT P(E'), E_c=31 kcal/mol, and a RRKM-AM P(E') calculated assuming that 4 modes with frequencies in the range 700 - 800 cm^{-1} are active in energy redistribution and with B_m' = 0.40 kcal/mol (Fig. 8). Note that the q parameter determines the curvature of the experimental P(E') which in turn reflects the number of active modes in the complex. Thus, the data seem to indicate that only a limited number of

degrees of freedom participate in energy sharing prior to Cl elimination.

Such a mechanism is not unexpected. Endoergic substitution at elevated collision energies must occur in a quasi-direct fashion or not occur at all since, as more vibrational modes participate in energy redistribution, the probability of Cl elimination, η_{Cl}, drops relative to η_{Br}. This is due to the fact that η_X is proportional to the density of states at the TS for X elimination. The smaller the number of active vibrational modes, the smaller the difference between the state densities for the exoergic and endoergic channels and the more Cl elimination will compete with Br elimination. For example, taking η_X to be the microcanonical RRKM rate constant for X elimination (classically, $\eta_X \propto (\varepsilon^\dagger/E^*)^{s-1}$, where $\varepsilon^\dagger$ is the excess energy, E^*-E_0, at the X elimination TS and s is the number of active vibrational modes [33]), at E_c=30 kcal/mol, η_{Br}/η_{Cl} = 270 with 12 active modes (ν = 800 - 300 cm^{-1}) whereas with 4 active modes, η_{Br}/η_{Cl} = 6.

We attempted to determine the relative importance of the Br elimination channel in reaction 3, E_c=21 kcal/mol, and reaction 1, E_c=31 kcal/mol, by measuring the TOF of CT from the channel BCMC → Br + CT near the center-of-mass angle. In both cases, the TOF of nonreactively scattered CT obtained by substituting Kr for Br was very similar to that obtained with Br. This indicates that the Br addition cross section is substantially smaller that the elastic/inelastic scattering

cross section. Yet, if η_{Br} were indeed two orders of magnitude larger than η_{Cl} (as one would predict from a 12-mode RRKM calculation), we would have been able to see a substantial peak in the o-CT TOF spectrum corresponding to slow o-CT travelling at the velocity of the center of mass since the fast and slow components of the elastic scattering TOF spectrum were well resolved at E_c=31 kcal/mol. Thus, our inability to observe slow o-CT provides additional (though indirect) evidence that only a few modes are active during the reaction.

Further support for a reduced mode mechanism comes from an examination of the excitation functions. The measured relative cross sections can be expressed as the product of the cross section for forming the BCMC adduct and the relative probability of decomposition of the adduct through Cl elimination, $S_r = \sigma_{add}[\eta_{Cl}/(\eta_{Cl}+\eta_{Br})]$. If intramolecular energy randomization were complete prior to atomic elimination, the quantity in brackets would be equivalent to the RRKM branching ratio, S_{RRKM}. For an endoergic reaction, this quantity will be a strongly increasing function of energy. Based on our previous findings [5], we initially used 3- and 6-mode S_{RRKM} functions to represent $S_{r,p\text{-}BT}$ and $S_{r,o\text{-}BT}$ respectively. These curves needed to be modified very little to fit the data. The 3-mode (ν = 800 - 700 cm^{-1}) and 6-mode (ν = 900 - 700 cm^{-1}) RRKM curves are plotted in point-form in Fig. 10 alongside the experimental excitation functions.

It is certainly plausible that the o-BCMC collision complex has a larger number of active vibrational modes than p-BCMC. (We have already noted that the o-BT P(E') distributions have slightly lower values of $\langle E'/E_{avl} \rangle$ than those for p-BT.) The reduced symmetry of the o-BCMC complex may allow for enhanced vibrational energy redistribution through state mixing. As noted above, coupling of methyl group torsion to the ring vibrations is believed to be responsible for accelerated IVR in S_1 p-fluorotoluene. Although the barrier to methyl torsion is likely to be higher in o-CT than in p-CT [29], the methyl group is closer to the collision site in the ortho isomer.

The normalization factor used to scale S_{RRKM}(6-mode) to $S_{r,o\text{-}BT}$ at E_c=44 kcal/mol is ≈5 times that used to scale S_{RRKM}(3-mode) to $S_{r,p\text{-}BT}$ at the same energy. If the probability of C-Br bond formation is independent of collision energy, this suggests that σ_{add}(o-CT) is approximately 5 times larger than σ_{add}(p-CT). A larger addition cross section for o-CT can be rationalized along the above lines. The greater number of active modes in o-BCMC might serve to dissipate the energy of the collision better, allowing Br to add more readily to o-CT than to p-CT.

Two points should be made regarding the way in which we interpret our results. Firstly, in saying that a product P(E') or excitation function is reproduced well by a limited-mode RRKM calculation, we do not maintain that a small number

of modes are in microcanonical equilibrium prior to bond rupture. In fact, IVR competes with bond rupture in the present reactions and RRKM theory cannot, in principle, be applied. The number of active modes is thus a relative measure of the extent of intramolecular energy transfer prior to Cl elimination. Secondly, it seems rather tenuous to divide the substitution reaction into addition and decomposition steps when C-Br bond formation is endoergic and so few vibrational degrees of freedom participate in the reaction. However, both the moderate amount of backward scattering and the change in the effective number of modes as the substituents near the collision site are changed (see also Section IV.b) indicate that these reactions proceed through a (short-lived) collision complex and that we may divide them into two steps for conceptual purposes.

In arriving at a value for the number of active vibrational modes in o-BCMC and p-BCMC, we assumed that the cross section for Br addition to o-CT and p-CT does not vary with E_c. However, the probability of C-Br bond formation might indeed depend on collision energy. In particular, steric blocking of the chlorinated carbon by the methyl group in o-CT might cause σ_{add}(o-CT) to change more drastically with energy than σ_{add}(p-CT). Thus, assuming that the number of active modes in o-BCMC and p-BCMC is the same, the lower substitution cross section for reaction 1 below 25 kcal/mol could result from a narrowing of the acceptance angle of the

Br + o-CT potential energy surface (PES) relative to that of the Br + p-CT PES. The number of approach geometries that can lead to reaction should grow with increasing energy. As noted in the previous section, the CM angular distributions for reaction 1 do suggest that the approach angle widens at higher E_c. With a greater number of low frequency modes in the vicinity of the collision, o-CT could therefore have a larger addition cross section than p-CT at collision energies above 25 kcal/mol. In addition, the increased amount of energy remaining in the C-Br coordinate of p-BCMC (relative to o-BCMC) might cause σ_{add}(p-CT) to <u>decrease</u> above 25 kcal/mol and thereby cause $S_{r,p\text{-}BT}$ to level off.

Hase <u>et al.</u> [34] have carried out a classical trajectory study of the H + C_2H_4 addition reaction on two semi-empirical potential energy surfaces (I and III of ref. 34) having the same classical barrier height but differently shaped entrance channels. The potential energy surface with the narrower range of approach angles (surface III) has a longer range H + C_2H_4 interaction potential which manifests itself in a more gradual attenuation of the H-C-C bending force constant with C-H distance. They found that the cross section for H atom addition on both surfaces rises with collision energy in the range 2 - 20 kcal/mol, begins to level off at 30 kcal/mol and declines above 60 kcal/mol. The decrease in cross section above E_c=60 kcal/mol results from an increase in the number of non-reactive collisions in which the incipient C-H bond

either never reaches its equilibrium length or, having reached this length, breaks in less than one vibrational period. In the collision energy range 4 - 20 kcal/mol, the cross sections on surface III are smaller than those on surface I, as one would expect. The reverse is true, however, at energies above 20 kcal/mol. This rise in cross section is attributed to the longer range H-C_2H_4 interaction on surface III which becomes dominant at higher energies when the H atom can add over a wider range of angles.

It should be noted that a longer range atom-molecule interaction potential is not a necessary consequence of restricting the range of approach angle on the PES. In addition, since C_2H_5 is bound by ≈40 kcal/mol with respect to reactants, H + C_2H_4 is not an ideal model for the Br + CT → [BCMC] reactions. However, Hase's study does show that at elevated collision energies the surface with the narrower range of approach angles can give a larger addition cross section. Thus, it is evident that the addition excitation functions for o-CT and p-CT may influence the forms of $S_{r,o\text{-}BT}$ and $S_{r,p\text{-}BT}$ and that the steeper slope of $S_{r,o\text{-}BT}$ need not necessarily be due to a larger number of active modes in o-BCMC than in p-BCMC.

Could differences between the thermodynamic stabilities of the o-BCMC and p-BCMC radicals also be influencing the substitution cross sections? One way to assess the stabilities of these radicals is to consider the hypothetical

"residual" species that result from removing the halogenated carbon from o-BCMC and p-BCMC [35]. In this manner, o-BCMC is represented by a linear conjugated methyl pentadienyl radical whereas p-BCMC is represented by a branched conjugated radical. One might expect that the greater degree of π-electron delocalization allowed in the linear conjugated radical makes it more thermodynamically stable and there is evidence from the kinetics of nucleophilic aromatic substitution reactions that this is the case [36]. Although there are no values for the heats of formation of the methyl pentadienyl radicals, we can compare the heats of formation of the methyl allyl (MA) and 2-methyl allyl radicals (2-MA):

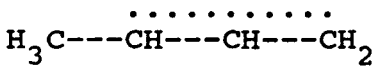

(MA)

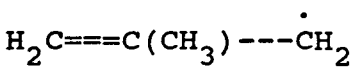

(2-MA)

Experiments on the iodine catalyzed isomerization of butene by Benson and co-workers [37] lead to ΔH°_{f298}(MA) = 30.4 ± 1.4 kcal/mol. Trenwith [38] obtains 29.4 ± 1.5 kcal/mol for the same quantity from pyrolysis of 3-methyl-1-butene. Trenwith and Wrigley [39] and Tsang [40] arrive at values of 30.0 ± 1.0 and 29.6 kcal/mol respectively for ΔH°_{f298}(2-MA). Thus, within experimental error, these two radicals have the same heats of formation. This would lead us to believe that the o-BCMC and p-BCMC radical have similar heats of formation. Subtle differences between the slopes of the Br + o-CT and p-CT potential energy surfaces along their reaction coordinates

cannot be ruled out, however (see below).

Based on our experimental signal levels, the substitution cross section for m-CT at E_c=29 kcal/mol is estimated to be at least a factor of 10 lower than for o-CT at 31 kcal/mol. It is well known that the methyl group is an ortho-para directing substituent in electrophilic (ionic and atomic) substitution reactions. This phenomenon is usually explained in terms of the electron donating capability of the methyl group [35,36], which stabilizes the o- and p- adducts by either increasing the o- and p- frontier electron populations in the reactant molecule or lowering the total π-electron energy of the o- and p- adducts relative to the m-adduct.

There have been no rigorous quantum mechanical calculations of the heats of formation of the isomeric methyl cyclohexadienyl radicals (much less halogenated methyl cyclohexadienyl radicals such as BCMC). However, using a modified version of Huckel theory, Wheland [41] calculated the energy change associated with localizing an electron at the ortho, meta, and para positions of various aromatic molecules, thereby removing it from conjugation with the ring. Although this "localization" energy has traditionally been correlated with the activation energy for addition to a particular ring position, we may associate it with the thermodynamic stability of the resulting radical. This approach is analogous to the one taken above in assessing the stabilities of the o-

BCMC and p-BCMC radicals. For toluene, Wheland found a mere 0.8 kcal/mol difference between the o- and m- localization energies. Such small differences in thermodynamic stability will not have an observable effect on the dynamics of aromatic substitution reactions at high collision energies.

Let us suppose that the reduced cross section for reaction 2 results from barriers of equal magnitude in the entrance and exit channels of the PES. Assuming that there are four active vibrational modes in the m-BCMC complex and that σ_{add} for Br + m-CT is 50% smaller than σ_{add} for Br + o-CT (where we correlate the magnitude of σ_{add} with the position of the methyl group relative to the chlorinated carbon), RRKM calculations indicate that a barrier of ≈13 kcal/mol above threshold in the entrance and exit channels would be needed for $S_{r,m\text{-}BT}$ to be one order of magnitude smaller than $S_{r,o\text{-}BT}$ at E_c=30 kcal/mol. Considering that the activation energies for halogen atom addition to unsaturated molecules are generally in the range of 0 - 2 kcal/mol, it seems unlikely that a barrier of such magnitude could be the cause of the lower reactivity of m-CT.

An alternative explanation is that the reactivities of the isomers of CT are governed by the shape of the Br-CT PES rather than by fixed barriers. The increased electron populations ortho and para to the methyl group in CT could enhance the long range attraction between Br and these sites, but such an attraction might not be strong at high collision

energies. The shape of the potential in the exit valley might be the key. Since the ΔH° are nearly the same for the three isomeric reactions, the ΔG° and K_{eq} for all three reactions will also be roughly the same. Therefore, the rates of the reverse reactions, Cl + o-,p-BT → Br + o-,p-CT, must be accelerated relative to the rate of Cl + m-CT → Br + m-CT. A longer range attraction between Cl and o- and p-BT, manifesting itself in a more gradually sloping potential in the reverse endoergic direction, might be responsible for such a rate enhancement. Alternatively, the lower π-electron energies of the o- and p- complexes may cause the o- and p-surfaces to rise more gradually. In either case, translational energy will be better able to promote the endoergic reaction. Classical trajectory studies on several different potential energy surfaces lend support to these ideas. Polanyi and co-workers [42] have observed that translational energy is favored over vibrational energy in endoergic reactions with a gradual ascent to the barrier crest. Likewise, Chapman [43] has found that the curvatures of the Be + HF → BeF + H and $NO + O_3 \rightarrow NO_2 + O_2$ surfaces have marked effects on the excitation functions and product energy distributions of these reactions. Of course, the slope of the PES will affect the translational energy dependence of the reaction cross section most when only a few vibrational modes participate in energy sharing prior to bond breakage and when reactant translational energy can couple directly into the bond

breaking coordinate. Although the substitution reactions under study are not "direct", they do seem to satisfy these criteria.

B. Br + CB, PFCB

As discussed in relation to the Br + CT reactions, Br addition to CB should be endoergic by ≈2 kcal/mol. However, because of the weakness of the π-bond in fluorinated unsaturated molecules, Br addition to PFCB should be somewhat exoergic. From photodissociation experiments on several fluorinated bromo-iodoalkanes, Lee and co-workers have calculated the C-Br bond dissociation energies (D_0°) in CF_2CF_2Br and CFHCFHBr to be 20 and 12 kcal/mol respectively [44]. Neglecting the effect of resonance stabilization, let us assume that D°(C-Br)=15 kcal/mol in the pentafluoro-chloro-bromocyclohexadienyl (PFCBC) radical. Therefore, a loss of 11 kcal/mol in resonance stabilization energy would make Br addition to PFCB exoergic by approximately 4 kcal/mol.

As we noted at the beginning of Section III(a), ΔH°_{298} = 15 kcal/mol for reaction 4. The overall endoergicity of reaction 5 is uncertain, however. Krech et al. [45] measured $\Delta H^\circ_{f298}(C_6F_5Br)$ = -170.1 kcal/mol. With $\Delta H^\circ_{f298}(C_6F_5Cl)$ = -193.6 kcal/mol from experiment [46] and known heats of formation for Cl and Br [18], this gives ΔH°_{298} = 25.8 kcal/mol for reaction 5. From group additivity, $\Delta H^\circ_{f298}(C_6F_5X)$= -197.8 kcal/mol (X = Cl) and -183.3 (X = Br) [47]. Together these

yield ΔH°_{298} = 16.8 kcal/mol. With experimental values for the heats of formation of the products or reactants, these calculated $\Delta H^\circ_{f298}(C_6F_5X)$ give ΔH°_{298} = 30.0 kcal/mol and 12.6 kcal/mol respectively. Thus, lacking a firm value for the endoergicity of this reaction, we have assumed ΔH°_0 = 15 kcal/mol.

Considering the larger number of low frequency vibrational modes in the fluorinated complex (C-F stretching, $\approx$1000 cm^{-1}, and C-C-F bending, $\approx$500 cm^{-1}), one would expect IVR in PFCBC to be even more rapid than in BCMC. Interestingly, Reddy et al. [25] obtain 3ν and 5ν C-H overtone lifetimes of 200 fs and 120 fs respectively in C_6F_5H (as compared to 230 fs and >51 fs for the same states in benzene). They attribute the relatively low relaxation rate in C_6F_5H to poor frequency matching between the C-H overtone state and the C-F stretch bath states. It seems clear, however, that the lower average product translational energy that we observe for the Br + PFCB reaction as compared to the Br + CT reactions results from the higher density of states of the PFCBC complex at its exit transition state.

The experimental E_c=35 kcal/mol P(E') plotted in Fig. 14a (q=3.2) is in fair agreement with an 8-mode (ν = 650 - 440 cm^{-1}) RRKM-AM P(E') (B'_m = 0.20 kcal/mol). Since it is possible to fit both the o-BT and PFBB data with P(E')'s having the same q parameter (e.g., q=3.2), we cannot conclude from the distributions in Figs. 8 and 14a that there are more

active modes in PFCBC than in o-BCMC. However, the PFBB, E_c=35 kcal/mol, data could be fit reasonably well with a q=7.0 P(E') (Fig. 14b) whereas the o-BT and p-BT data could not. This P(E') agrees with a 10-mode (ν = 700 - 440 cm^{-1}) RRKM-AM P(E') (B'_m = 0.40 kcal/mol).

This is noteworthy in light of Quack's argument that an apparently non-statistical P(E') for a substitution reaction with a "loose" TS need not imply incomplete energy redistribution in the collision complex [48]. He has been able to reproduce experimental P(E') distributions for substitution reactions reasonably well by including an angular contribution to the interaction potential in the adiabatic channel model while assuming that all vibrational modes in the collision complex are active. However, the differences that we observe between the BT and PFBB P(E') distributions imply that more vibrational modes participate in energy sharing in PFCBC than in BCMC.

The slope of the PFBB excitation function also supports this view. The excitation function used to fit the PFBB data (solid curve in Fig. 15) was derived from the 10-mode RRKM branching ratio calculation. The experimental and RRKM curves agree reasonably well. The 20 kcal/mol threshold for the dashed curve indicates that our data are consistent with a higher endoergicity than 15 kcal/mol for reaction 5.

The marked difference in cross section between reactions 4 and 5 is likely to be due to differences in σ_{add} for the

two reactions. As discussed above in relation to reactions 1 and 3, Br will "stick" better to the molecule with the larger number of low frequency dissipative modes in the vicinity of the collision. The slight exoergicity of Br addition to PFCB will increase the density of dissipative states and render the Br-PFCB interaction more "attractive" than the Br-CB interaction. Considering that the contribution of the statistical branching ratio to the total substitution cross section will be smaller for the complex with the larger number of active vibrational modes (i.e., $\eta_{Cl}/(\eta_{Cl} + \eta_{Br})$ decreases as the number of modes increases, see above), $\sigma_{add}(5)/\sigma_{add}(4)$ will be greater than a simple comparison of the signal levels for the two reactions would suggest.

Halogen substituents are known to deactivate aromatic molecules to electrophilic attack but their ability to back-donate p-electrons to the ring makes them ortho-para directing [49]. A CNDO study of fluorobenzene and p-difluorobenzene has shown increased π-electron populations ortho and para to the F atoms [50]. It is not clear, however, whether p-electron back-bonding stabilizes PFCBC relative to BCB, and thereby enhances the substitution cross section for Br + PFCB.

Finally, in comparing our results for reactions 1 and 3 with those for reaction 4, we note how strongly the methyl group enhances the cross section for Br addition to the ring. The features of the PES that are responsible for this large

difference in cross section should be analogous to those responsible for the greater reactivity of o- and p-CT relative to m-CT.

V. CONCLUSIONS

A complex interplay of phenomena underlies our observations for these endoergic aromatic substitution reactions. Competition between intramolecular vibrational energy redistribution and Cl elimination results in asymmetric, forward peaked product CM angular distributions and translational energy distributions and excitation functions that can be modeled by assuming that a limited number of vibrational modes participate in energy sharing in the energized radicals. Ring substituents appear to affect the dynamics by influencing both the orientation and probability of Br addition and the extent of energy redistribution in the radicals. The electronic effects responsible for the different reactivities of the CT isomers may manifest themselves in the slope of the potential energy surface along the reaction coordinate.

REFERENCES

1. (a) G. H. Williams, Homolytic Aromatic Substitution (Pergamon, New York, 1960); (b) M. J. Perkins, in Free Radicals, edited by J. Kochi (Wiley, New York, 1973), vol. 2, pp. 231-271; (c) J. March, Advanced Organic Chemistry (Wiley, New York, 3rd ed., 1985), Ch. 14.
2. K. Shobatake, J. M. Parson, Y. T. Lee, and S. A. Rice, J. Chem. Phys. 59, 1427 (1973); K. Shobatake, Y. T. Lee, and S. A. Rice, ibid., 1435 (1973).
3. S. J. Sibener, R. J. Buss, P. Casavecchia, T. Hirooka, and Y. T. Lee, J. Chem. Phys. 72, 4341 (1980); R. J. Baseman, R. J. Buss, P. Casavecchia, and Y. T. Lee, J. Am. Chem. Soc. 106, 4108 (1984).
4. R. J. Brudzynski, Ph. D. Thesis, University of California, Berkeley, 1987.
5. G. N. Robinson, R. E. Continetti, and Y. T. Lee, Faraday Discuss. Chem. Soc. 84, 0000 (1987).
6. Y. T. Lee, J. D. McDonald, P. R. LeBreton, and D. R. Herschbach, Rev. Sci. Inst. 40, 1402 (1969).
7. R. K. Sparks, Ph. D. Thesis, University of California, Berkeley, 1979.
8. J. J. Valentini, M. J. Coggiola, and Y. T. Lee, Rev. Sci. Inst. 48, 58 (1977).
9. J. D. Cox and G. Pilcher, Thermochemistry of Organic and Organometallic Compounds (Academic, New York, 1970).

10. CRC Handbook of Chemistry and Physics (CRC, Cleveland, 64th ed., 1983).

11. R. J. Buss, Ph. D. Thesis, University of California, Berkeley, 1979.

12. (a) W. B. Miller, S. A. Safron, and D. R. Herschbach, Faraday Discuss. Chem. Soc. 44, 108 (1967); (b) G. A. Fisk, J. D. McDonald, and D. R. Herschbach, ibid., 228.

13. Rather than use the formal nomenclature for the BCMC radicals, we identify them with a prefix corresponding to the aromatic reagent.

14. H. B. Schlegel and C. Sosa, J. Phys. Chem. 88, 1141 (1984).

15. D. R. Stull, E. F. Westrum, Jr., and G. C. Sinke, The Chemical Thermodynamics of Organic Compounds (Wiley, New York, 1969).

16. T. Holm, J. Organometal. Chem. 56, 87 (1973).

17. M. Szwarc and D. Williams, Proc. Royal Soc. A 219, 353 (1953).

18. H. M. Rosenstock, K. Draxl, B. W. Steiner and J. T. Herron, J. Phys. Chem. Ref. Data 6, suppl. 1 (1977).

19. D. F. McMillan and D. M. Golden, Ann. Rev. Phys. Chem. 33, 493 (1982).

20. S. W. Benson and H. E. O'Neal, Kinetic Data on Gas Phase Unimolecular Reactions (NSRDS-NBS 21, US Dept. of Commerce, Washington, DC, 1970).

21. D. G. L. James and R. D. Stuart, Trans. Faraday Soc. 64,

2752 (1968).

22. A. S. Rodgers, D. M. Golden, and S. W. Benson, J. Am. Chem. Soc. 89, 4578 (1967).

23. RRKM algorithm of W. L. Hase and D. L. Bunker, Quantum Chemistry Program Exchange, University of Indiana, Bloomington, Indiana.

24. (a) L. M. Sverdlov, M. A. Kovner and E. P. Krainov, Vibrational Spectra of Polyatomic Molecules (Wiley, New York, 1974); (b) A. Amano, O. Horie and N. H. Hanh, Int. J. Chem. Kin. 8, 321 (1976).

25. K. V. Reddy, D. F. Heller and M. J. Berry, J. Chem. Phys. 76, 2814 (1982).

26. R. H. Page, Y. R. Shen, and Y. T. Lee, Phys. Rev. Lett. 59, 1293 (1987); R. H. Page, Y. R. Shen, and Y. T. Lee, J. Chem. Phys. submitted (1987).

27. C. S. Parmenter and B. M. Stone, J. Chem. Phys. 84, 4710 (1986).

28. D. B. Moss, C. S. Parmenter and G. E. Ewing, J. Chem. Phys. 86, 51 (1987).

29. K. Okuyama, N. Mikami and M. Ito, J. Phys. Chem. 89, 5617 (1985).

30. P. S. Skell and K. J. Shea, in Free Radicals, edited by J. Kochi (Wiley, New York, 1973), vol. 2, pp. 809-852.

31. S. A. Safron, N. D. Weinstein, D. R. Herschbach and J. C. Tully, Chem Phys. Lett. 12, 564 (1972).

32. J. A. Kerr and M. J. Parsonage, Evaluated Kinetic Data

on Gas Phase Addition Reactions (CRC, Cleveland, 1972).

33. P. J. Robinson and K. A. Holbrook, Unimolecular Reactions (Wiley, New York, 1972).

34. W. L. Hase, D. M. Ludlow, R. J. Wolf and T. Schlick, J. Phys. Chem. 85, 958 (1981).

35. See for example, (a) L. Salem, The Molecular Orbital Theory of Conjugated Systems (W. Benjamin, New York, 1966); (b) R. McWeeny, Coulson's Valence (Oxford University Press, Oxford, 3rd ed., 1979).

36. I. Fleming, Frontier Orbitals and Organic Chemical Reactions (Wiley, New York, 1978).

37. D. M. Golden and S. W. Benson, Chem. Rev. 69, 125 (1969).

38. A. B. Trenwith, Trans. Faraday Soc. 66, 2805 (1970).

39. A. B. Trenwith and S. P. Wrigley, J. Chem. Soc. Faraday Trans. 1 73, 817 (1977).

40. W. Tsang, Int. J. Chem. Kinet. 5, 929 (1973).

41. G. W. Wheland, J. Am. Chem. Soc. 64, 900 (1942).

42. J. C. Polanyi and N. Sathyamurthy, Chem. Phys. 33, 287 (1978).

43. (a) H. Schor, S. Chapman, S. Green, and R. N. Zare, J. Chem. Phys. 69, 3790 (1978); (b) S. Chapman, J. Chem. Phys. 74, 1001 (1981).

44. D. Krajnovich, L. J. Butler, and Y. T. Lee, J. Chem. Phys. 81, 3031 (1884); T. K. Minton, Ph. D. Thesis, University of California, Berkeley, 1986; T. K. Minton,

G. M. Nathanson, and Y. T. Lee, J. Chem. Phys. 86, 1991 (1987).

45. M. J. Krech, S. J. W. Price, and H. J. Sapiano, Can. J. Chem. 55, 4222 (1977).

46. J. D. Cox, H. A. Gundry, D. Harrop, and A. J. Head, J. Chem. Thermodyn. 1, 77 (1969).

47. S. W. Benson, F. R. Cruickshank, D. M. Golden, G. R. Haugen, H. E. O'Neal, A. S. Rodgers, R. Shaw, and R. Walsh, Chem. Rev. 69, 279 (1969).

48. M. Quack, Chem. Phys. 51, 353 (1980).

49. C. K. Ingold, Structure and Mechanism in Organic Chemistry (Cornell University Press, Ithaca, 2nd ed., 1969).

50. J. S. Yadav, P. C. Mishra, and D. K. Rai, Mol. Phys. 26, 193 (1973).

Table 1. Relevant experimental quantities for reactions 1 - 3.

Reaction	E_c[a]	$\langle E'/E_{avl} \rangle$[b]	$n_{Br} n_{RCl} v_{rel}$[c]	p[d]	B[d]
Br/He + o-CT	31	0.27	1.00	0.033	0.06
Br/Ne + o-CT	25	0.27	0.54	0.035	0.03
Br/Ar + o-CT	21	0.30	0.44	0.20	0.00
Br/He + m-CT	29	---	(e)		
Br/He + p-CT	31	0.30	0.98	0.23	0.02
Br/Ne + p-CT	25	0.30	0.59	0.21	0.00
Br/Ar + p-CT	21	0.33	0.53	0.41	-0.01

(a): All energies are in kcal/mol; collision energies reflect cross section weighting.

(b): Fraction for most-probable collision energy.

(c): Arbitrary units.

(d): P(E') parameters; q=1.85.

(e): The m-CT reaction was studied several weeks after the o- and p-CT experiments were completed. The Br/He + o-CT angular distribution was re-measured at this time, however. The o-BT and Br elastic signal levels indicated that the Br beam intensity was ≈50% lower than during the earlier experiments; the o-BT signal-to-noise ratio had dropped by 20%. However, given the presence of elastic scattering background in the m-CT experiment (≈2 Hz at 46°), it is doubtful that we would have been able to see signal even if the Br beam were twice as intense.

Table 2. Relevant experimental quantities for reactions 4 and 5.[a,b]

Reaction	E_c	$\langle E'/E_{avl} \rangle$	$n_{Br} n_{RCl} v_{rel}$	p	B
Br/He + CB	30	---	1.29	---	---
Br/He + PFCB	35	0.18	1.00	-0.10	0.08
Br/Ne + PFCB	25	0.21	0.68	0.050	0.1
Br/Ar + PFCB	20	---	0.50	---	---

(a): These experiments were carried out with a different inductor circuit, or "high-Q head", on the quadrupole mass filter than were the CT experiments so the transmission function of the mass spectrometer was different.

(b): See legend to Table 1; q=3.20 for these fits.

FIGURE CAPTIONS

Fig. 1: Generalized reaction coordinate diagram. Shaded region indicates approximate collision energy range. Numbers represent the five reactions studied.

Fig. 2: o-BT (m/e=170) laboratory angular distributions. ◐: E_c=31 kcal/mol; ○: E_c=25 kcal/mol; □: E_c=21 kcal/mol. Signal is normalized to constant reactant flux but peak of E_c=31 distribution is scaled to unity. Br beam is at 0°. Solid lines are fits to data using CM distributions in Figs. 7 and 8 and excitation function in Fig. 10. Error bars represent 90% confidence limits. Arrows indicate positions of center-of-mass angles with collision energy decreasing from left to right.

Fig. 3: p-BT (m/e=170) laboratory angular distributions. See Fig. 2.

Fig. 4: p-BT (m/e=170) time-of-flight spectra at E_c=31 kcal/mol at five laboratory angles. Solid lines represent fits to data using CM distributions in Figs. 7 and 8 and excitation function in Fig. 10.

Fig. 5: p-BT (m/e=170) time-of-flight spectra.
(a) E_c=25 kcal/mol; (b) E_c=21. See Fig. 4.

Fig. 6: o-BT (m/e=170) time-of-flight spectra.
(a) E_c=31 kcal/mol; (b) E_c=25; (c) E_c=21.
See Fig. 4.

Fig. 7: Center-of-mass frame product angular distributions used in fits. (a) o-BT; (b) p-BT.
——— E_c=31 kcal/mol; — — E_c=25; — - — E_c=21.

Fig. 8: Center-of-mass product translational energy distributions used in fits.
(a) Br + o-CT: ——— E_c=31 kcal/mol; — — E_c=25;
— - — E_c=21; - - - 4-mode RRKM-AM calculation.
(b) Br + p-CT: same as (a).

Fig. 9: Center-of-mass frame product flux contour diagram for reaction 3, E_c=31 kcal/mol. Scale is for contours; scale for kinematic ("Newton") diagram is half of contour scale.

Fig. 10: Excitation functions for reactions 1 (— —) and 3 (———). Arrows indicate most-probable experimental collision energies. Shaded regions indicate uncertainty in S_r above the highest most-probable collision energy.

□: 6-mode RRKM branching ratio calculation.

○: 3-mode RRKM calculation.

Fig. 11: PFBB (m/e=246) laboratory angular distributions. ○: E_c=35 kcal/mol; □: E_c=25 kcal/mol. Signal is normalized to constant reactant flux. Br beam is at 0°. Solid lines are fits to data using CM distributions in Figs. 13 and 14 and solid line excitation function in Fig. 15. Error bars represent 90% confidence limits.

Fig. 12: PFBB (m/e=246) time-of-flight spectra. (a) E_c=35 kcal/mol; (b) E_c=25 kcal/mol. Solid lines represent fits to data using CM distributions in Figs. 13 and 14 and solid line excitation function in Fig. 15.

Fig. 13: Center-of-mass frame product angular distributions used in fits to PFBB data. ——— E_c=35 kcal/mol; — — E_c=25.

Fig. 14: Center-of-mass frame product translational energy distributions used in fits to PFBB data.

(a) ——— E_c=35 kcal/mol (q=3.2);

— — E_c=25 kcal/mol (q=3.2);

– – – 8-mode RRKM-AM calculation

(b) ——— E_c=35 kcal/mol (q=7.0);

– – – 10-mode RRKM-AM calculation.

Fig. 15: Excitation functions for reaction 5. See Fig. 10.

O: 10-mode RRKM branching ratio calculation.

"For number sequence only"

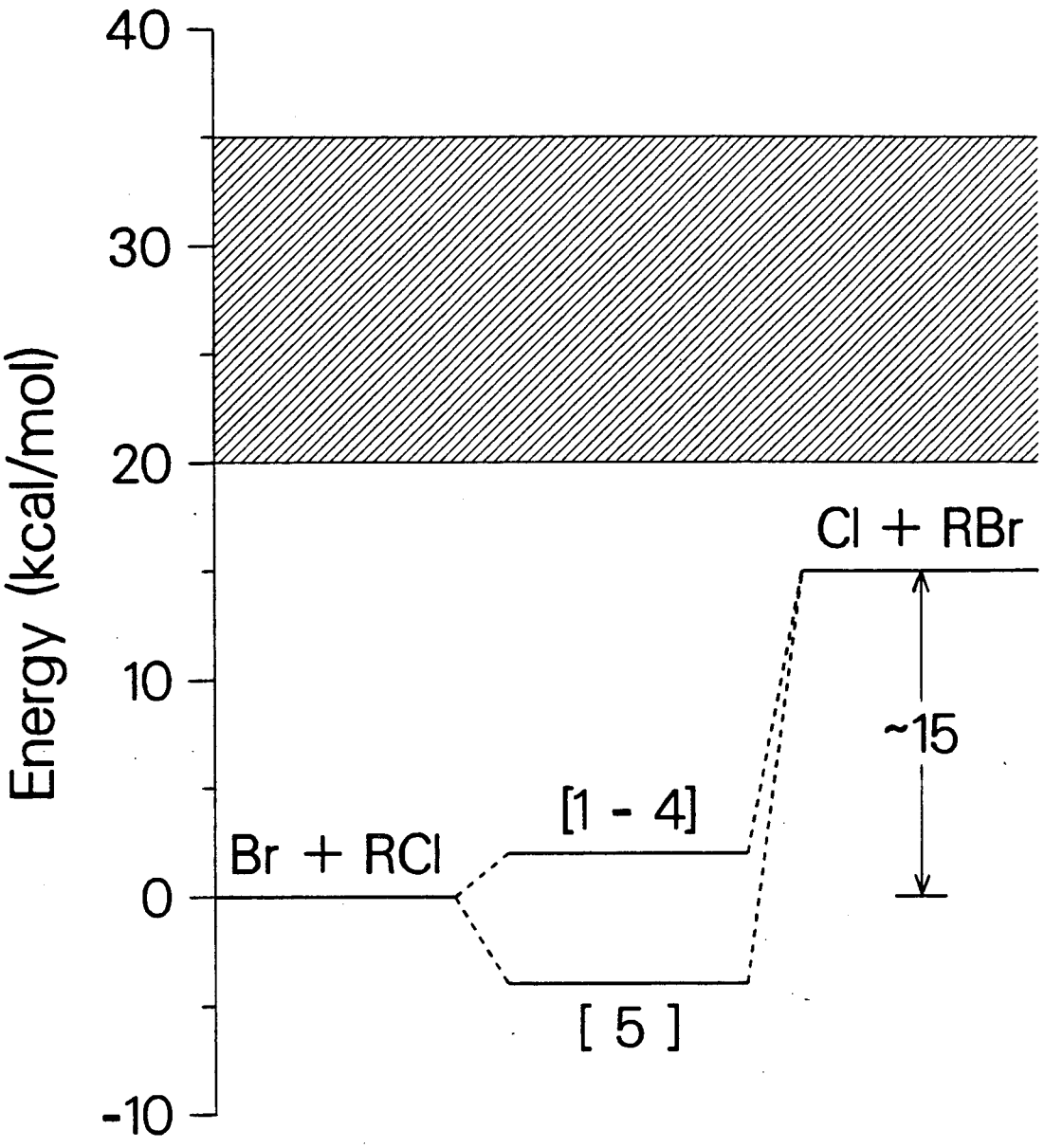
40
30
20
10
0
-10
Energy (kcal/mol)
Cl + RBr
~15
[1 - 4]
Br + RCl
[5]
XBL 8712-5289

Figure 1

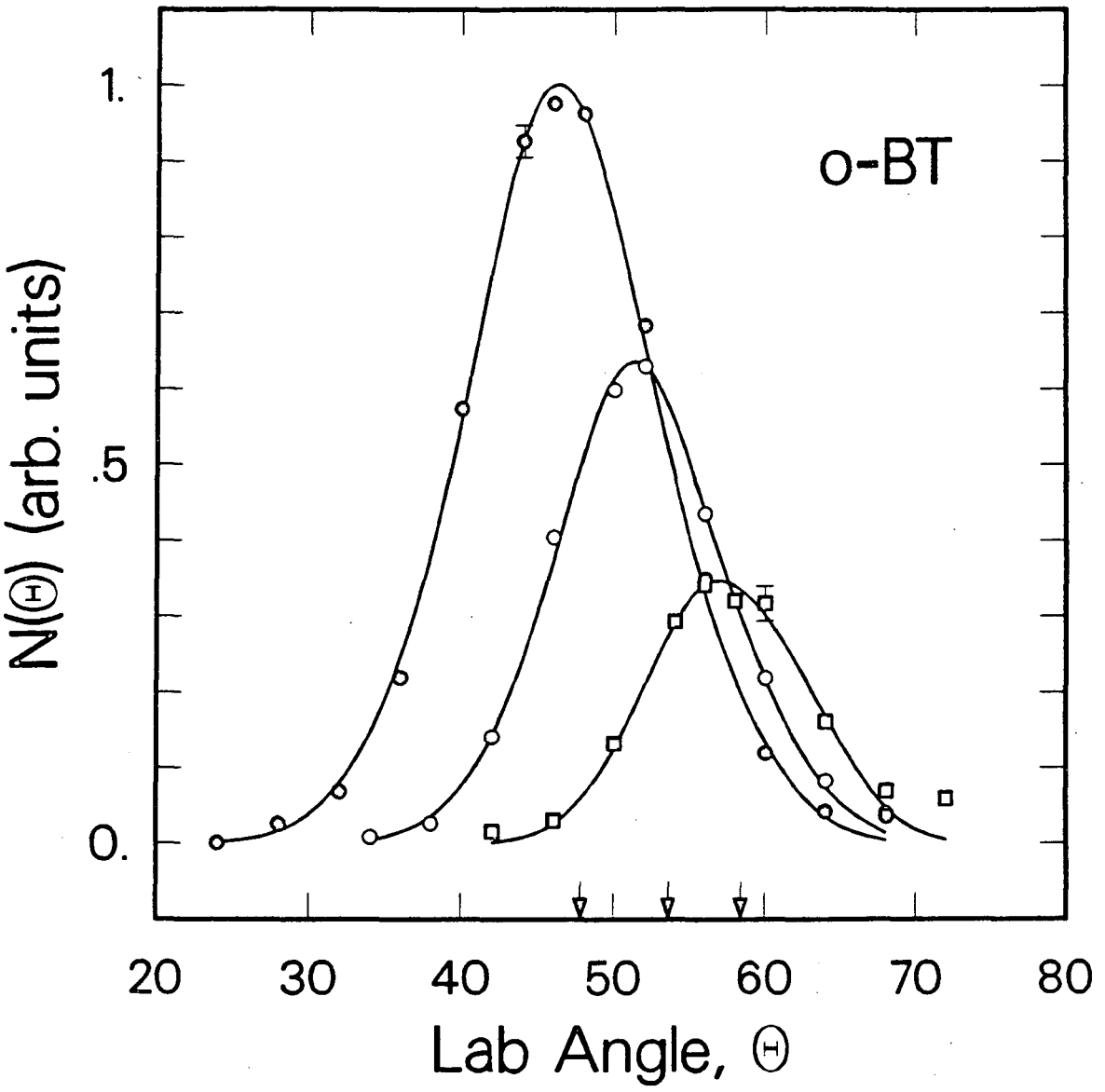

XBL 8712-5287

Figure 2

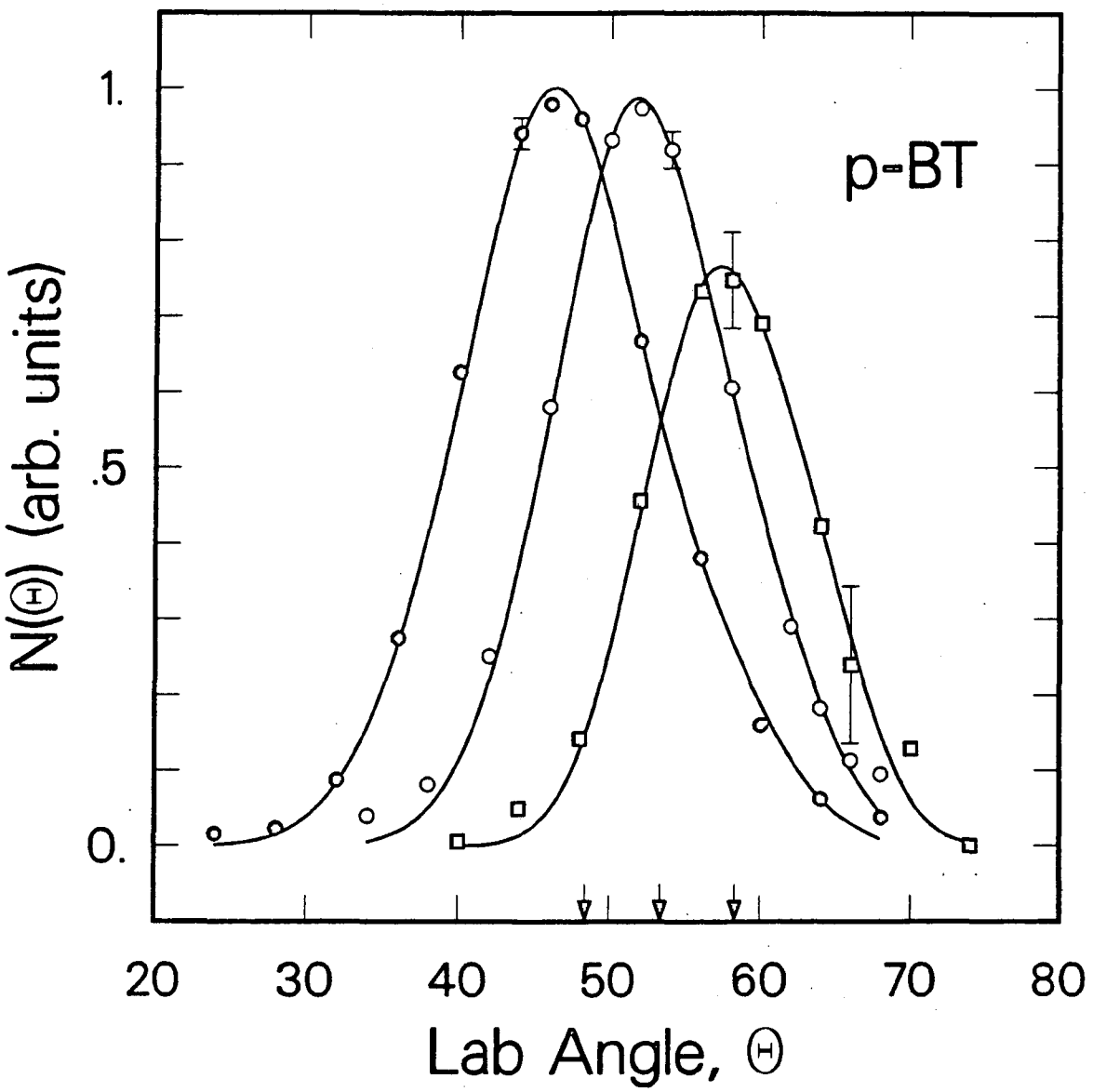

XBL 8712-5288

Figure 3

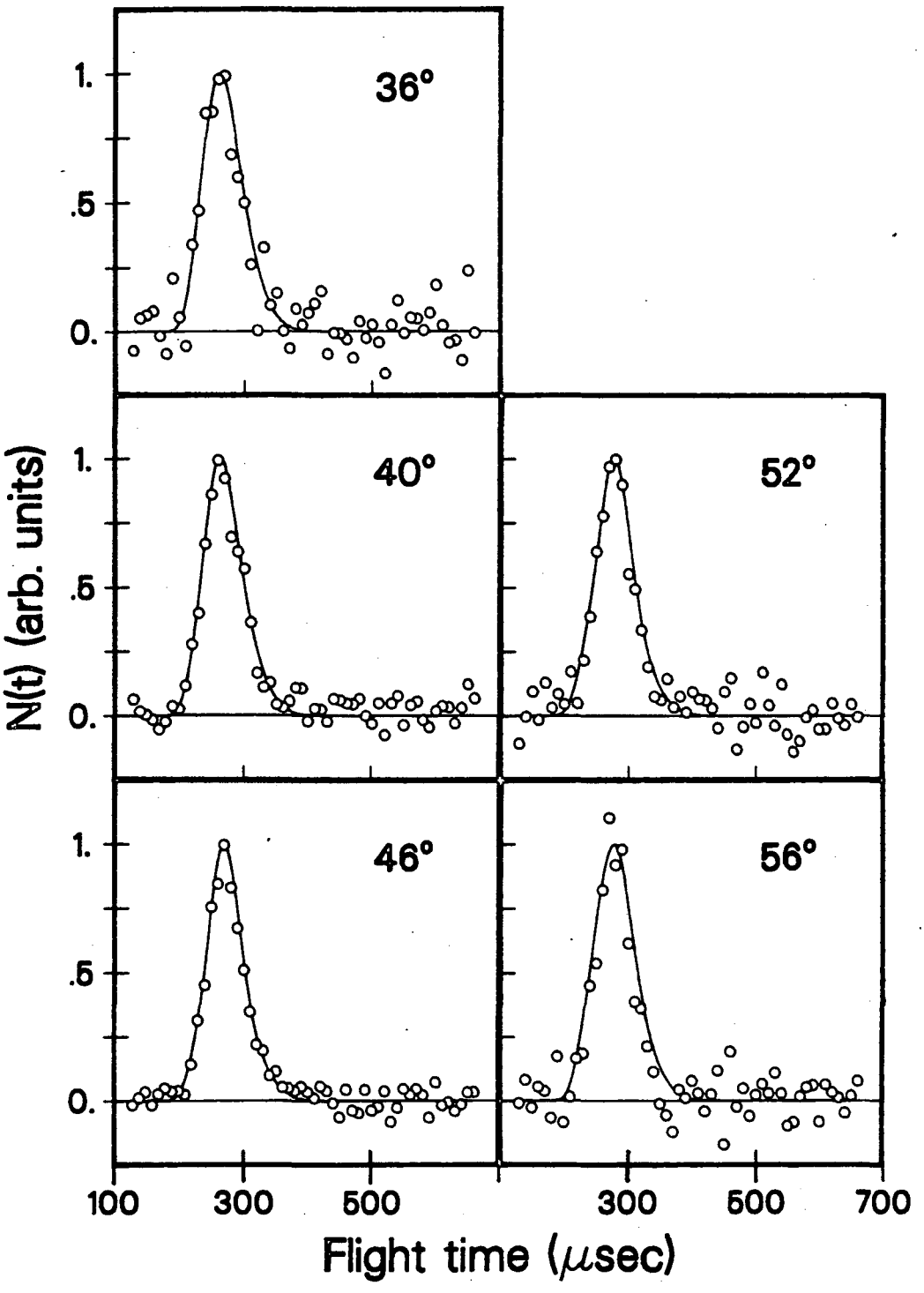

XBL 8712-5149

Figure 4

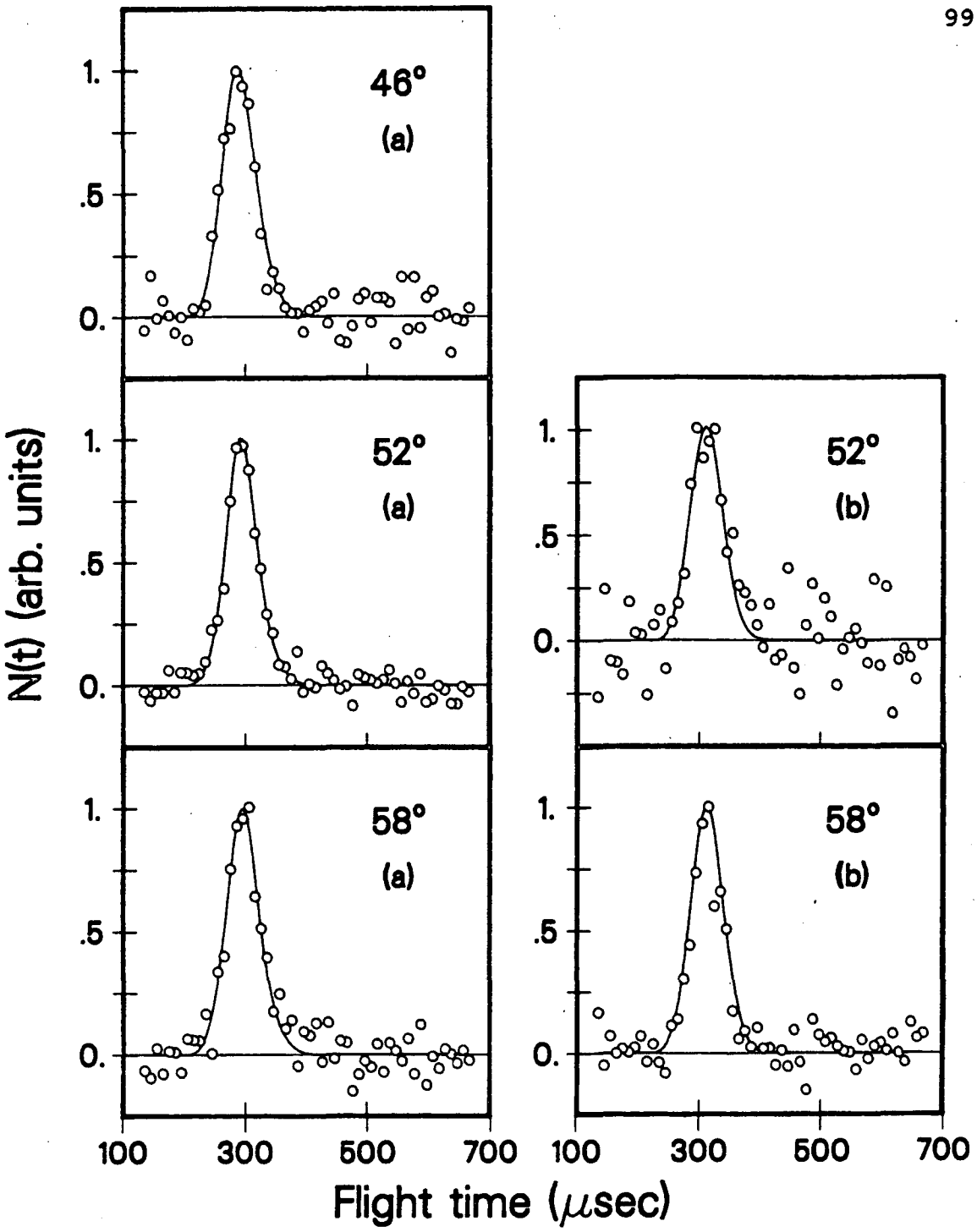
46°
(a)
52°
(a)
52°
(b)
58°
(a)
58°
(b)
1.
.5
0.
100
300
500
700
N(t) (arb. units)
Flight time (μsec)
XBL 8712-5148

Figure 5

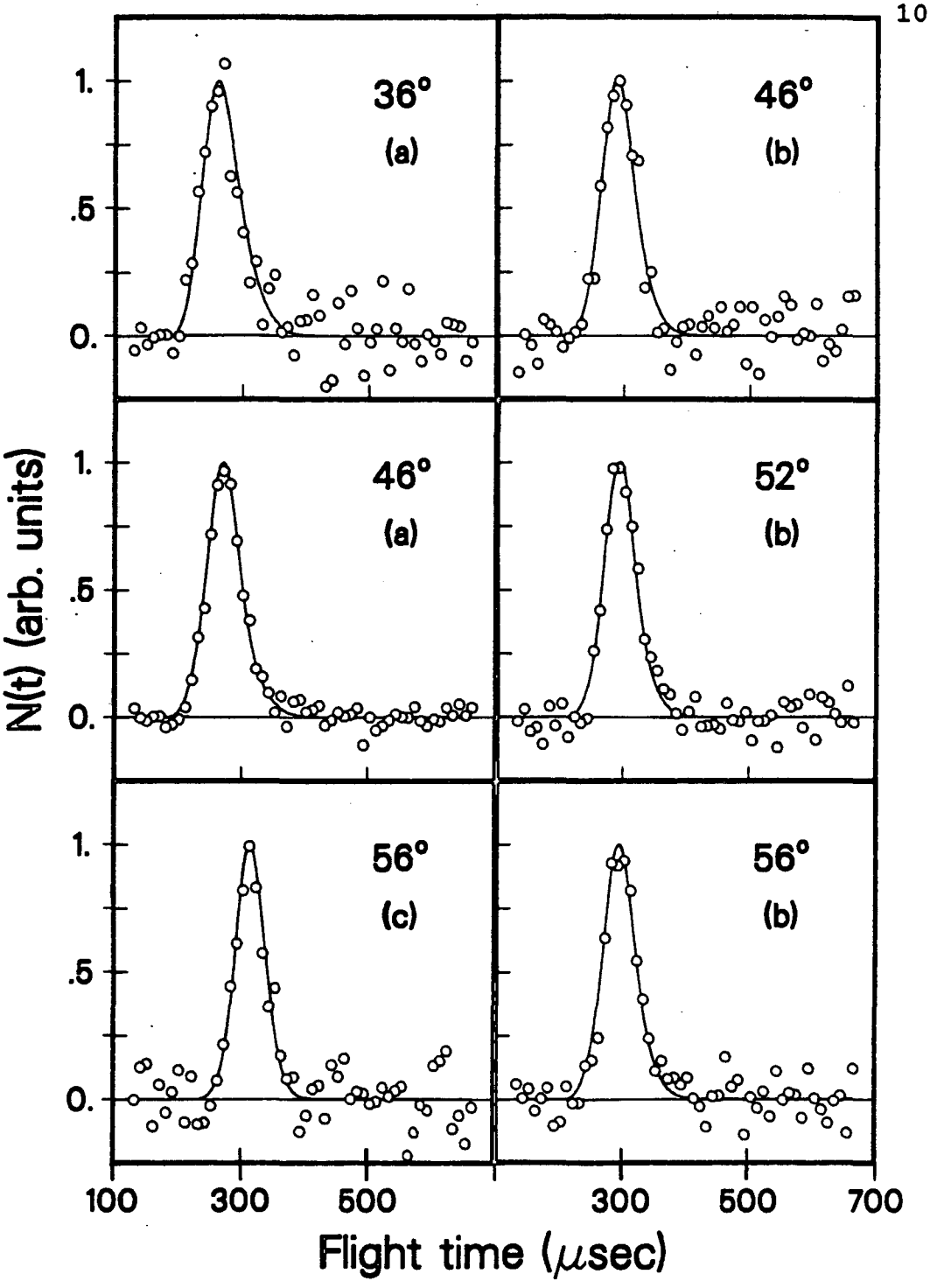
36°
(a)
46°
(b)
46°
(a)
52°
(b)
56°
(c)
56°
(b)
1.
.5
0.
N(t) (arb. units)
100
300
500
300
500
700
Flight time (μsec)
XBL 8712-5147

Figure 6

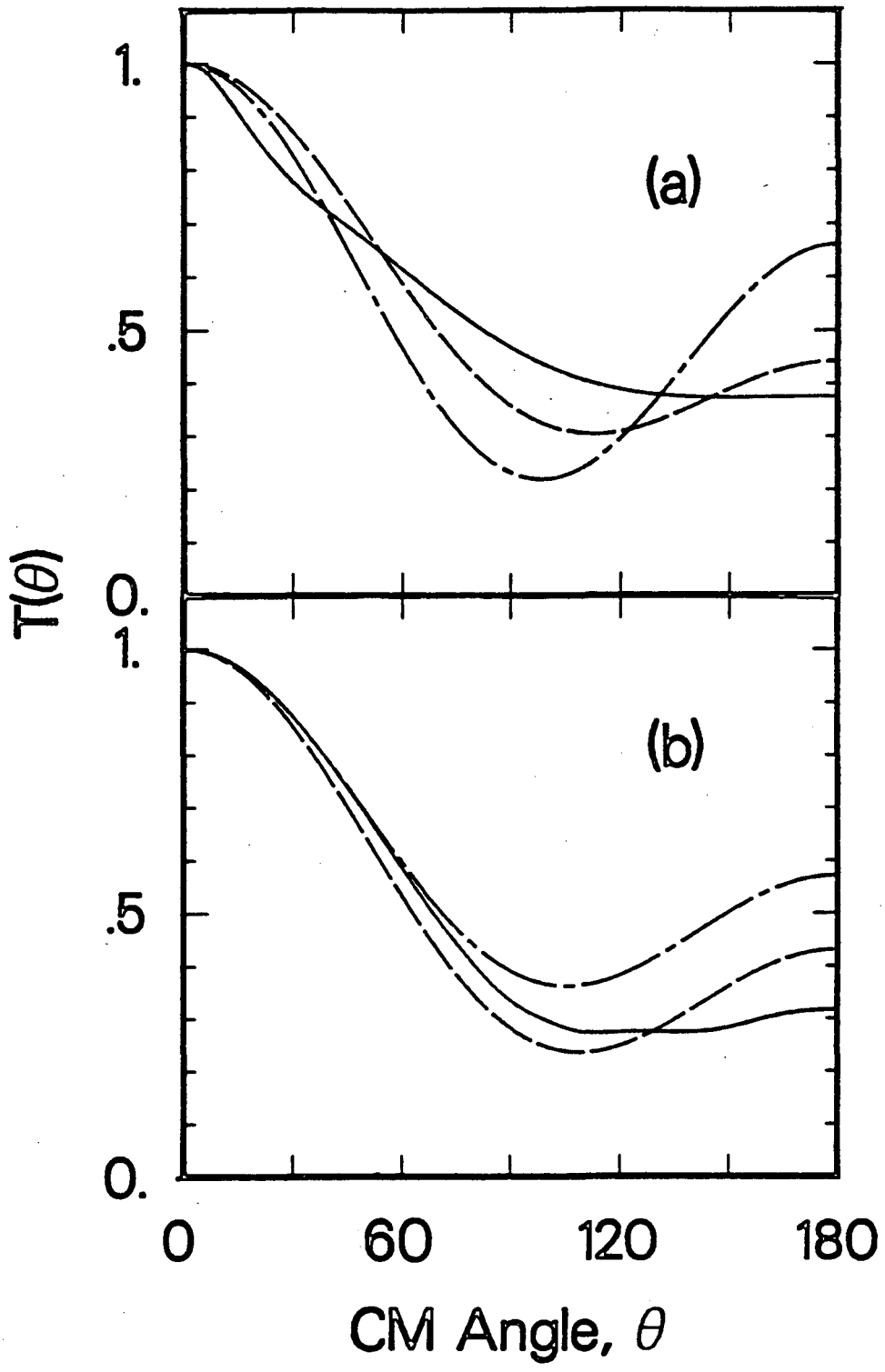

XBL 8712-5150

Figure 7

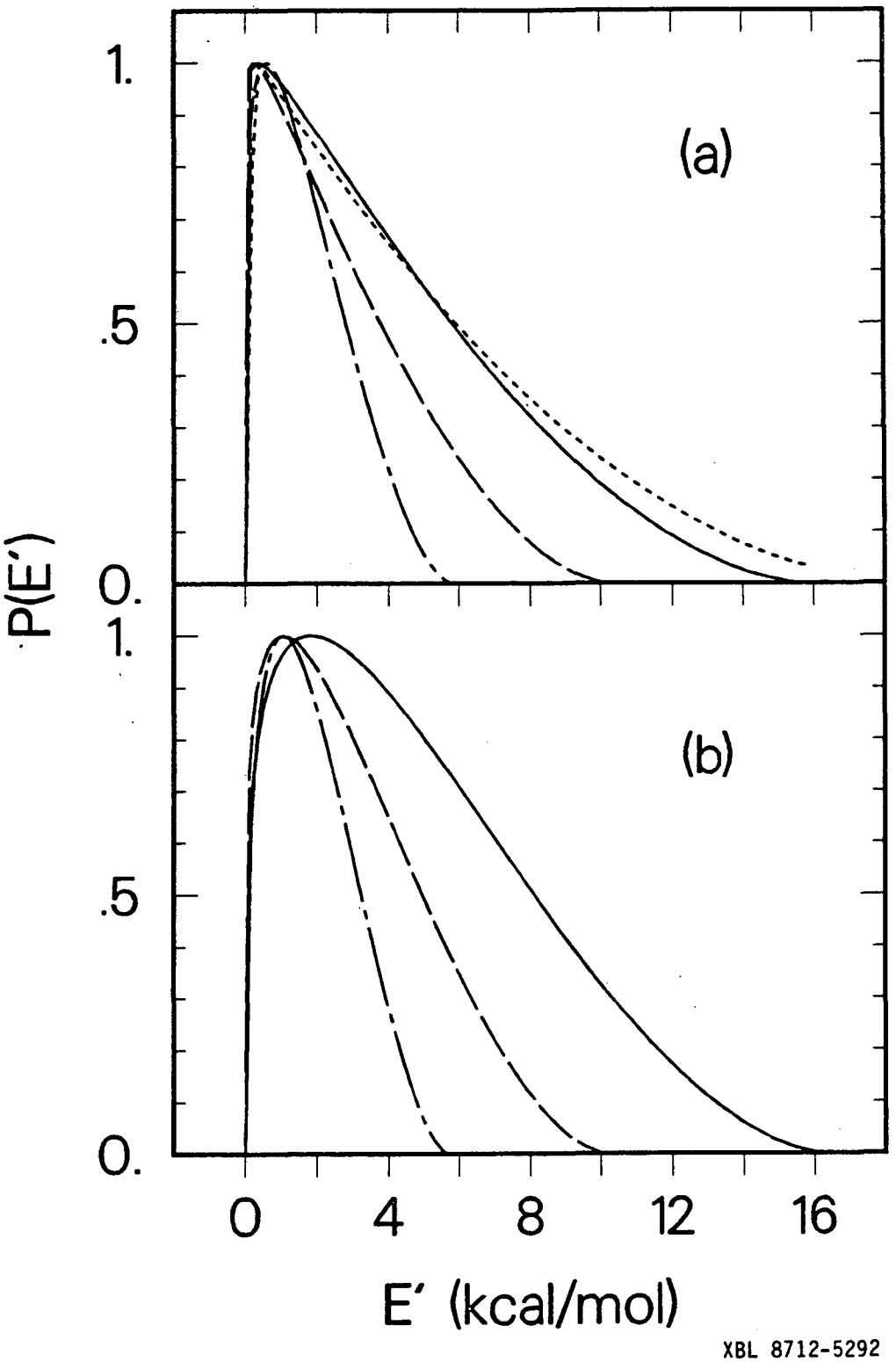

Figure 8

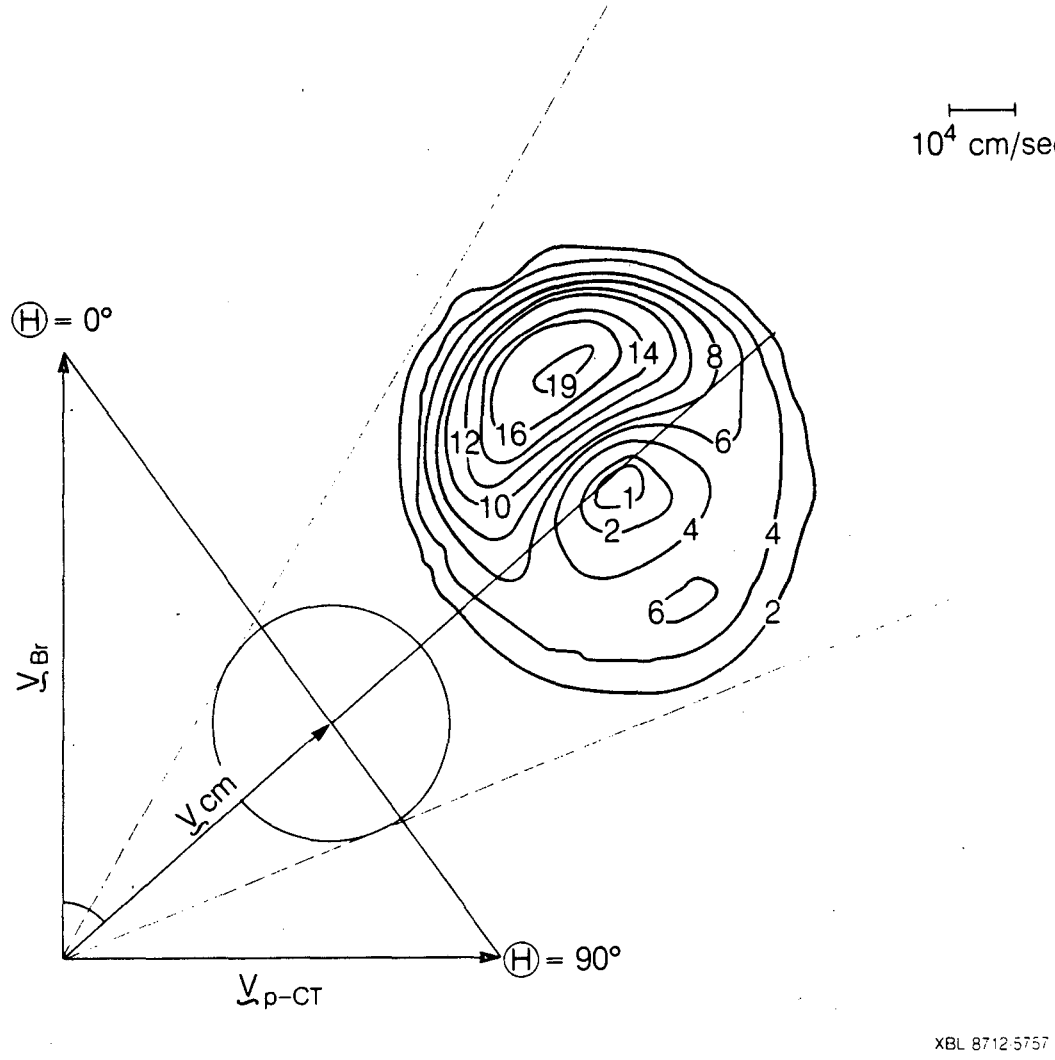

XBL 8712-5757

Figure 9

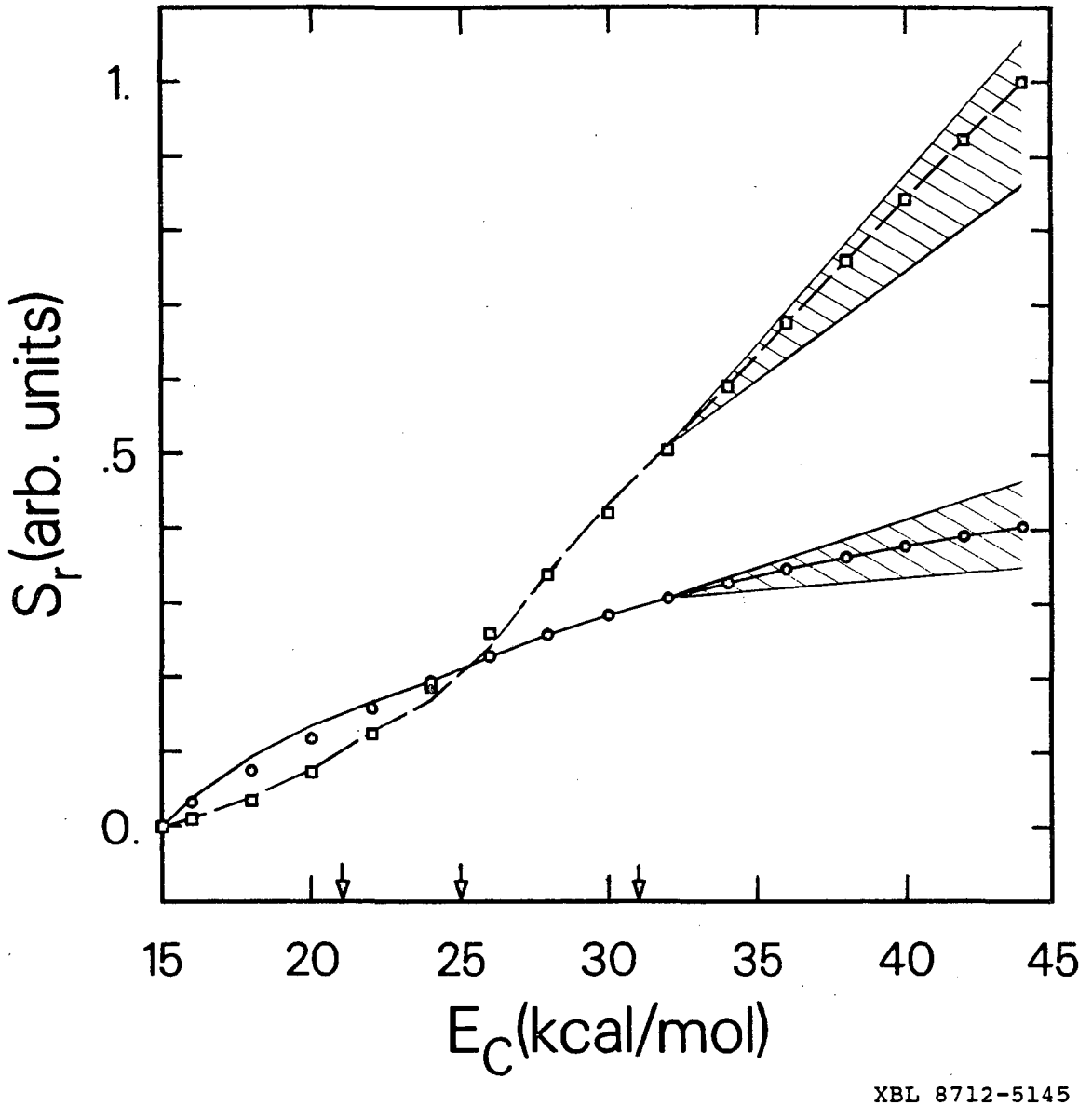

Figure 10

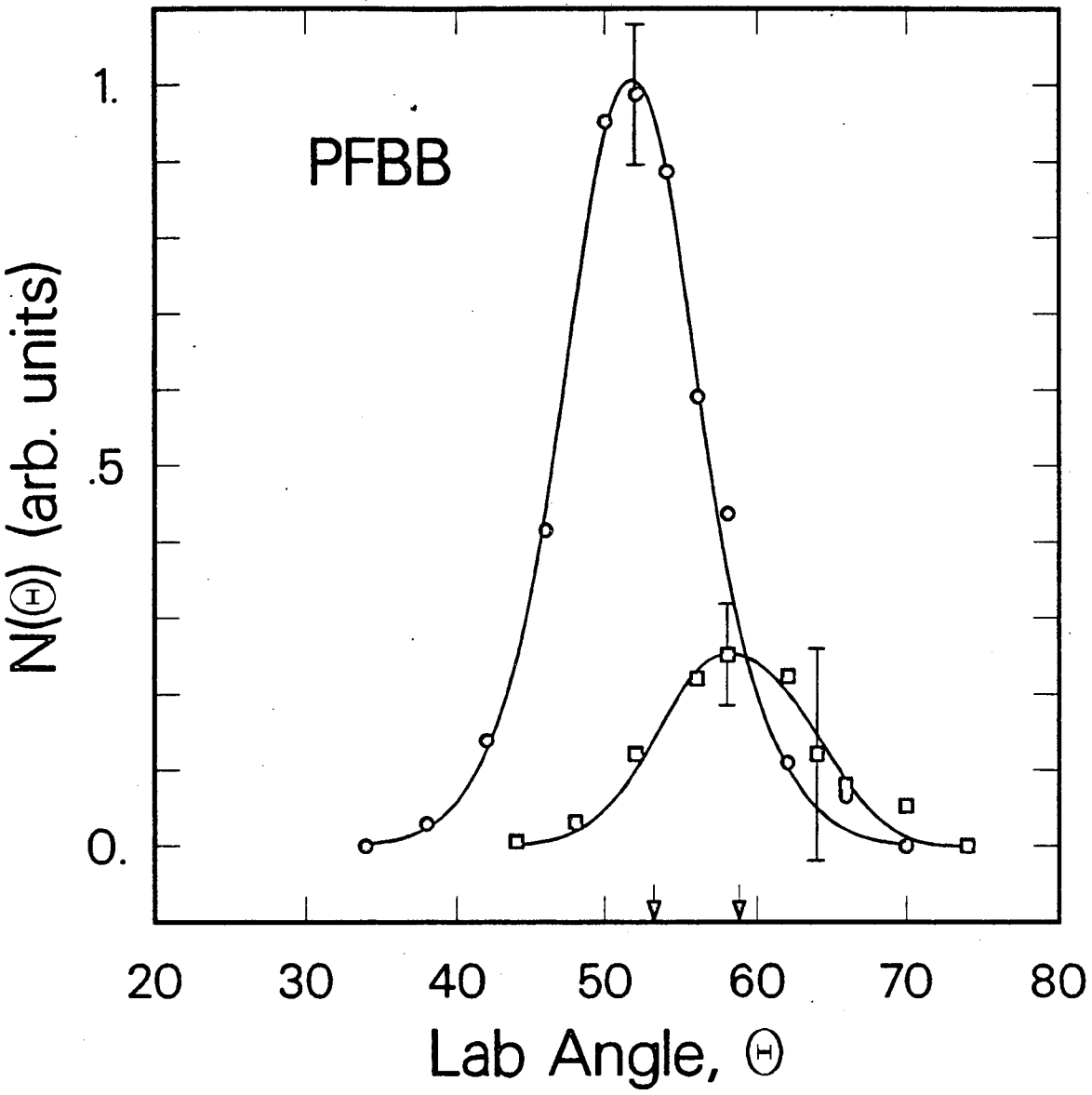

XBL 8712-5334

Figure 11

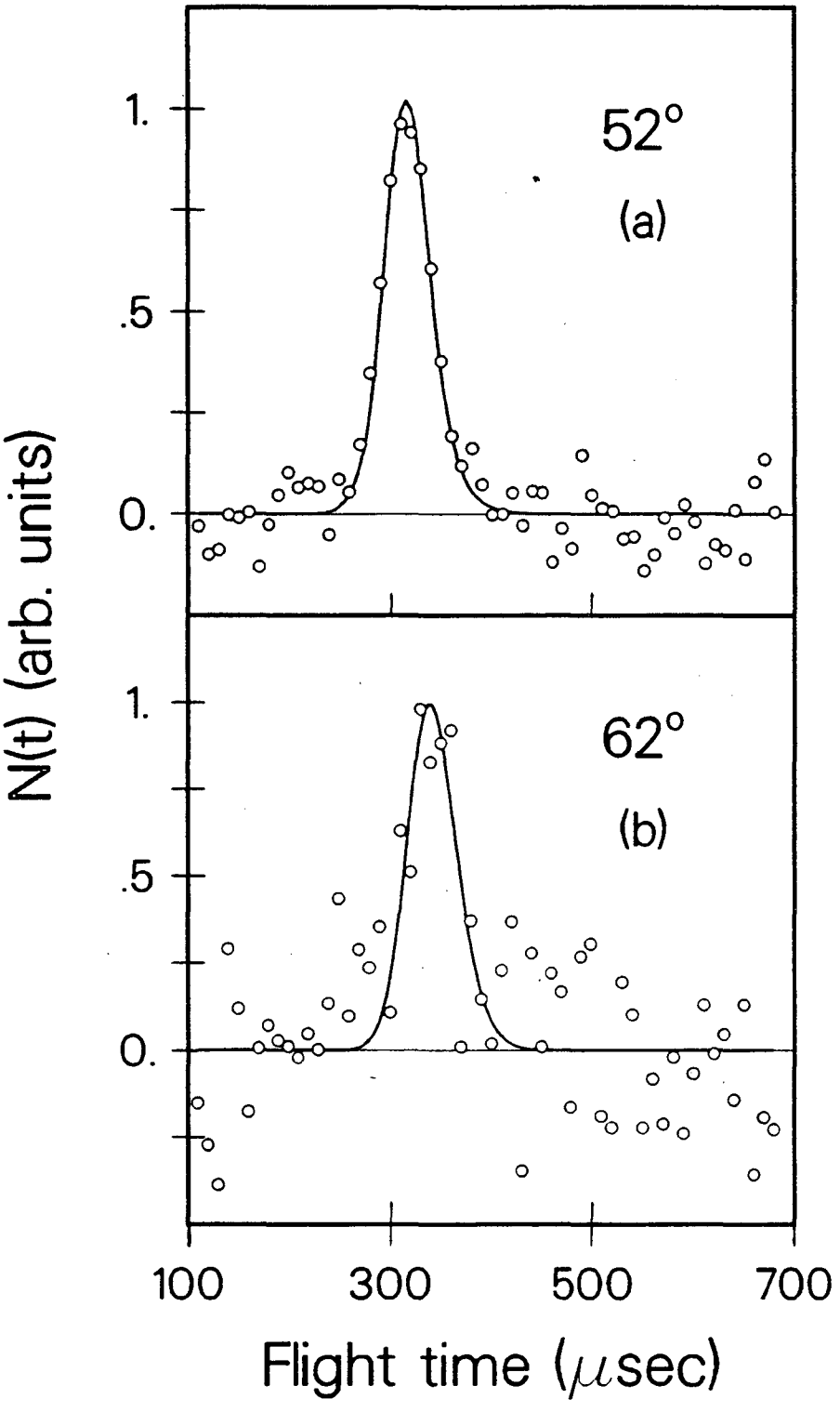
52°
(a)
62°
(b)
1.
.5
0.
N(t) (arb. units)
100
300
500
700
Flight time (μsec)
XBL 8712-5146

Figure 12

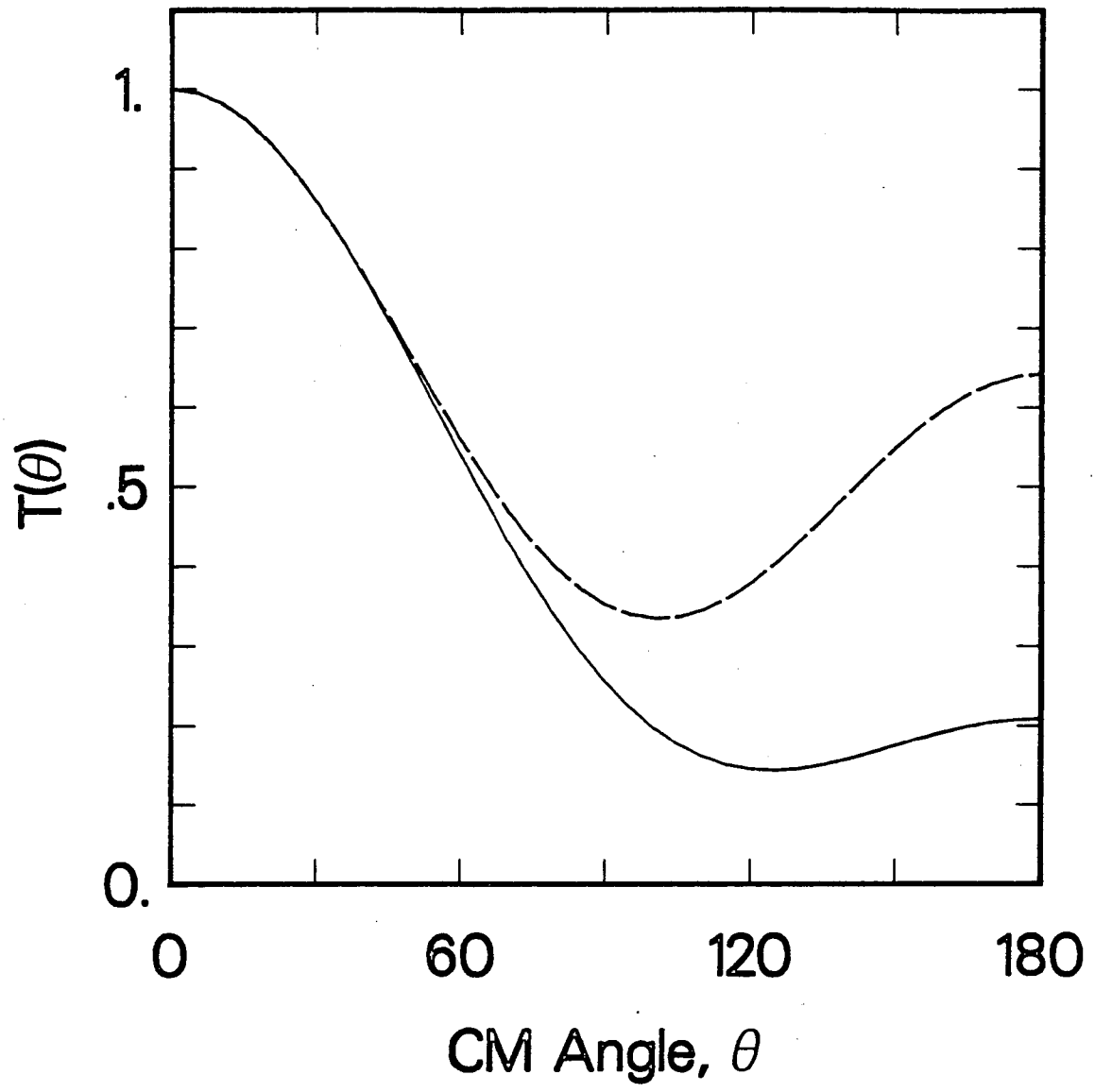

XBL 8712-5295

Figure 13

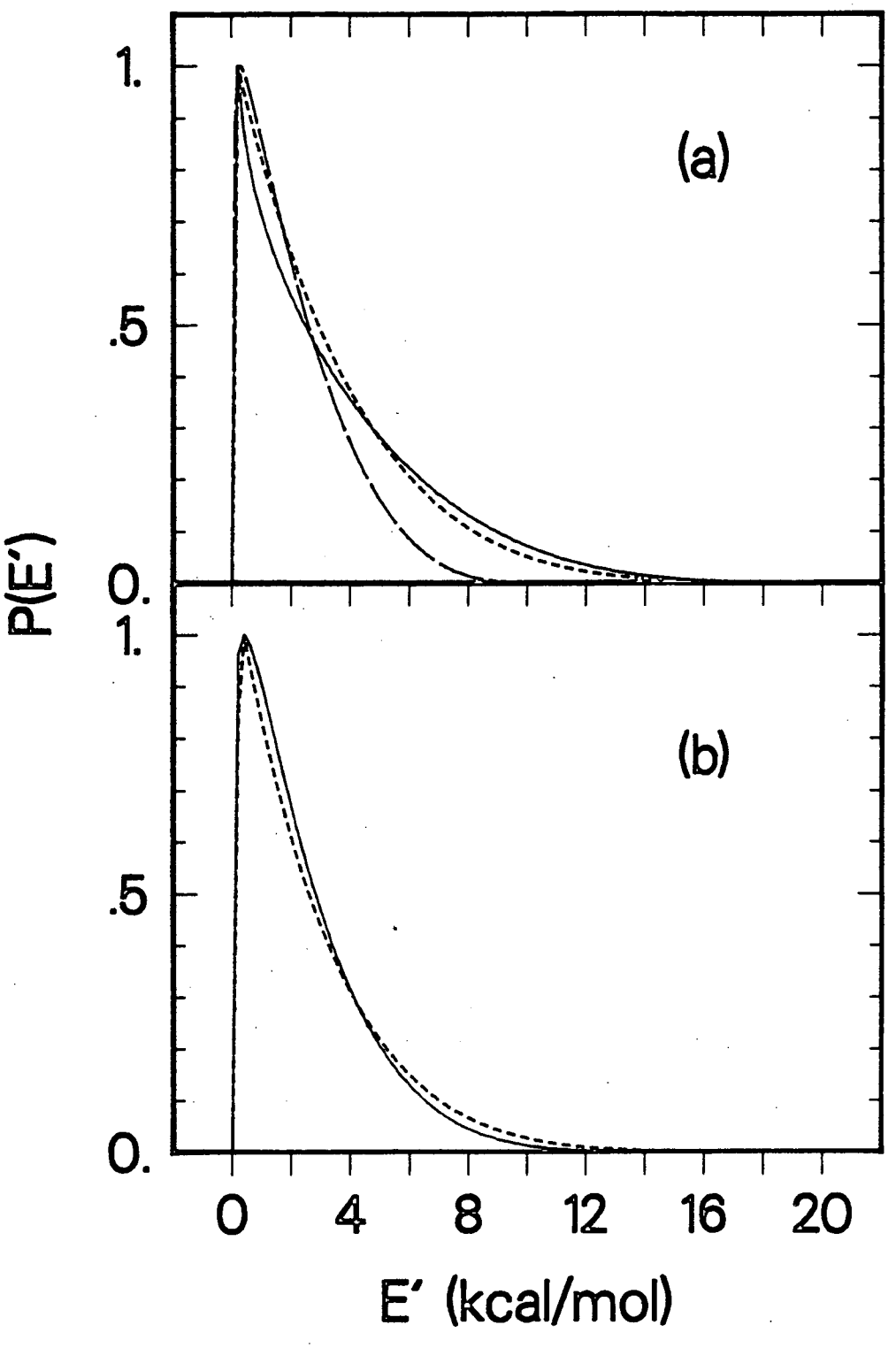

XBL 8712-5294

Figure 14

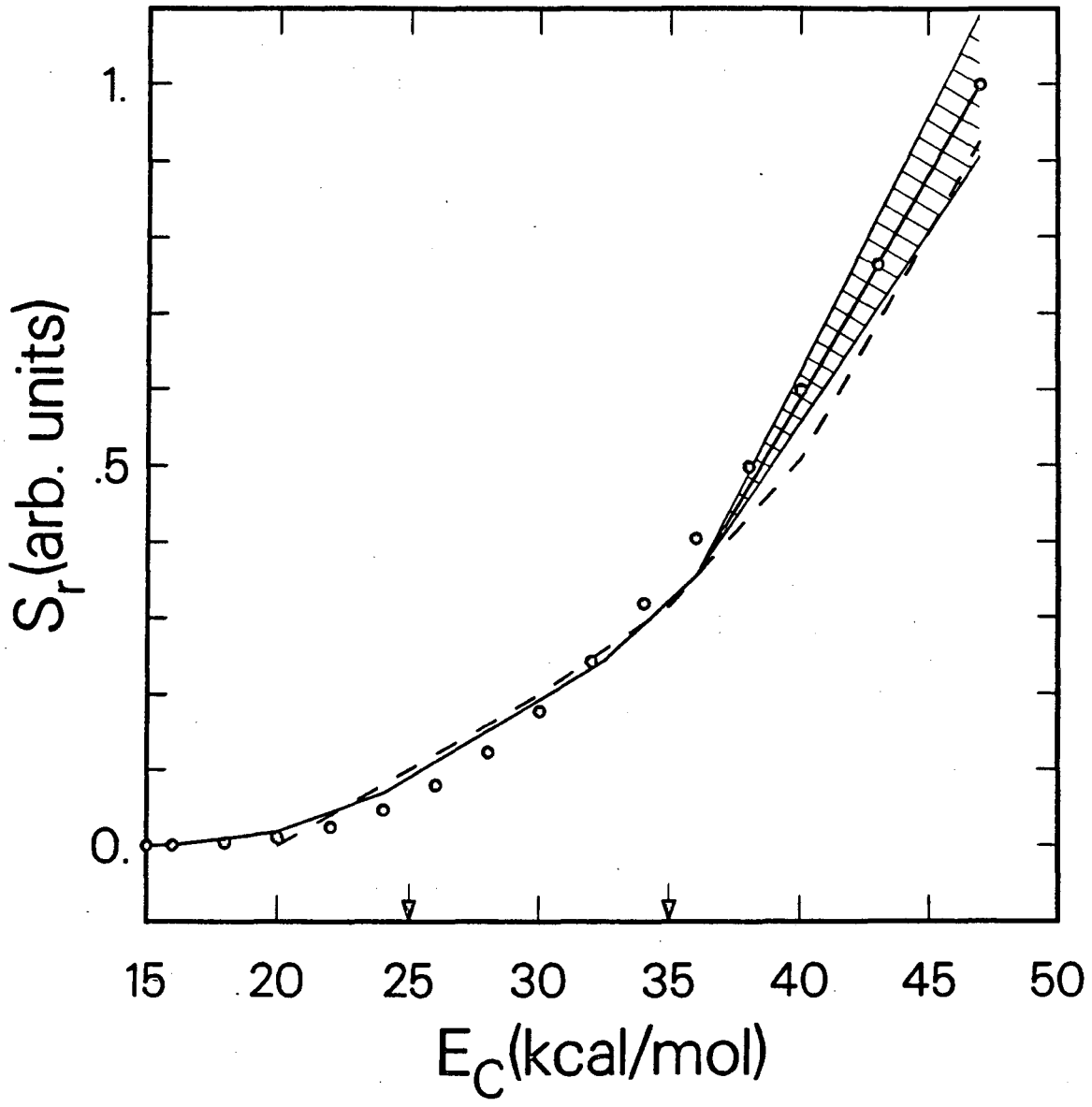

XBL 8712-5291

Figure 15

Chapter 3: Dynamics of Endoergic Substitution Reactions. II. Br + $\{C_2H_2Cl_2\}$ → Cl + $\{C_2H_2ClBr\}$

I. INTRODUCTION

Gas phase substitution reactions involving unsaturated molecules are generally divided into three steps: addition of the atom/radical to the double bond to form a vibrationally excited collision complex, energy redistribution within the complex and finally emission of another atom/radical. In the 50 years since Kharasch and co-workers discovered the homolytic bromination of alkenes [1], much experimental and theoretical work has been directed towards understanding the many facets of radical addition reactions [2]. Several factors are believed to influence the kinetics and site-specificity of such reactions, including the relative bulk and polarity of the reagents, and the stability of the adduct radical. However, our quantitative knowledge of the potential energy surfaces for atom/radical-alkene addition reactions has come entirely from molecular beam scattering and

chemiluminescence experiments [3] and ab initio quantum chemical calculations [4].

The energy redistribution and bond fission steps of the substitution process have been the focus of numerous bulk gas phase kinetic studies designed to determine if the unimolecular decomposition of chemically activated radicals is a statistical process. In a series of classic experiments [5], Rabinovitch and co-workers found that the rates of decomposition of alkyl radicals formed from the addition of H and D atoms to alkenes were in good agreement with the predictions of RRKM theory, implying that energy was randomized among all of the vibrational and internal rotational degrees of freedom of the activated radicals prior to unimolecular decay. Evidence for non-statistical energy redistribution in chemically activated radicals began to appear in the early 1970's with the work of Rynbrandt and Rabinovitch on the reaction of singlet methylene with hexafluorovinylcyclopropane [6] and with the crossed molecular beams experiments of Lee and coworkers on the reactions of F atoms with a number of unsaturated molecules, $F + R\text{-}X \rightarrow X + R\text{-}F$ (where X = H and CH_3) [3a,7,8].

In these crossed beam studies, the experimental product translational energy distributions, P(E'), were compared to ones derived from statistical calculations to arrive at a value for the "effective" number of vibrational modes in the collision complexes. The P(E') is sensitive to the distribu-

tion of vibration-rotation states along the reaction coordinate at the exit channel transition state but when there is a potential energy barrier in the exit channel, as there is for reactions involving elimination of H and CH_3, repulsive forces between the departing products will channel more energy into translation than would be expected on the basis of this internal state distribution [9]. A more straightforward comparison of experimental and statistical P(E')'s can be made for reactions that do not have exit channel barriers, such as substitution reactions involving halogen atom elimination [10].

The results of crossed beam studies of such reactions are by no means uniform, however. Experiments on F + (1,1-, cis-, and trans-) $C_2H_2Cl_2 \rightarrow Cl + C_2H_2ClF$ by Shobatake, Lee, and Rice [11] yielded P(E') distributions that were consistent with nearly complete energy randomization in the $[C_2H_2Cl_2F]^*$ collision complexes. Cheung, McDonald, and Herschbach [12] obtained statistical P(E') distributions for the reactions Cl + R-Br → Br + RCl for R-Br = C_2H_3Br and 1- and 2-C_3H_5Br, and a non-statistical distribution for R-Br = 3-C_3H_5Br. Their results were taken as evidence that the vinylic reactions proceed via 1,2 Cl migration whereas the allylic Br + 3-C_3H_5Br reaction involved 1,2 bond migration. However, in higher velocity resolution experiments, Buss et al. [13] found that the products of these Cl + R-Br reactions had far more translational energy than would be expected if

all of the vibrational modes of the collision complex participated in energy redistribution. Product vibrational energy distributions from chemiluminescence studies of these same reactions were also non-statistical [14]. Steele et al. [15] have recently reinvestigated $Cl + C_2H_3Br \rightarrow Br + C_2H_3Cl$ at a somewhat higher collision energy than ref. 13. Their results are in agreement with those of the earlier experiments.

In order to extend our understanding of intramolecular energy transfer in chemically activated radicals and of free radical substitution in general, we undertook crossed molecular beam studies of the endoergic reactions,

$$Br + \left\{ \begin{array}{c} CH_2CCl_2 \\ \text{trans-}CHClCHCl \end{array} \right\} \rightarrow Cl + \left\{ \begin{array}{c} CH_2CClBr \\ CHClCHBr \end{array} \right\} \quad \begin{array}{l} (1) \\ (2), \end{array}$$

($\Delta H_0^\circ \simeq 13$ kcal/mol) at four collision energies in the range 15 - 27 kcal/mol. Our motivations for studying endoergic substitution reactions were outlined at the start of the previous chapter. By investigating statistically unfavored channels for a series of isomeric reactions, one can potentially gain a deeper insight into the dynamics of the substitution process at different points along the reaction coordinate. One may begin, for instance, to establish a microscopic basis for familiar rules of chemical kinetics such as the reactivity-selectivity principle, according to which reactions with higher activation energies tend to be more regio-selective [16]. Towards this end, we have studied not only the translational energy distribution of the prod-

ucts but the collision energy dependence of the reaction cross sections, or excitation functions, as well.

Our results for the present reactions reinforce our conclusions in the previous chapter regarding the limited extent of intramolecular energy transfer in the bromo-chloro-cyclohexadienyl systems prior to Cl elimination. In fact, these smaller atom-alkene reactions may serve as heuristic models for endoergic substitution in larger molecular systems.

II. EXPERIMENTAL

The apparatus and Br atom source were described in the previous chapter. The Br source stagnation pressures, oven temperature, and nozzle-skimmer configuration were the same as described previously.

The dichloroethylene beam was formed by bubbling 450-500 torr of He through the cooled (-30°C) liquid reagent and expanding the resulting mixture through a 0.21 mm diameter nozzle. A conical stainless steel skimmer with an orifice diameter of 0.74 mm was positioned 0.9 cm from the nozzle. The vapor pressures of the reagents at -30°C are: 40 torr CH_2CCl_2 (1,1-DCE) and 17 torr trans-CHClCHCl (t-DCE). 1,1-DCE was purchased from Aldrich and t-DCE from Pfaltz and Bauer.

The collision energy was varied by seeding Br_2 in

different rare gases and by heating the DCE beam nozzle with a coaxial heater wire. A list of nozzle temperatures, peak laboratory beam velocities, speed ratios, and most-probable collision energies, E_c, is given in Table 1 along with values for the relative reactant flux at each energy, $n_{Br}n_{DCE}v_{rel}$, determined by measuring Br on DCE elastic scattering at a laboratory angle of 16° (see Section II of Chapter 2).

The 1,1- and 1,2-bromochloroethylene (1,1-, 1,2-BCE) products were monitored at m/e=140 ($C_2H_2Cl^{79}Br$) but the mass spectrometer resolution was set sufficiently low to allow some of the ^{81}Br containing product to be detected as well. Angular distributions were measured by modulating the DCE beam with a 150 Hz tuning fork chopper. Counting times were 6 - 18 minutes per angle. Product time-of-flight spectra were measured using the cross correlation method with a resolution of 10 μs/channel. The flight path from wheel to ionizer was 30.0 cm. Counting times ranged from 0.5-3 hr per angle.

A liquid nitrogen cooled copper cold finger was placed against the differential wall inside of the scattering chamber and facing the detector. This improved the signal-to-noise of the 1,1-BCE angular distribution, E_c=27 kcal/mol, by a factor of ≈3. The DCE reagents were distilled under dry nitrogen prior to use and stored under rare gas. Nonetheless, at all collision energies there was background at m/e=140 at angles near both beams from elastic and inelastic

scattering of impurities in the beams. This was most problematic at the lower collision energies where the product signal was weakest. The background near each beam was measured by substituting a properly diluted beam of Kr for the other beam. The in/elastic scattering angular distribution was then scaled to the product angular distribution and subtracted from it. However, for a few product angular distributions it was not possible to reproduce the slope of the in/elastically scattered signal near one or both beams with the Kr measurements. As a result, we either approximated the non-reactive angular distribution or used a non-reactive distribution obtained at another collision energy which had a similar slope.

III. RESULTS AND ANALYSIS

The BCE product angular distributions and TOF spectra for both reactions are plotted in Figs. 1 - 6. The peak m/e=140 count rates for the E_c=27 kcal/mol angular distributions were 50 Hz and 320 Hz for reactions 1 and 2 respectively.

The method of analyzing the data was essentially the same as that described in the previous chapter. At the two highest collision energies for each reaction the data were fit with a point form CM angular distribution, $T(\theta)$. We assumed ΔH°_0 = 13 kcal/mol for both reactions (see Section IV).

The product translational energy distributions, P(E'), for both reactions are similar in shape, with the 1,2-BCE distributions peaking at slightly higher energies than those for 1,1-BCE (Fig. 7, Table 2). $\langle E'/E_{avl} \rangle \approx 0.3$ for both reactions (where E_{avl} is the total energy available to the products). Note that we obtained approximately the same value of $\langle E'/E_{avl} \rangle$ for the Br + o-, p-chlorotoluene (CT) reactions [17]. The P(E') for reaction 1 at E_c=27 kcal/mol is in fair agreement with a RRKM-AM P(E') calculated assuming 4 active vibrational modes with frequencies in the range 250 - 550 cm^{-1} [18] and a maximum centrifugal barrier, B_m', of 0.70 kcal/mol (Fig. 7a). The 1,1-BCE angular distribution at this collision energy could not be fit well by a P(E') in which q=4 [17]. The similarity between the falling slopes of the P(E')'s for both reactions is particularly interesting considering that the angular dependence of the Cl + BCE interaction potential is likely to be different for the two reactions [10] (see discussion of S_r in Section IV).

Although the $T(\theta)$ distributions for reaction 1 (Fig. 8a) at E_c=27 and 21 kcal/mol are asymmetric, the areas, A, under the forward (0°-90°) and backward (90°-180°) parts of each distribution are comparable. At E_c=27 kcal/mol, R = A(0°-90°)/A(90°-180°) = 0.94 whereas at E_c=21 kcal/mol, R = 0.92. The E_c=17 kcal/mol data could be fit with a symmetric $T(\theta)$ composed of two Legendre polynomials. At this energy, the uncertainties associated with subtracting the m/e=140

background were relatively large. At E_c=15 kcal/mol, the signal-to-noise ratio is so poor that the laboratory angular distribution could be fit with an isotropic $T(\theta)$. We did not collect any TOF data at this collision energy.

Forward scattering of 1,2-BCE from reaction 2 is slightly favored at the three highest experimental collision energies (Fig. 8b). R = 1.07, 1.09, and 1.09, at E_c=27, 23, and 18 kcal/mol respectively. At E_c=17 kcal/mol, we had to guess at the slope of the non-reactive scattering angular distribution near the t-DCE beam so the uncertainties in the product angular distribution (especially for $\theta > 50°$) are large. This angular distribution could be fit with an isotropic $T(\theta)$. A CM flux contour diagram for reaction 2, E_c=23 kcal/mol, is presented in Fig. 9.

The differences between the CM angular and translational energy distributions for reactions 1 and 2 can be rationalized by considering the reactant orbital angular momenta, **L**, for the two reactions. Since the distance between the chlorinated carbon and the center of mass of the molecule is larger in t-DCE than in 1,1-DCE (≈0.7 vs. ≈0.4 Å), we would expect $\mathbf{L}_{(2)} > \mathbf{L}_{(1)}$ and $\tau_{rot(2)} < \tau_{rot(1)}$ if the two radicals had about the same moments of inertia, where τ_{rot} is the rotational period of the collision complex. Assuming that the Br atom approaches the chlorinated carbon perpendicular to the plane of the C=C bond, $\mathbf{L}_{(1)} \simeq 70\ \hbar$ and $\mathbf{L}_{(2)} \simeq 100\ \hbar$ at E_c=27 kcal/mol. The moments of inertia of the 2-bromo-2,2-

dichloroethyl (2,2-BDCE) and 2-bromo-1,2-dichloroethyl (1,2-BDCE) radicals about their rotation axes will be ≈350 and ≈400 amu·Å^2 respectively assuming that the β- (or 2-) carbon is sp^3 hybridized with C-Br and C-Cl bond lengths of 2.0 and 1.8 Å and that the C_α-Cl and C_α-H bonds lie in the original C=C plane. Therefore, neglecting the small rotational angular momenta of the reactants, τ_{rot} ≈ 5 ps for 2,2-BDCE and ≈4 ps for 1,2-BDCE. If the lifetimes of the BDCE radicals are comparable, we might expect slightly more forward scattering from reaction 2. The higher peak energies of the P(E')'s for (2), which indicate that $\mathbf{L'}_{(2)} > \mathbf{L'}_{(1)}$ (where the prime refers to products), also accord with $\mathbf{L}_{(2)}$ being greater than $\mathbf{L}_{(1)}$.

The approximate forward-backward symmetry in $T(\theta)$ for both of these reactions contrasts with the marked asymmetry in $T(\theta)$ for the Br + chlorotoluene (CT) reactions. Unlike Br + CT → BCMC, which is endoergic by ≈2 kcal/mol, Br addition to DCE is exoergic by ≈8 kcal/mol (see Section IV). This difference in exoergicity might explain the apparently larger values of τ/τ_{rot} for BDCE (where τ is the lifetime of the complex). We have calculated RRKM lifetimes for the bromodichloroethyl collision complex using approximate frequencies for the 15 vibrational modes of the energized radical and the 14 modes of the activated complex (Table 3). With E_0=8 and 21 kcal/mol for the Br and Cl elimination channels, we obtain lifetimes, τ_{RRKM}, of ≈0.5 and ≈0.3 ps for 2,2-BDCE and 1,2-

BDCE respectively at E_c=27 kcal/mol. As we found for BCMC, the calculated rotational periods for the BDCE complexes are considerably longer than the RRKM lifetimes. However, $\tau_{rot}/\tau_{RRKM} \approx 10$ for BDCE whereas the same ratio is ≈250 for BCMC [17]. Thus, the symmetry of the product angular distributions for the present reactions is most likely due to the longer lifetimes of the reaction intermediates.

The curvatures of the $T(\theta)$ distributions from θ=0°-40° and 140°-180° have a pronounced effect on the widths of the TOF spectra. The more suddenly $T(\theta)$ changes over a range of CM angles, the narrower the calculated TOF spectra at LAB angles in that range will be. In order for the calculated and experimental TOF spectra to agree in reaction 1, E_c=27 and 21 kcal/mol, and reaction 2, E_c=27 kcal/mol, $T(\theta)$ must rise more steeply at wide (140°-180°) than at small (0°-40°) CM scattering angles. The reverse is true for reaction 2 at E_c=23 kcal/mol.

The data at the highest collision energies might actually reflect a narrowing of the product translational energy distribution at wider angles. It is possible that, as a consequence of angular momentum conservation, the CM product translational energy and scattering angle distributions are coupled. When the initial reactant rotational angular momentum is negligible and **L** and **L'** are of comparable magnitude, high **L** collisions will contribute most strongly to scattering at 0° and 180° in a reaction that proceeds through

a long-lived complex. The rotational energy of the complex at its exit transition state will go into product translation so the P(E') distributions for scattering near 0° and 180° would be expected to peak at higher energies [13]. When the lifetime of the collision complex is comparable to or shorter than its rotational period, an asymmetry in the θ-**L** coupling might arise, with small **L** (long τ_{rot}) collisions dominating scattering at wide angles and large **L** (small τ_{rot}) contributing most strongly to scattering at small angles. In such a case, we would expect the translational energy distributions for backward scattered products to peak at lower energies than those for forward scattered products.

A comparison of the reduced masses and the most-probable relative velocities of the reactants and products for both reactions indicates that, in all cases, the average exit impact parameter would have to be ≈3 - 4 times larger than the average entrance impact parameter for **L'** ≃ **L**. However, the relatively strong peaking in $T(\theta)$ at 0° and 180° [19] and the fact that the peak energies of the P(E')'s, E'_{pk}, which are proportional to $|\mathbf{L}'|^2$, increase with **L** (i.e., $E'_{pk} \propto E_c$ and $E'_{pk}(2) > E'_{pk}(1)$) indicate that **L'** may be sufficiently large in the present reactions for us to observe a moderate coupling between CM scattering angle and recoil velocity.

The excitation functions, S_r, used to reproduce the relative intensities of the LAB angular distributions are plotted in Figs. 10 - 12. The shaded regions indicate the

uncertainties in S_r above the highest most-probable collision energies. The thresholds were set at 13.5 kcal/mol since this helped in obtaining the proper scaling factor for the 1,1-BCE, E_c=15 kcal/mol, angular distribution. The poor signal-to-noise of the low energy angular distributions and relatively wide spread in collision energy prevents us from determining the thresholds to these reactions accurately. (Note that at E_c=15 kcal/mol, a large fraction of the Br + 1,1-DCE collisions have insufficient energy to overcome the endoergicity to Cl substitution.)

The slopes of the two experimental excitation functions do not differ drastically from one another. S_r(1,2-BCE) agrees well with an 8-mode (ν = 200 - 800 cm^{-1}; E_0=8 and 21.5 kcal/mol) RRKM branching ratio curve, S_{RRKM}, whereas S_r(1,1-BCE) is in qualitative agreement with a 6-mode RRKM function (ν = 200 - 650 cm^{-1}) (Figs. 11,12) [17]. Near threshold, S_r(1,1) agrees best with a 5-mode RRKM curve but, as just noted, the excitation functions are inaccurate in this region. The relative magnitudes of the substitution cross sections for the two reactions will be discussed below.

We tried to determine the extent of Br elimination, $[BDCE]^* \rightarrow Br + DCE$, in both reactions by measuring TOF spectra at m/e=79 and m/e=96 near the center-of-mass angle at several collision energies. At all energies, however, in/elastic scattering of the reactants dominated the spectra.

1,1-DCE has C-C-Cl (B_1) and Cl-C-Cl (A_1) bending modes

at 375 and 299 cm^{-1}; t-DCE has C-C-Cl bending modes of A_g and B_u symmetry at 349 and 250 cm^{-1} [20]. Assuming no relaxation of these vibrations during supersonic expansion, the fraction of DCE molecules in the beam that has at least one quantum of C-C-Cl or Cl-C-Cl bend ($f_{v>0}$) is ≈50% at a nozzle temperature of 30°C. For each reaction, $f_{v>0}$ changes by ≈10% over the experimental nozzle temperature range (Table 1). It is possible that energy in these bending vibrations can couple into the C-Cl reaction coordinate and thereby affect our measurements of the translational energy dependence of the substitution cross sections near threshold. Manning et al. [21] found no enhancement in the rate constant for the reaction(s) O + C_2H_4 → [products] with vibrationally excited C_2H_4, but their analysis is based upon a complicated kinetic scheme for excitation and deactivation of the reagent involving rate constants of unknown magnitude. Also, Hase et al. [22] concluded from classical trajectory calculations that two quanta in the CH_2 wagging mode of ethylene has little effect on the H + C_2H_4 addition cross section.

IV. DISCUSSION

Reactions 1 and 2 are not likely to differ much in endoergicity. Rosenstock et al. [23] report the heats of formation (ΔH°_{f0}) of 1,1-DCE and t-DCE to be 2.01 and 2.76 kcal/mol respectively. The heats of formation of the

C_2H_2ClBr isomers are unknown. However, ΔH°_0 = 12.4 kcal/mol for the reaction Br + $C_2H_3Cl \rightarrow C_2H_3Br$ + Cl [23,24]. We assume that the C-X (X = Br, Cl) bond dissociation energies in the isomers of $C_2H_2Cl_2$ and C_2H_2ClBr differ by less than 1 kcal/mol from those in C_2H_3Br and C_2H_3Cl and take ΔH°_0 = 13 kcal/mol for reactions 1 and 2.

The activation energies for halogen atom addition to alkenes are known to be very small or zero [25]. From experiments on the photochemical bromination of t-DCE, Schumacher [26] concluded that there is no activation energy to the reaction Br + t-DCE → 1,2-BDCE. The activation energies for Cl addition to ethylene and its chlorinated derivatives are uniformly ≈0 kcal/mol [27].

As mentioned in the previous chapter, the thermochemistry of Br addition to unsaturated molecules is not well understood. Benson and O'Neal [28] report ΔH°_{298} = -8.8 kcal/mol for the reaction Br + $C_2H_4 \rightarrow C_2H_4Br$. With ΔH°_0 = 12.4 kcal/mol for Br + $C_2H_3Cl \rightarrow$ Cl + C_2H_3Br and D°_0(C-Cl) = 19.3 kcal/mol for $CH_2CHClBr$ [4c,23,29], ΔH°_0 = -7.0 kcal/mol for the same reaction. The C=C bond dissociation energies in $C_2H_2Cl_2$ and C_2H_4 (D°_{298} ≈ 143 vs. 172 kcal/mol [30]) do not differ enough for Br + $C_2H_2Cl_2 \rightarrow C_2H_2Cl_2Br$ to be significantly more exoergic than Br + $C_2H_4 \rightarrow C_2H_4Br$. (Br addition to CH_2CF_2, in which D°_{298}(C=C) = 130 kcal/mol [30], is just ≈4 kcal/mol more exoergic than Br addition to C_2H_4 [31].) Indeed, the reactions (a) Cl + $C_2H_4 \rightarrow C_2H_4Cl$ and (b) Cl +

$CHClCHCl \rightarrow CHClCHCl_2$ have the same exothermicity within experimental error (ΔH°_{298} = -20.2 [4c,23] vs. -19.7 ± 3 [32] kcal/mol). There is evidence that CH_2CCl_3 is an unstable species which undergoes rapid 1,2 Cl migration [33,34]. But, using group additivity, Franklin and Huybrechts [32] calculate ΔH°_{298} = -15.3 kcal/mol for Cl + $CH_2CCl_2 \rightarrow CH_2CCl_3$, which agrees with ΔH°_{298} for (b) within the stated uncertainties. Thus, the C-Br bond energies in 2,2- and 1,2-BDCE may not differ greatly from that in CH_2CH_2Br.

As for the Br + CT reactions, the P(E') distributions and excitation functions for the Br + DCE reactions imply that only a limited number of vibrational modes in the energized radicals participate in energy redistribution prior to Cl elimination. Our analysis suggests that the fraction of active modes is roughly the same in 2,2- and 1,2-BDCE. This is noteworthy considering that 2,2-BDCE has more low frequency Cl-C-X (X = Cl, Br) bending modes (ν = 200 - 300 cm^{-1}) than 1,2-BDCE and that these modes are principally associated with the carbon atom that was attacked. It is thus possible that a similar subset of modes is excited in both reactions. Most striking, however, is that the number of active modes remains approximately the same for both the Br + DCE and Br + CT reactions. This finding reinforces our earlier conclusion that substitution of Cl for Br in Br + CT is a localized, or quasi-direct, process and suggests that endoergic atom-alkene substitution reactions can serve as

models for endoergic atom-aromatic molecule reactions.

The crossed beam studies of the exoergic substitution reactions F + (1,1-, trans-) $C_2H_2Cl_2$ → Cl + C_2H_2ClF ($\Delta H^\circ \simeq$ -30 kcal/mol; $E_c \simeq$ 2.5 kcal/mol) [11] yielded CM frame C_2H_2ClF angular distributions for both reactions that were isotropic and product translational energy distributions that were consistent with collision complexes in which nearly all of the vibrational modes participated in energy redistribution. Whereas $\langle E'/E_{avl} \rangle \simeq 0.16$ for these reactions, earlier experiments gave $\langle E'/E_{avl} \rangle \simeq 0.11$ for the roughly isoenergetic F + C_6H_5Cl → Cl + C_6H_5F reaction [35]. This difference in average translational energy was attributed to a smaller number of active vibrational modes in the $[C_2H_2Cl_2F]^*$ collision complexes. However, the <u>fraction</u> of active modes in these complexes was found to be larger than that in $[C_6H_5ClF]^*$.

Although the additional C_β-Cl bond in 2,2-BDCE may not appreciably enhance intramolecular energy transfer, the presence of this bond in 1,1-DCE appears to have a pronounced effect on the magnitude of the substitution cross section for reaction 1. At E_c=27 kcal/mol, $S_r(1,1)$ is ≈6 times smaller than $S_r(1,2)$. (Note that although t-DCE has two identical carbon atoms available for Br attack, the reaction path degeneracy for Cl elimination from 2,2-BDCE is twice that for 1,2-BDCE.) Thus, if the two BDCE isomers have roughly the same number of active modes, the cross section for Br

addition, σ_{add}, to 1,1-DCE must be lower than that to t-DCE.

The original theory of anti-Markownikoff addition, formulated to explain the kinetics of HBr addition to alkenes in the presence of peroxides or ultraviolet light, postulated that the preferred site of radical attack is determined by the relative stabilities of the two possible adducts [36]. Thus, addition to the least substituted carbon atom would be favored since the resulting adduct radical will be resonance stabilized. There is, however, a paucity of data on the heats of formation of halogenated alkyl radicals so it is difficult to argue on thermodynamic grounds about preferred pathways for addition. As mentioned above, the experimental evidence for the chlorinated ethyl radicals indicates that $D^{\circ}(C_{\beta}\text{-Cl})$ is relatively independent of the extent of chlorination [32]. Johari et al. [37] have shown that the rate of addition of CCl_3 to the CF_2 end of $CHClCF_2$ is 25 times greater than the rate of addition to the CHCl end, a result that is inconsistent with the notion that resonance stabilization of the adduct determines the preferred position of attack. Indeed, Tedder and Walton have argued convincingly that the orientation of many radical addition reactions can be correlated straightforwardly with the bulk of the radical and the substituents on the alkene as well as with the relative electronegativities of the reagents [2a,c].

Experiments on radical addition to alkenes indicate that Cl substituents strongly influence rate constants for addi-

tion. Chiltz et al. [27] report values of log A for the reactions Cl + C_2H_4 → C_2H_4Cl and Cl + C_2Cl_4 → C_2Cl_5 of 10.2 and 9.4 respectively. Since these reactions have no activation energy, this is equivalent to a six-fold difference in rate constant. Bertrand et al. [38] studied the products of the Cl-photosensitized oxidation of C_2HCl_3 and isomers of $C_2H_2Cl_4$ and concluded that the rate constant for Cl addition to the less chlorinated carbon atom in C_2HCl_3 is at least 8 times greater than that for addition to the more chlorinated carbon. Johari et al. [37] have found that CCl_3 adds ≈300 times more readily to the CHCl end of $CHCl=CCl_2$ than to the CCl_2 end. The simplest explanation of these data and our results for Br + 1,1-DCE is that Cl substituents hinder approach of the attacking atom and thereby reduce the probability of addition.

The slopes of the excitation functions suggest that the two BDCE complexes have about the same number of active modes but if σ_{add} were dependent on collision energy, the curvature of S_r would not simply reflect the energy dependence of the statistical branching ratio [17]. According to the classical RRK theory [39],

$$\eta_{Cl}/(\eta_{Cl} + \eta_{Br}) \propto [(\varepsilon^{\dagger}_{Br}/\varepsilon^{\dagger}_{Cl})^{s-1} + 1]^{-1},$$

(where η_X is the probability of X elimination, $\varepsilon^{\dagger}_X$ is the excess energy at the critical configuration, E^*-E_0, and s is the number of active vibrational modes) so, for two reactions with the same energetics, the one with the larger number of

modes involved in energy sharing should have the lower substitution cross section and the steeper excitation function. Thus, $S_r(1,1)$ could be lower than $S_r(1,2)$ partly because 2,2-BDCE has more active modes but, in order for the slopes of the two excitation functions to be similar, $\sigma_{add}(1,1)$ would have to decrease, or $\sigma_{add}(1,2)$ would have to increase, with increasing collision energy.

Based on our discussion of the Br + CT excitation functions [17], however, the cross section for Br addition to the sterically hindered 1- carbon of 1,1-DCE would be more likely to show a positive energy dependence. We would also not expect the Br + t-DCE interaction potential to depend more strongly on approach angle than that for Br + 1,1-DCE. So, it does not appear reasonable to invoke differences in the number of active modes along with an energy dependent addition cross section to explain the lower substitution cross section for reaction (1). It is more likely that steric effects cause $\sigma_{add}(1,1) < \sigma_{add}(1,2)$ at all collision energies. Note, however, that the number of low frequency vibrational modes in the vicinity of the collision appears to have a much smaller effect on the Br addition cross section in the present reactions than in the Br + chlorinated aromatic reactions.

In their crossed beam study of the F + 1,1- and t-DCE reactions, Shobatake et al. [11] found that $S_r(1,1)$ was only slightly ($\approx$20%) smaller than $S_r(1,2)$. (The substitution

cross section for cis-DCE was comparable to that for 1,1-DCE). Indeed, we would not expect F atom addition reactions to be very site selective considering their large exoergicity ($-\Delta H^\circ_0$ = 40 - 50 kcal/mol). In the endoergic Br + DCE reactions, where Br addition is less exoergic and the substitution process is more direct, subtle differences among the isomeric potential energy surfaces (i.e., in the angular dependence of the Br-DCE interaction potential and in the slope of the potential energy surface along the reaction coordinate) [17] will manifest themselves more strongly in the reaction cross sections. In particular, long range atom-molecule attractive forces will cause the transition state for F atom addition at low collision energies to occur "earlier" along the reaction coordinate, i.e., at a larger C-X (X = F, Br) internuclear distance, than that for Br addition at elevated energies [3d]. Thus, steric effects are more likely to dominate the Br addition cross section.

The question of migration

Given the evidence that atoms and radicals add preferentially to the less substituted end of chlorinated derivatives of ethylene, it is worth considering the likelihood that 1,1-dichloro-2-bromoethyl radicals formed from Br addition to the CH_2 end of 1,1-DCE rearrange via Br or Cl migration and subsequently decompose to give Cl + 1,1-BCE. There is a large body of data on the stereo-specific addition of HBr to al-

kenes that has been interpreted as evidence for 1,2 bridged bromoalkyl radicals [40]. ESR experiments on 2-chloroethyl radical [41] and 2-bromo-tert-butyl radical ($BrCH_2\dot{C}(CH_3)_2$) [42] suggest that these species do exist in preferred conformations, the former with a planar radical center and the C-Cl bond eclipsing the unpaired electron orbital and the latter with a nonplanar radical center and the C-Br bond gauche staggered with respect to the unpaired orbital. (The bromoethyl radical has not been observed by ESR spectroscopy [43].) However, no evidence for symmetrical bridging of the halogen atom was found in these studies. Ab initio calculations on 2-chloroethyl radical predict that the chlorinated carbon atom is tetrahedral [4c,44] and that the symmetrically bridged structure is unstable with respect to dissociation to $Cl + C_2H_4$ [44].

In a study of the $Cl + C_2H_3Br$ reaction using radioactive ^{38}Cl atoms and HI as a radical scavenger, Iyer and Rowland [45] found that the yields of (I) $CH_2{}^{38}ClCH_2Br$ (the product of the reaction of the stabilized adduct $CH_2{}^{38}ClCHBr$ with HI) and (II) $CH_2{=}CH^{38}Cl$ were both pressure dependent, the dominant product being (I) at higher pressures and (II) at lower pressures. The yield of $CH_3CH^{38}ClBr$ (from $CH_2CH^{38}ClBr$) was always less than 0.1%. They rule out a mechanism in which unimolecular decomposition of $CH_2CH^{38}ClBr$ through Br elimination is much more rapid than its collisional stabilization and explain their results by invoking halogen atom

migration (either Cl or Br) to give the substitution product (II).

We see no reason why Br or Cl migration should be important in the present reactions. The reduced substitution cross section observed for 1,1-DCE is straightforwardly explained by a lower probability for Br addition to the chlorinated carbon. Although the rotational barrier to 2 → 1 Br migration in 2-bromo-1,1-dichloroethyl radical is only ≈3 kcal/mol at E_c=27 kcal/mol, it seems unlikely that a migrating Br atom will have as good a chance of displacing a Cl atom as one that directly attacks the 1-carbon of 1,1-DCE. The translational energy distribution and excitation function for reaction 1 both suggest that fewer vibrational degrees of freedom are active in the endoergic substitution process than one might expect if Br had to migrate to displace Cl. Also, the similarity between the P(E')'s and excitation functions for (1) and (2) argues that the dynamics of the two reactions (after the initial addition step) are rather similar.

V. CONCLUSIONS

Our results for the Br + DCE → Cl + BCE reactions are consistent with the model described in the previous chapter whereby endoergic substitution occurs most readily when it is a quasi-direct process. Exoergic Br elimination is always the statistically favored mode of decay of the BDCE collision

complex but Cl elimination becomes a competitive channel when vibrational energy redistribution is limited. Although the slopes of the P(E')'s and excitation functions for both reactions are comparable, $S_r(1,1)$ is substantially lower than $S_r(1,2)$ at most collision energies, suggesting that steric effects play a dominant role in determining the relative magnitudes of the substitution cross sections. Such effects are likely to be observable only in reactions that have large energetic thresholds. Finally, the similarity between the "effective" number of vibrational modes in the Br + DCE and Br + CT reactions offers the intriguing possibility that endoergic aromatic substitution reactions can be modeled by analogous atom-alkene reactions.

REFERENCES

1. M. S. Kharasch, H. Engelmann, and F. R. Mayo, J. Org. Chem. 2, 288 (1937); D. H. Hey and W. A. Waters, Chem. Rev. 21, 169 (1937).

2. For overviews see: (a) J. M. Tedder and J. C. Walton, Accts. Chem. Res. 9, 183 (1976); (b) D. C. Nonhebel and J. C. Walton, Free Radical Chemistry (Cambridge University Press, Cambridge, 1974); (c) J. M. Tedder, Angew. Chem. Int. Ed. Engl. 21, 401 (1982); (d) B. Giese, Angew. Chem. Int. Ed. Engl. 22, 753 (1983).

3. (a) J. M. Farrar and Y. T. Lee, Ann. Rev. Phys. Chem. 25, 357 (1974); (b) J. G. Moehlmann, J. T. Gleaves, J. W. Hudgens, and J. D. McDonald, J. Chem. Phys. 60, 4790 (1974); (c) J. G. Moehlmann and J. D. McDonald, J. Chem. Phys. 62, 3052 (1975); (d) Chapter 1 of this thesis.

4. (a) C. S. Sloane and W. L. Hase, Faraday Discuss. Chem. Soc. 62, 210 (1977); (b) W. L. Hase, G. Mrowka, and R. J. Brudzynski, J. Chem. Phys. 69, 3548 (1978); (c) H. B. Schlegel and C. Sosa, J. Phys. Chem. 88, 1141 (1984); (d) H. B. Schlegel, J. Phys. Chem. 86, 4878 (1982); (e) C. Sosa and H. B. Schlegel, J. Am. Chem. Soc. 109, 4193 (1987); (f) S. Kato and K. Morokuma, J. Chem. Phys. 72, 206 (1980); (g) H. B. Schlegel, K. C. Bhalla, and W. L. Hase, J. Phys. Chem. 86, 4883 (1982); (h) J. R. Hoyland, Theoret. Chim. Acta 22, 229 (1971).

5. For a review see: B. S. Rabinovitch and M. C. Flowers, Quart. Rev. 18, 122 (1964).

6. J. D. Rynbrandt and B. S. Rabinovitch, J. Chem. Phys. 54, 2275 (1971); J. D. Rynbrandt and B. S. Rabinovitch, J. Phys. Chem. 75, 2164 (1971).

7. J. M. Farrar and Y. T. Lee, J. Chem. Phys. 65, 1414 (1976).

8. For related observations in an ion-molecule reaction see: A. Lee, R. L. Leroy, Z. Hermann, and R. Wolfgang, Chem. Phys. Lett. 12, 569 (1972).

9. (a) R. A. Marcus, Faraday Discuss. Chem. Soc. 55, 379, 381 (1973); (b) R. A. Marcus, J. Chem. Phys. 62, 1372 (1975); (c) W. L. Hase and K. C. Bhalla, J. Chem. Phys. 75, 2807 (1981).

10. Quack has argued that, even in the absence of a potential energy barrier along the reaction coordinate, the angular dependence of the atom-molecule interaction potential can cause the P(E') to appear non-statistical when all vibrational modes are active; see: M. Quack, Chem. Phys. 51, 353 (1980).

11. K. Shobatake, Y. T. Lee, and S. A. Rice, J. Chem. Phys. 59, 6104 (1973).

12. J. T. Cheung, J. D. McDonald, and D. R. Herschbach, J. Am. Chem. Soc. 95, 7889 (1973).

13. R. J. Buss, M. J. Coggiola, and Y. T. Lee, Faraday Discuss. Chem. Soc. 67, 162 (1979).

14. J. F. Durana and J. D. McDonald, J. Chem. Phys. 64, 2518 (1976).

15. T. A. Steele, N. Bradshaw, and R. Grice, Mol. Phys. 56, 1117 (1985).

16. (a) S. W. Benson, Thermochemical Kinetics (Wiley, New York, 2nd ed., 1976), Ch. 5; (b) B. Giese, Angew. Chem. Int. Ed. Engl. 16, 125 (1977).

17. Chapter 2 of this thesis.

18. S. A. Safron, N. D. Weinstein, D. R. Herschbach and J. C. Tully, Chem Phys. Lett. 12, 564 (1972).

19. W. B. Miller, S. A. Safron, and D. R. Herschbach, Faraday Discuss. Chem. Soc. 44, 108 (1967).

20. L. M. Sverdlov, M. A. Kovner and E. P. Krainov, Vibrational Spectra of Polyatomic Molecules (Wiley, New York, 1974).

21. R. G. Manning, W. Braun, and M. J. Kurylo, J. Chem. Phys. 65, 2609 (1976).

22. W. L. Hase, D. M. Ludlow, R. J. Wolf and T. Schlick, J. Phys. Chem. 85, 958 (1981).

23. H. M. Rosenstock, K. Draxl, B. W. Steiner and J. T. Herron, J. Phys. Chem. Ref. Data 6, suppl. 1 (1977).

24. Z. B. Alfassi, D. M. Golden, and S. W. Benson, J. Chem. Thermodyn. 5, 411 (1973). These authors report a group additivity value for ΔH°_{f298} (C_2H_3Cl) that is 3.5 kcal/mol lower than the value given in ref. 23 which would yield ΔH°_{298} = 16.1 kcal/mol for this reaction.

ΔH°_{298} = 12.5 kcal/mol from ref. 23.

25. J. A. Kerr and M. J. Parsonage, Evaluated Kinetic Data on Gas Phase Addition Reactions (CRC, Cleveland, 1972).

26. K. L. Muller and H. J. Schumacher, Z. Phys. Chem. B42, 327 (1939).

27. G. Chiltz, P. Goldfinger, G. Huybrechts, G. Martens, and G. Verbeke, Chem. Rev. 63, 355 (1963).

28. S. W. Benson and H. E. O'Neal, Kinetic Data on Gas Phase Unimolecular Reactions (NSRDS-NBS 21, US Dept. of Commerce, Washington, DC, 1970).

29. This calculation assumes that D°_{0}(C-Cl) in $CH_2CHClBr$ is the same as that in CH_2CH_2Cl.

30. E. A. Carter and W. A. Goddard III, J. Phys. Chem. 90, 998 (1986).

31. T. K. Minton, G. M. Nathanson, and Y. T. Lee, J. Chem. Phys. 86, 1991 (1987).

32. J. A. Franklin and G. H. Huybrechts, Int. J. Chem. Kinet. 1, 3 (1969).

33. P. B. Ayscough, F. S. Dainton, and B. E. Fleischfresser, Trans. Faraday Soc. 62, 1838 (1966).

34. W. H. Urry and J. R. Eiszner, J. Am. Chem. Soc. 74, 5822 (1952).

35. K. Shobatake, Y. T. Lee, and S. A. Rice, J. Chem. Phys. 59, 1435 (1973).

36. F. R. Mayo and C. Walling, Chem. Rev. 27, 351 (1940).

37. D. P. Johari, H. W. Sidebottom, J. M. Tedder, and J. C.

Walton, J. Chem. Soc. B, 95 (1971).

38. L. Bertrand, J. A. Franklin, P. Goldfinger, and G. Huybrechts, J. Phys. Chem. 72, 3926 (1968).

39. P. J. Robinson and K. A. Holbrook, Unimolecular Reactions (Wiley, New York, 1972).

40. (a) B. A. Bohm and P. I. Abell, Chem. Rev. 62, 599 (1962); (b) P. S. Skell and K. J. Shea, in Free Radicals, edited by J. Kochi (Wiley, New York, 1973), vol. 2, pp. 809-852.

41. (a) A. J. Bowles, A. Hudson, and R. A. Jackson, Chem. Phys. Lett. 5, 552 (1970); (b) T. Kawamura, D. J. Edge, and J. K. Kochi, J. Am. Chem. Soc. 94, 1752 (1972); (c) K. S. Chen, I. H. Elson, and J. K. Kochi, J. Am. Chem. Soc. 95, 5341 (1973); (d) I. H. Elson, K. S. Chen, and J. K. Kochi, Chem. Phys. Lett. 21, 72 (1973).

42. R. V. Lloyd and D. E. Wood, J. Am. Chem. Soc. 97, 5986 (1975).

43. D. J. Edge and J. K. Kochi, J. Am. Chem. Soc. 94, 6485 (1972).

44. A. C. Hopkinson, M. H. Lien, and I. G. Csizmadia, Chem. Phys. Lett. 71, 557 (1980).

45. R. S. Iyer and F. S. Rowland, Chem. Phys. Lett. 103, 213 (1983).

Table 1: Experimental conditions for the Br + DCE reactions.

Reaction		E_c[a]	$n_{Br}n_{DCE}v_{rel}$[b]	Br v_{pk}[d]	Br S[e]	T[c]	DCE v_{pk}	DCE S
Br/He	+ 1,1-DCE	27	1.00	18.1	6.2	192	12.5	12.8
Br/Ne	+ 1,1-DCE	21	0.87	15.2	7.4	192		
Br/Ar	+ 1,1-DCE	17	0.82	12.4	9.5	192		
Br/Ar	+ 1,1-DCE	15	0.77	*	*	107	10.6	12.6
Br/He	+ t-DCE	27	0.97	*	*	90	13.7	15.0
Br/Ne	+ t-DCE	23	0.74	*	*	90		
Br/Ar	+ t-DCE	18	0.64	*	*	90		
Br/Ar	+ t-DCE	17	0.51	*	*	37	12.2	14.3

(a): Energies are in kcal/mol; collision energies reflect cross section weighting.

(b): Arbitrary units.

(c): Nozzle temperature, °C.

(d): Peak laboratory velocity in units of 10^5 cm/s.

(e): Speed ratio.

(*): Given above.

Table 2: Fraction of available energy in product translation and P(E') parameters.[a]

Reaction	E_c[b]	$\langle E'/E_{avl} \rangle$[c]	p	q	B
Br + 1,1-DCE	27	0.26	0.080	2.1	0.08
	21	0.26	0.040	2.1	0.05
	17	0.26	0.040	2.1	0.06
	15	0.32	0.080	1.5	0.06
Br + t-DCE	27	0.28	0.12	1.9	0.08
	23	0.28	0.10	1.9	0.05
	18	0.29	0.12	1.9	0.06
	17	0.29	0.13	1.9	0.05

(a): See Chapter 2 for functional form of P(E').

(b): kcal/mol

(c): Fraction for most-probable collision energy.

Table 3: 2,2-BDCE and 1,2-BDCE vibrational frequencies used in statistical calculations.[a]

2,2-BDCE			1,2-BDCE		
complex	critical configuration		complex	critical configuration	
	[C-Cl]†	[C-Br]†		[C-Cl]†	[C-Br]†
3000	3000	*	3000	3000	*
2900	3000	*	2900	3000	*
1350	1550	*	1350	1550	*
1350	1400	*	1150	1200	*
1150	1200	*	1000	1100	*
1150	1200	*	1050	1000	*
650^{rc1}		750	950	600	950
650	750	*	800	900	400
550^{rc2}	650		700	750	*
350	250	350	650^{rc1}		750
350	350	*	550^{rc2}	650	
300	250	350	350	350	*
250	300	200	350	300	*
200	250	150	250	300	200
200	150	*	200	250	*

(a): Frequencies in cm^{-1}; moments of inertia of complex and critical configuration set equal to one another.

(*): Same as [C-Cl]† critical configuration.

($rc1$, $rc2$): Cl and Br elimination reaction coordinates respectively.

FIGURE CAPTIONS

Fig. 1: 1,1-BCE (m/e=140) product angular distribution from reaction 1.

⊙: E_c=27 kcal/mol; ○: E_c=21 kcal/mol;

□: E_c=17 kcal/mol; □: E_c=15 kcal/mol.

Signal is normalized to constant reactant flux but peak of E_c=27 distribution is scaled to unity. Br beam is at 0°. Solid lines are fits to data using CM distributions in Figs. 7 and 8 and excitation function in Fig. 11. Center-of-mass angles, in order of decreasing collision energy are: 38°, 44°, 50°, and 44°.

Fig. 2: 1,2-BCE (m/e=140) product angular distribution from reaction 2.

⊙: E_c=27 kcal/mol; ○: E_c=23 kcal/mol;

□: E_c=18 kcal/mol; □: E_c=17 kcal/mol.

See Fig. 1. Excitation function used in fit is plotted in Fig. 12. Center-of-mass angles, in order of decreasing collision energy, are: 42°, 46°, 53°, and 49°.

Fig. 3: 1,1-BCE (m/e=140) time-of-flight spectra at E_c=27 kcal/mol. Solid lines represent fits to data using CM functions in Figs. 7 and 8 and excitation

function in Fig. 11.

Fig. 4: 1,1-BCE (m/e=140) time-of-flight spectra. (a) E_c=21 kcal/mol; (b) E_c=17. See Fig. 3.

Fig. 5: 1,2-BCE (m/e=140) time-of-flight spectra. (a) E_c=27 kcal/mol; (b) E_c=23. See Fig. 3. Excitation function used in fit is plotted in Fig. 12.

Fig. 6: 1,2-BCE (m/e=140) time-of-flight spectra. (a) E_c=18 kcal/mol; (b) E_c=17. See Fig. 5.

Fig. 7: CM frame product translational energy distributions used in fits.
(a) Reaction 1: —— E_c=27 kcal/mol; — — E_c=21; — - — E_c=17; — - - - — E_c=15; - - - 4-mode RRKM-AM calculation.
(b) Reaction 2: —— E_c=27 kcal/mol; — — E_c=23; — - — E_c=18; — - - - — E_c=17.

Fig. 8: CM frame angular distributions used in fits.
(a) 1,1-BCE: —— E_c=27 kcal/mol; — — E_c=21; — - — E_c=17. E_c=15 distribution is isotropic.
(b) 1,2-BCE: —— E_c=27 kcal/mol; — — E_c=23; — - — E_c=18. E_c=17 distribution is isotropic.

Fig. 9: Center-of-mass frame product flux contour diagram for reaction 2, E_c=23 kcal/mol. Scale is for contours; scale for kinematic ("Newton") diagram is half of contour scale.

Fig. 10: Excitation functions for reactions 1 (— —) and 2 (———). Insert shows threshold region.

Fig. 11: Excitation function for reaction 1. Shaded region indicates uncertainty in S_r above the highest most-probable collision energy.

O: 6-mode RRKM branching ratio calculation.

Fig. 12: Excitation function for reaction 2. See Fig. 11.

O: 8-mode RRKM branching ratio calculation.

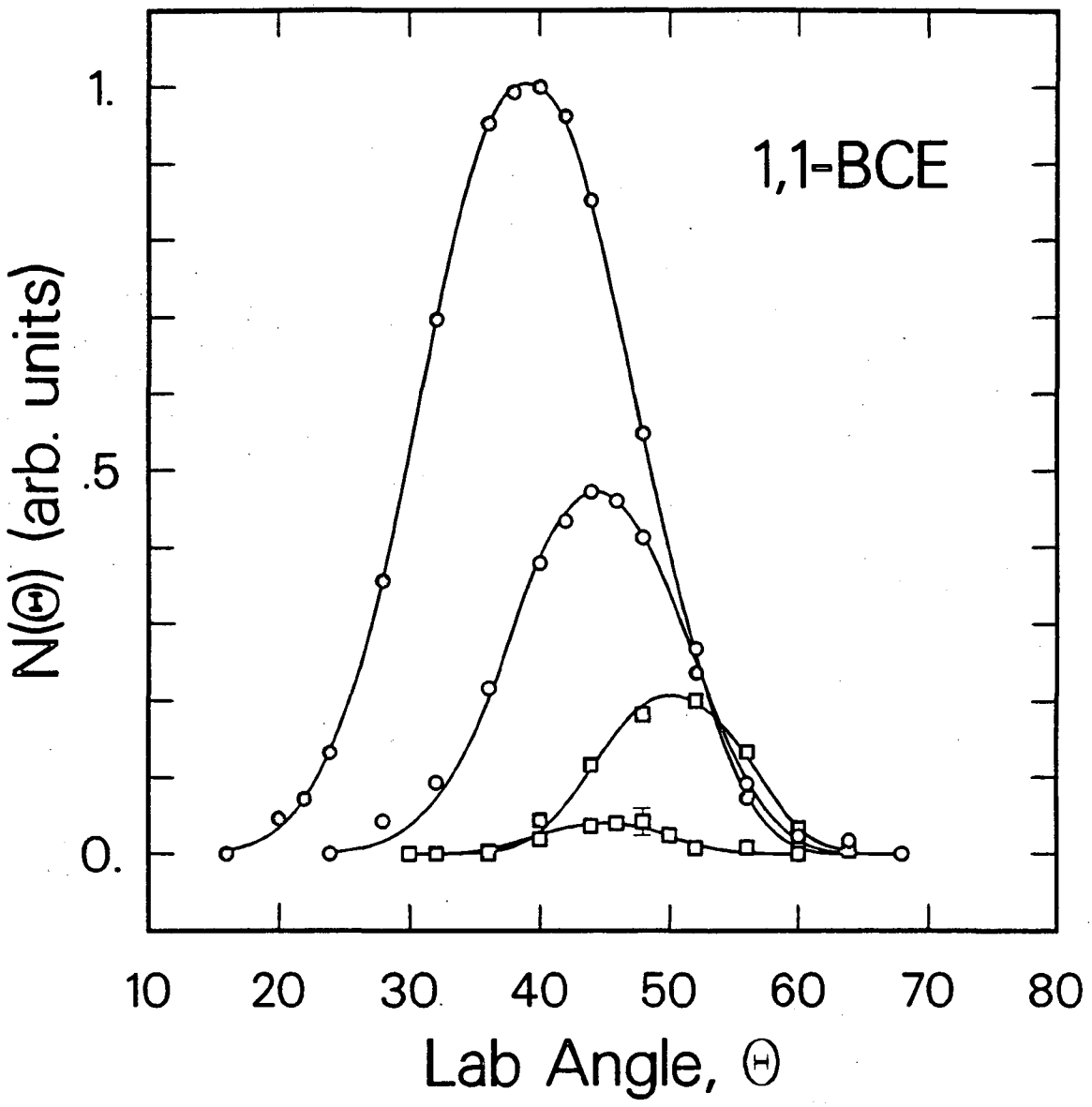

XBL 8712-5333

Figure 1

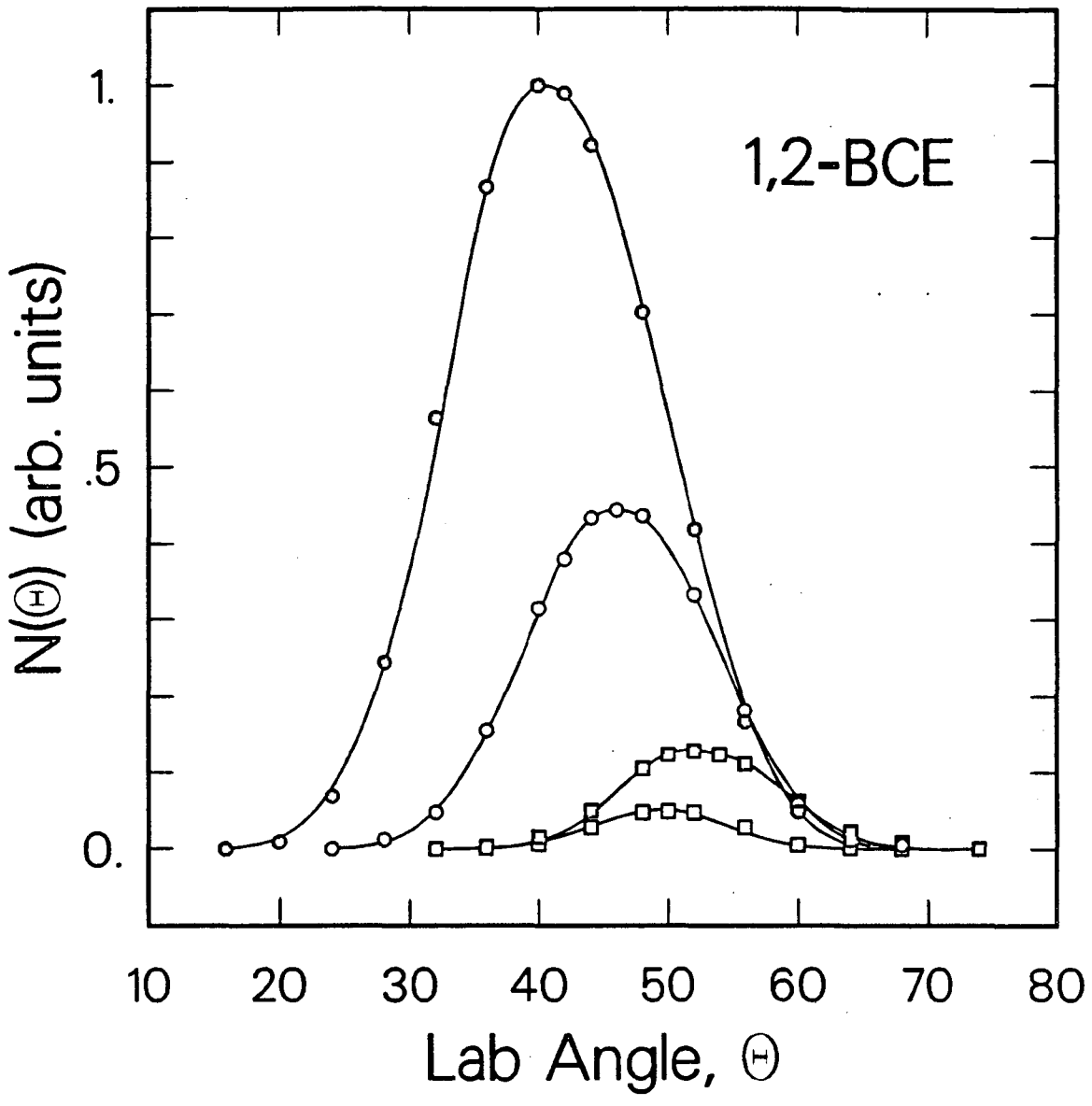

XBL 8712-5332

Figure 2

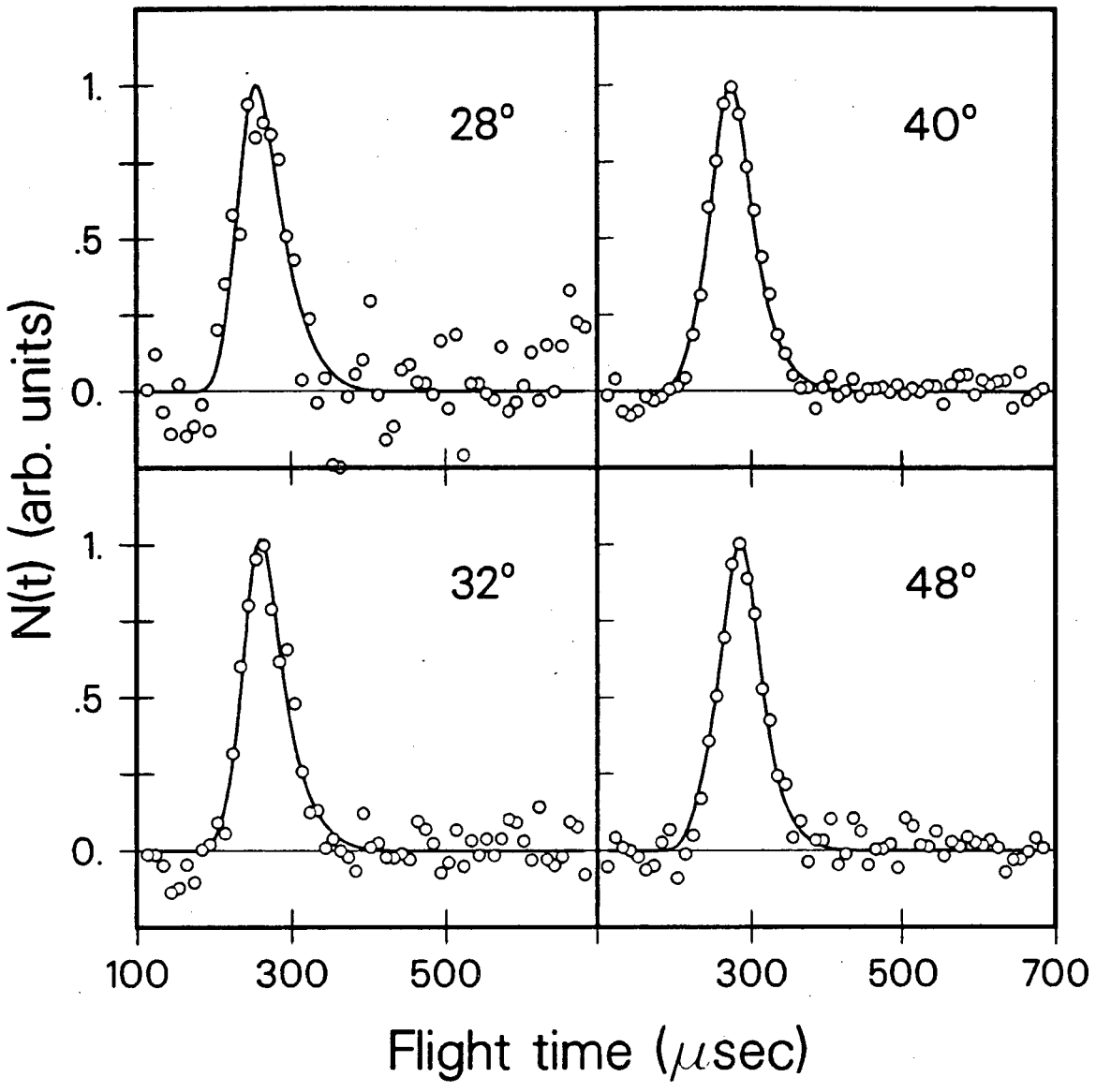
28°
40°
32°
48°
1.
.5
0.
N(t) (arb. units)
100
300
500
300
500
700
Flight time (μsec)
XBL 8712-5290

Figure 3

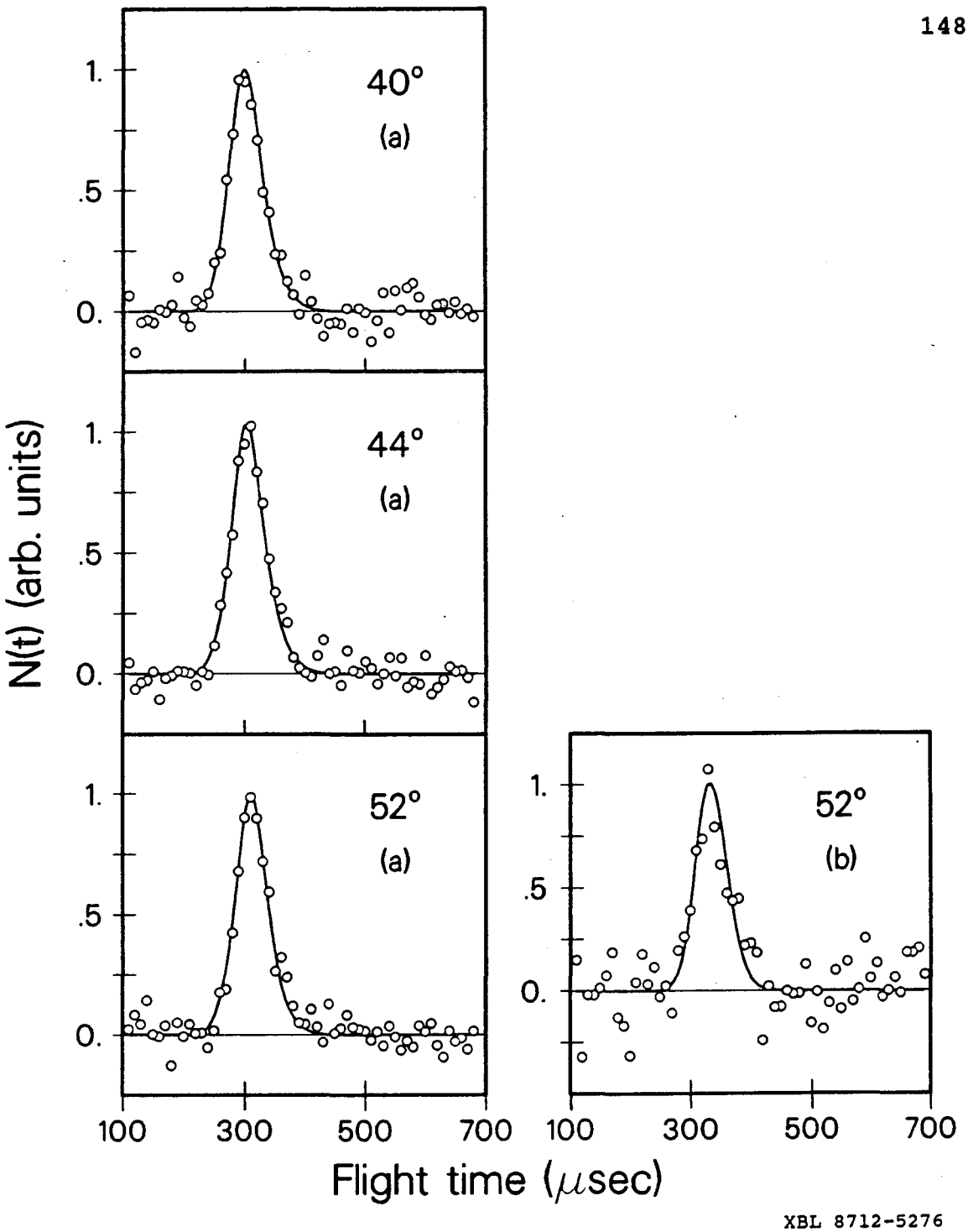
40°
(a)
44°
(a)
52°
(a)
52°
(b)
1.
.5
0.
N(t) (arb. units)
100
300
500
700
Flight time (μsec)
XBL 8712-5276

Figure 4

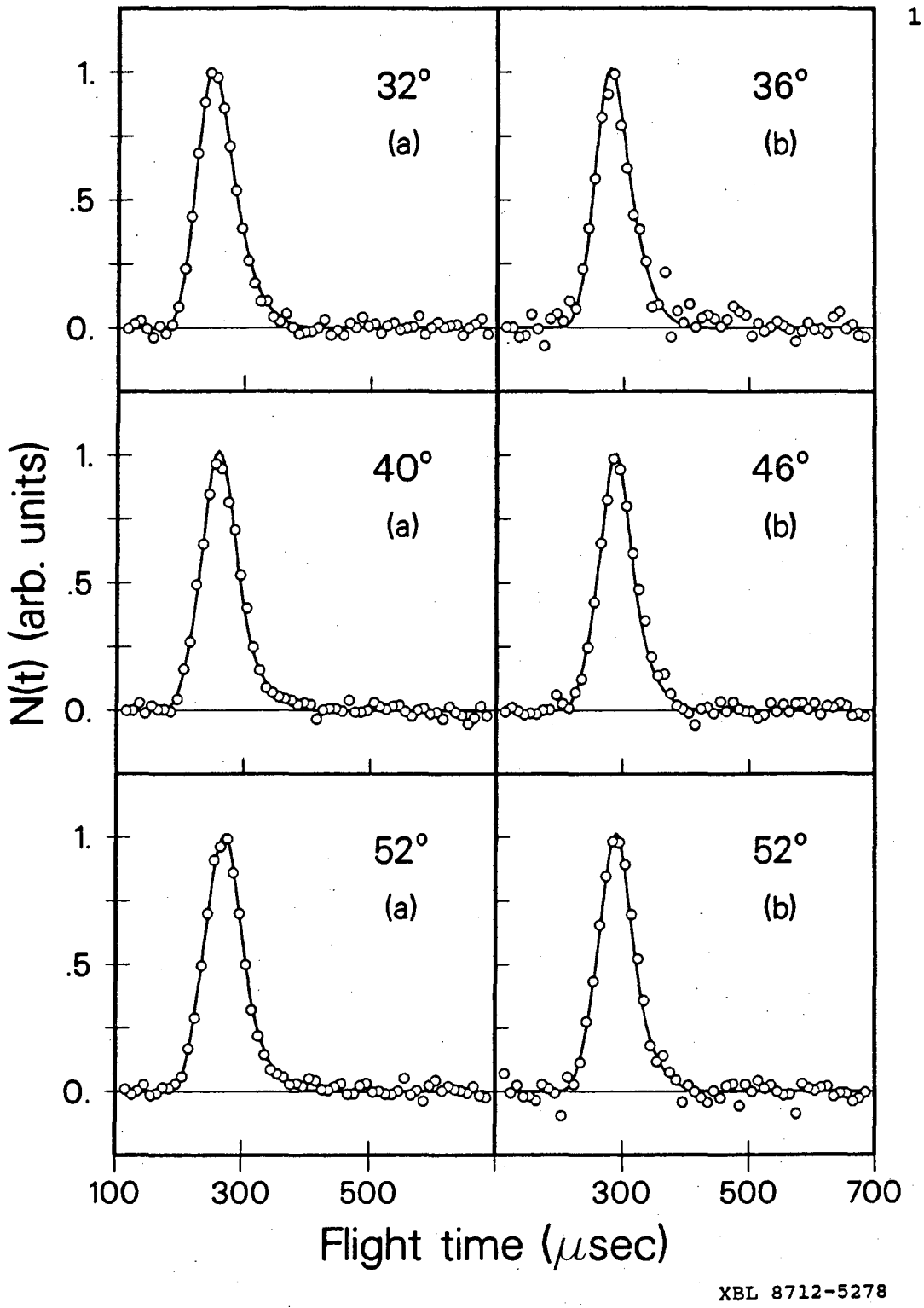
32°
(a)
36°
(b)
40°
(a)
46°
(b)
52°
(a)
52°
(b)
1.
.5
0.
N(t) (arb. units)
100
300
500
300
500
700
Flight time (μsec)
XBL 8712-5278

Figure 5

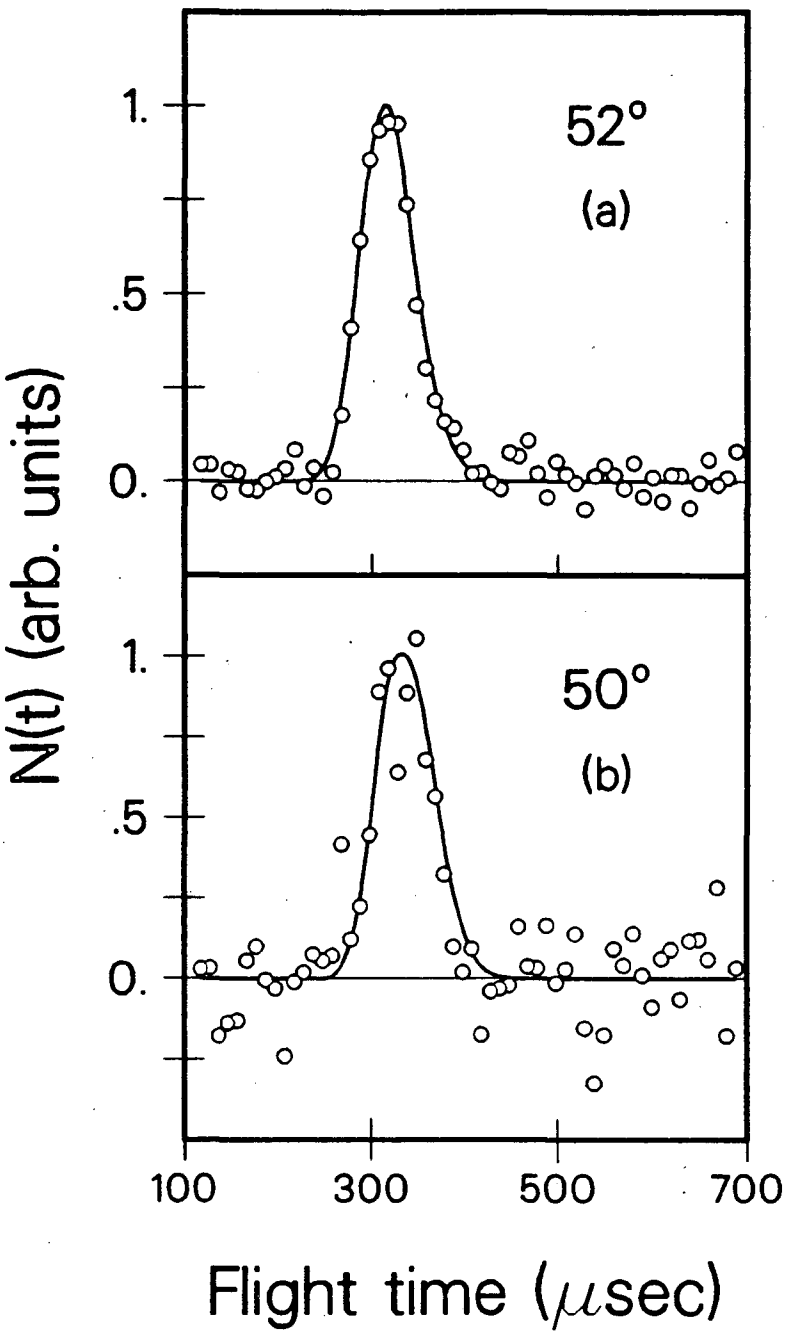

XBL 8712-5277

Figure 6

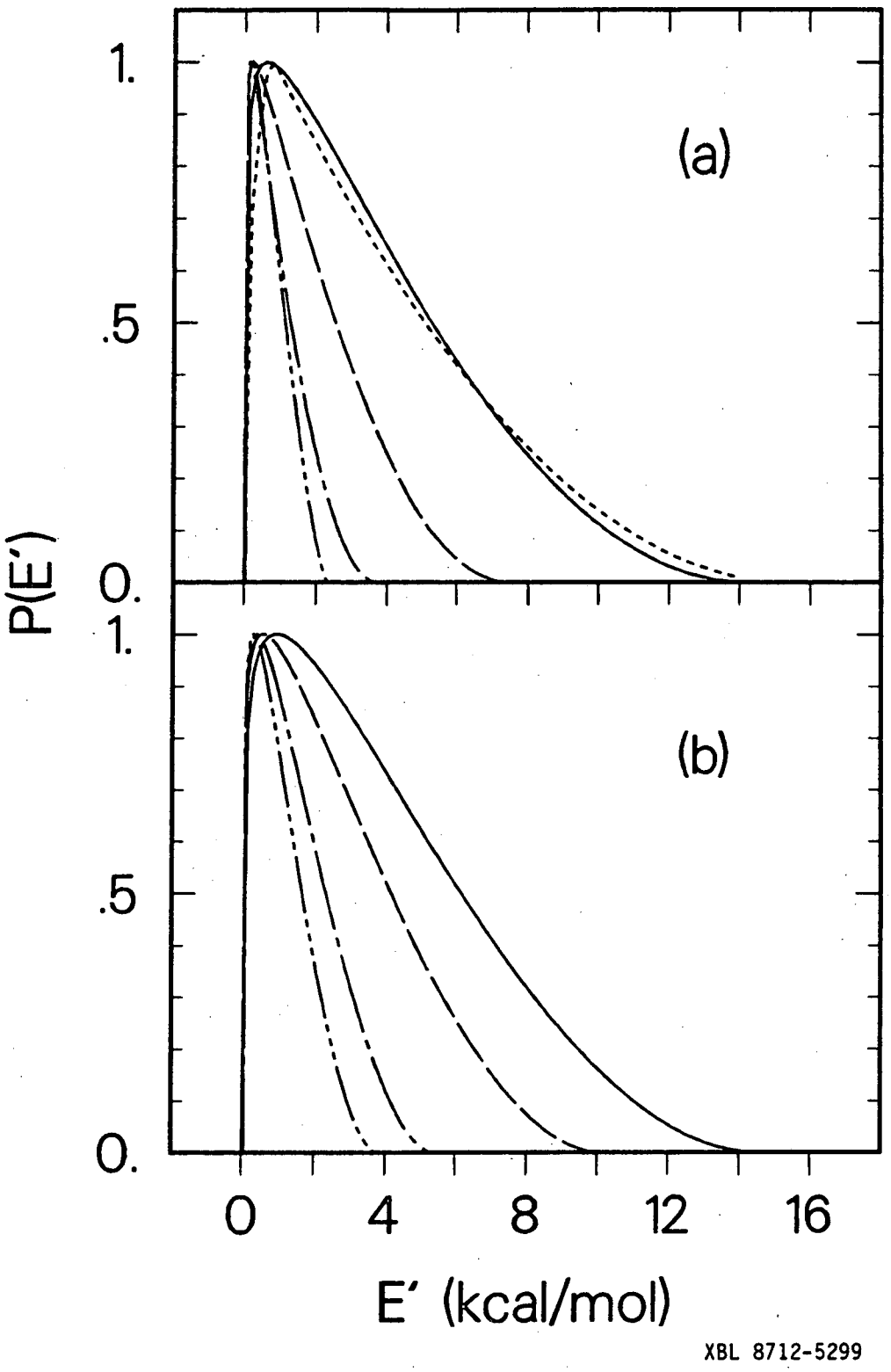

Figure 7

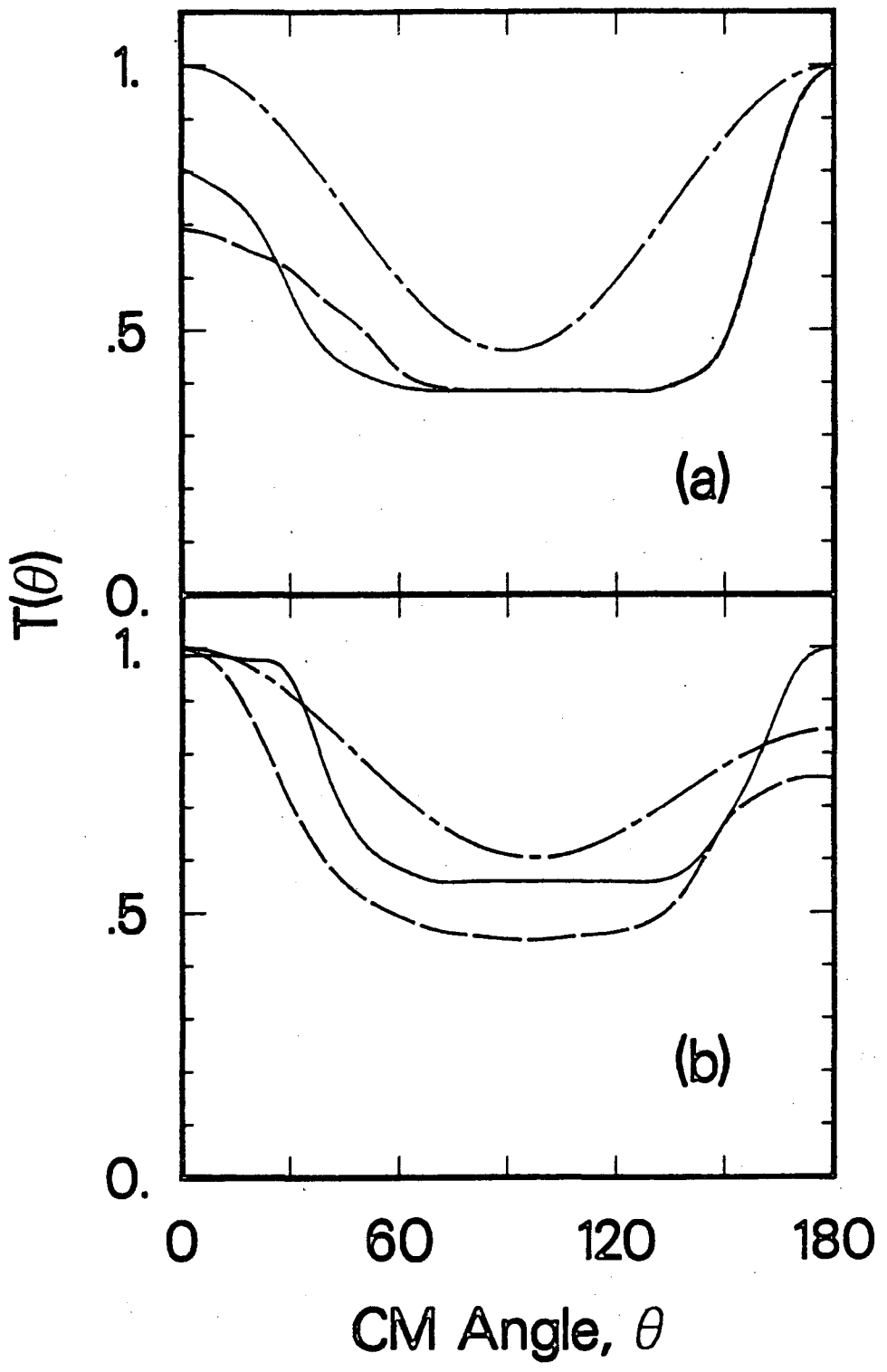

XBL 8712-5298

Figure 8

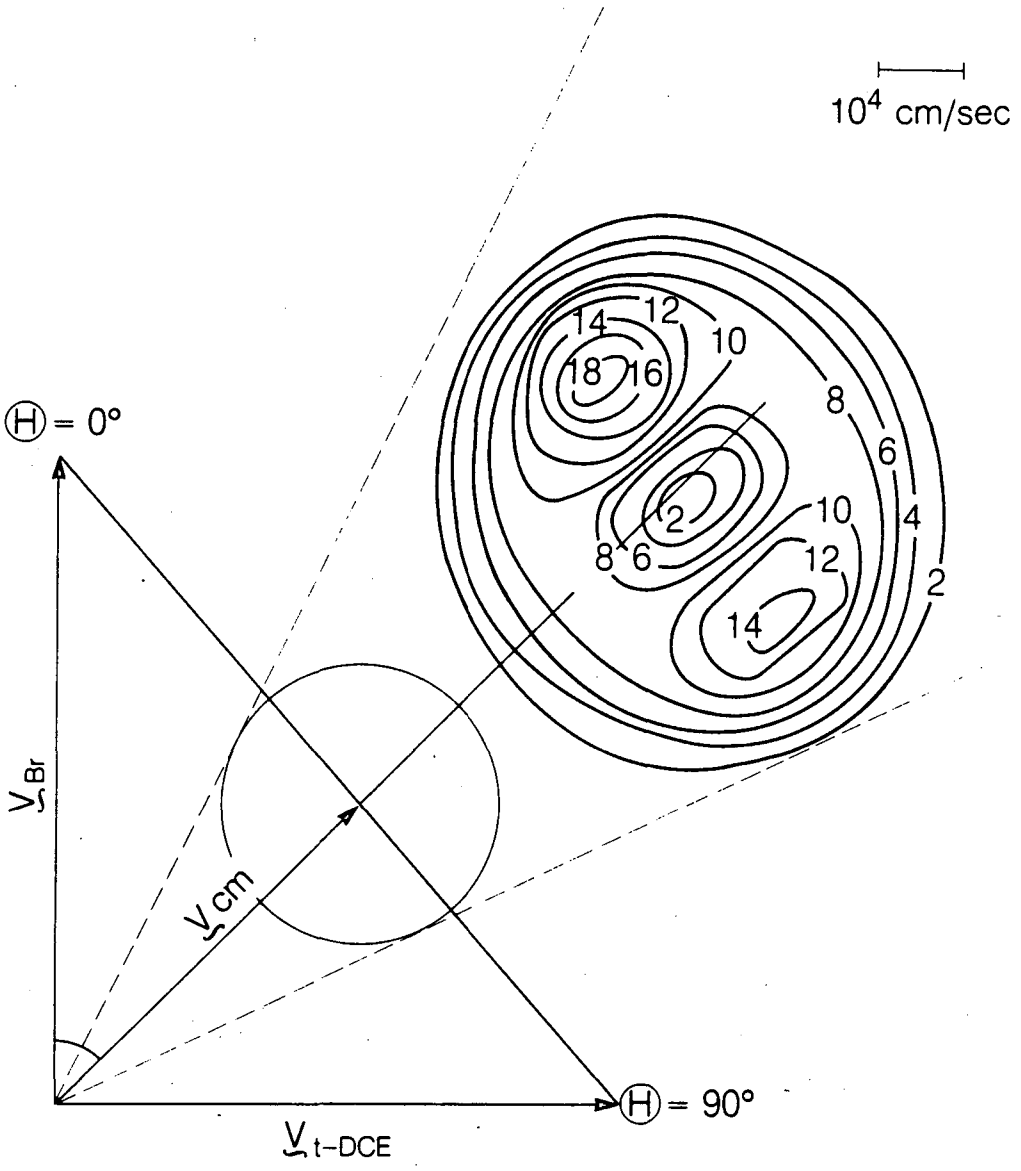
10^4 cm/sec
14
12
10
18
16
8
6
4
2
10
12
14
Ⓗ = 0°
Ⓗ = 90°
V_{Br}
V_{cm}
$V_{t\text{-}DCE}$
XBL 8712-5758

Figure 9

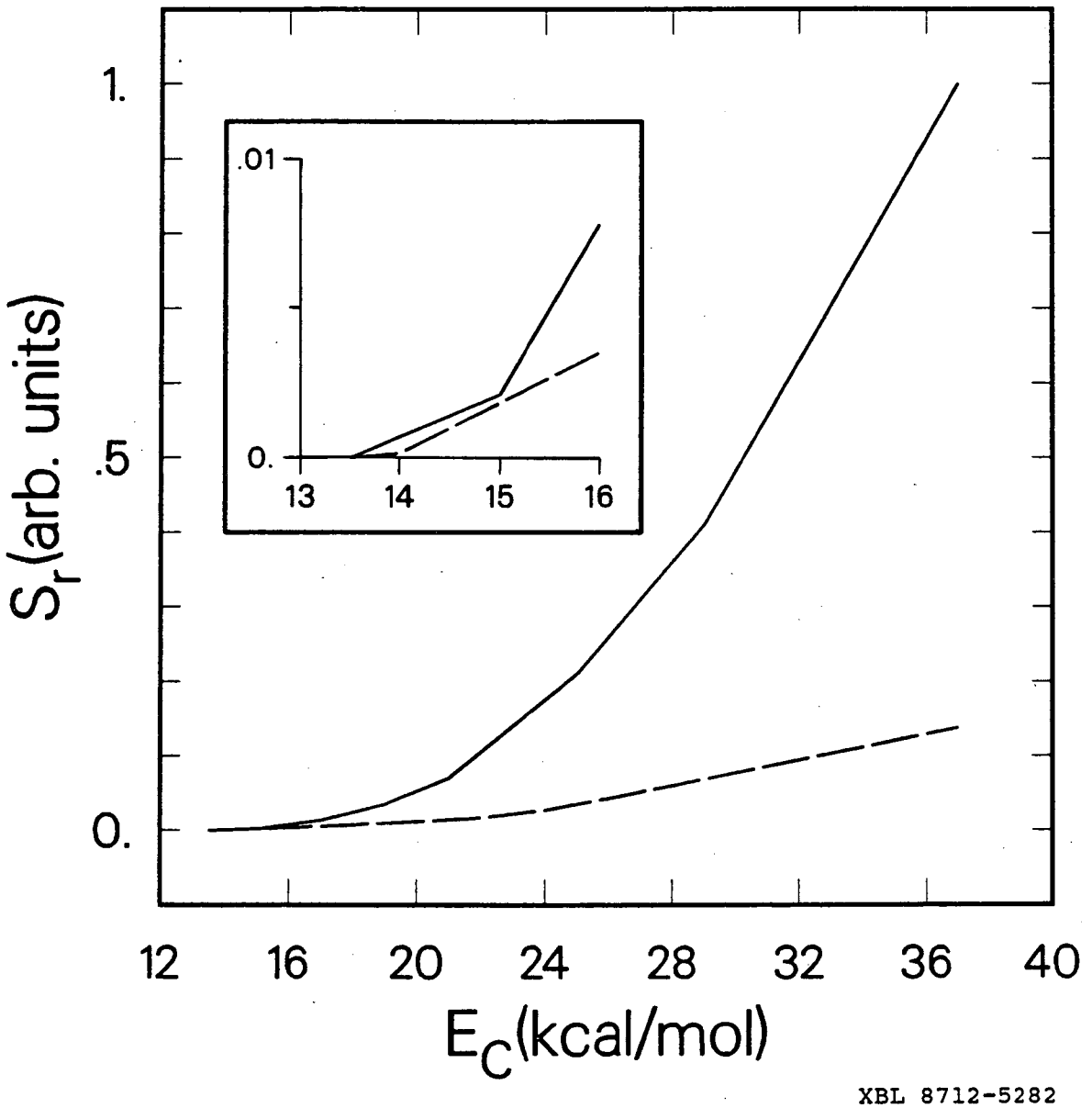
1.
.5
0.
S_r(arb. units)
.01
0.
13
14
15
16
12
16
20
24
28
32
36
40
E_C(kcal/mol)
XBL 8712-5282

Figure 10

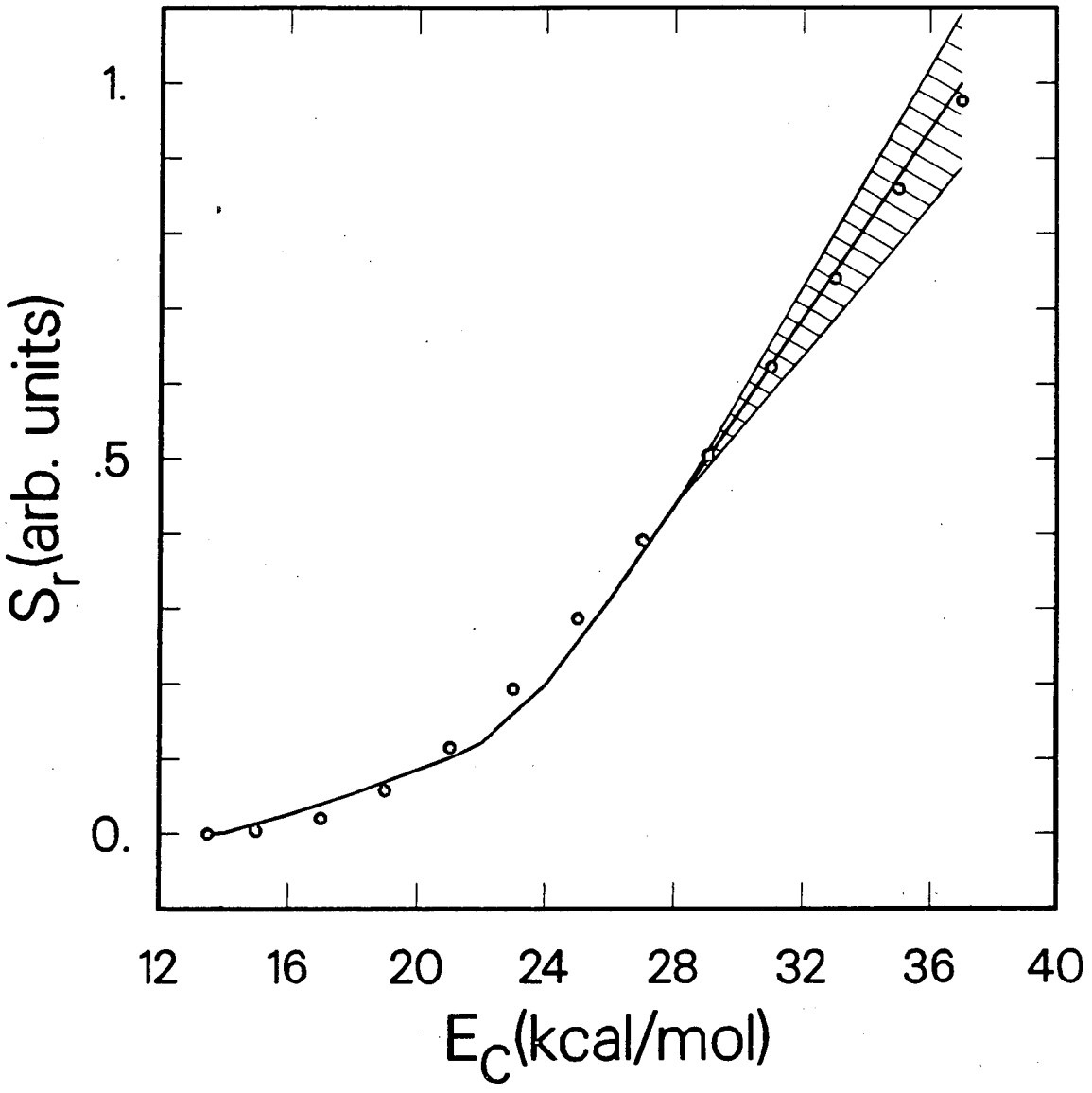

XBL 8712-5283

Figure 11

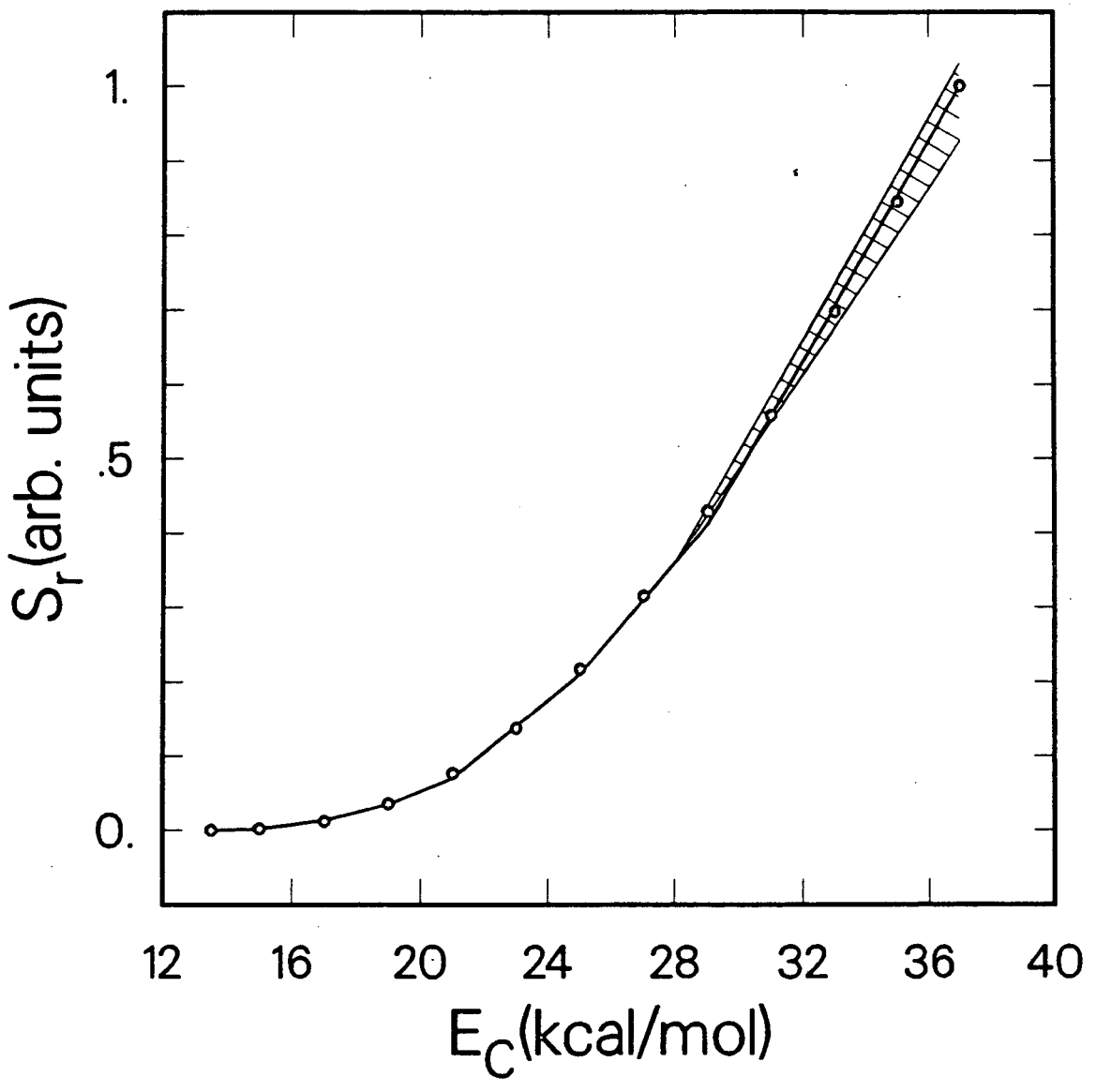

XBL 8712-5286

Figure 12

Chapter 4: Crossed Molecular Beams Studies of the Reactions of Methyl Radicals with Iodoalkanes

I. INTRODUCTION

Free radical abstraction reactions are of central importance in atmospheric and combustion chemistry. Although there have been numerous bulk gas-phase kinetic studies of such reactions (the majority of which have focused on H atom transfer [1]), very few free radical reactions of any sort have been investigated under single collision conditions.

Ross and co-workers [2,3] were the among the first to use the crossed beams technique to study radical reactions. Using a tantalum oven to generate effusive beams of methyl and ethyl radicals, they investigated the halogen abstraction reactions $CH_3 + XY \rightarrow CH_3X + Y$, (XY = Cl_2, Br_2, I_2, ICl, and IBr) [2,3] and $C_2H_5 + Br_2 \rightarrow C_2H_5Br + Br$ [2b]. Grice and co-workers also studied the reactions $CH_3 + IY \rightarrow CH_3I + Y$ (Y = I, Br, and Cl) with an effusive radical source [4,5]. More recently they employed a supersonic CH_3 source to reinvesti-

gate the IY and Br_2 reactions with improved velocity resolution [6]. In all of the above experiments, the RX product was observed to be predominantly backward scattered with respect to the incident radical beam. However, the CH_3I products from the IBr and ICl reactions were more sideways scattered than the CH_3X products from the homonuclear X_2 reactions. Product velocity measurements showed that the average fraction of available energy going into product translation, $\langle E'/E_{avl} \rangle$, was $\approx 0.30 \pm 0.05$ for all of these reactions. However, the translational energy distributions for the IY reactions peaked at lower values of E' than those for the X_2 reactions. Somssich et al. [7] observed the CH_3Br product from the reaction $CH_3 + Br_2$ to be translationally hotter and more sideways scattered than Ross and co-workers [3]; they obtained $\langle E'/E_{avl} \rangle = 0.56$ whereas Ross reported a value of 0.26. Although these differences were attributed to the higher collision energy of the German group's experiments, Grice's most recent work on $CH_3 + Br_2$ [6b], carried out at a comparable collision energy but with a supersonic radical beam, shows the CH_3Br product from this reaction to be strongly backward scattered with $\langle E'/E_{avl} \rangle = 0.33$.

The main conclusion from these studies was that the $CH_3 + X_2 \rightarrow CH_3X + X$ potential energy surfaces (PES) are largely repulsive, channeling a significant fraction of the available energy into product translation; the $CH_3 + IY \rightarrow CH_3I + Y$ surfaces are apparently more attractive. The results of

these experiments strongly resembled those for the reactive scattering of D atoms with diatomic halogen molecules [8,9] suggesting that, at least as far as halogen atom exchange reactions are concerned, methyl radicals and hydrogen atoms behave quite similarly.

Using the crossed beams method, we began to investigate the dynamics of methyl radical reactions with halogenated saturated and unsaturated organic molecules in order to learn how the internal degrees of freedom of both reactants couple to the reaction coordinate in abstraction and substitution reactions. In these studies, we used a pyrolysis source to generate a supersonic methyl radical beam. Unfortunately, we were unable to observe radical-for-atom substitution in any of the halogenated unsaturated systems that we studied, including those for which substitution was readily observed with Br [10] and Cl atoms [11]. This is due to the lower cross section for methyl radical (as compared to halogen atom) addition reactions which is related, at the macroscopic level, to the lower A-factor and higher activation energy for such reactions (for $CH_3 + C_2H_4 \rightarrow C_3H_7$, log A = 8.5 and E_{act} = 7.7 kcal/mol whereas for $Cl + C_2H_4 \rightarrow C_2H_4Cl$, log A = 10.7 and E_{act} = 0.0 kcal/mol [12]). The lower A-factor results in part from the fact that only certain orientations of the methyl radical allow it to add to the double bond. The difference in activation energy can be readily understood if we consider E_{act} to be proportional to the difference between

the ionization potential of the molecule and the electron affinity of the atom/radical [13]. The electron affinity of the methyl radical (0.08 eV [14]) is significantly lower than that of any halogen atom. The energy necessary to rehybridize the methyl carbon atom from sp^2 to sp^3 will also contribute to the activation energy to addition.

We were, however, able to carry out studies of the I atom exchange reactions, $CH_3 + RI \rightarrow CH_3I + R$, where R = CF_3 and $(CH_3)_3C$ at 12 - 13 kcal/mol collision energies. The most striking result of these experiments is that the additional vibrational degrees of freedom of the molecular reagent appear to play a very limited role in product energy partitioning. In fact, the fraction of energy available to the products of these reactions that is channeled into translation is greater than that for the CH_3 + XY reactions described above, suggesting that the CH_3-I-R and CH_3-X-Y potential energy surfaces are rather different from one another.

Thermochemistry

Tomkinson and Pritchard [15] have measured E_{act} = 7.5 ± 1.0 kcal/mol for the $CH_3 + CF_3I \rightarrow CH_3I + CF_3$ reaction. Alcock and Whittle [16] obtained an activation energy of 3.3 ± 0.2 kcal/mol for the reverse reaction implying that the forward reaction is endothermic by ≈4 kcal/mol. Molecular beam photodissociation studies have yielded D_0°(C-I) = 53.3 ±

0.7 [17] and 53.3 ± 0.2 [18] kcal/mol for CH_3I and $D_0^\circ(C-I)$ = 53.0 ± 0.5 kcal/mol [19] for CF_3I. According to these values, this reaction is essentially thermoneutral. However, a recent photodissociation experiment on CH_3I using a longer flight-path detector [20] gives $D_0^\circ(C-I)$ = 55 ± 0.5 kcal/mol, implying ΔH_0° = -2 kcal/mol.

Based on Benson's value of 51 kcal/mol for the C-I bond dissociation energy in $(CH_3)_3CI$ [13] and the above values for $D_0^\circ(C-I)$ in CH_3I, $CH_3 + (CH_3)_3CI \rightarrow CH_3I + (CH_3)_3C$ should be exoergic by 2 - 4 kcal/mol.

II. EXPERIMENTAL

The crossed beam apparatus used in these experiments has been described elsewhere [21,22]. Two seeded, doubly differentially pumped beams were crossed at 90° in a collision chamber held at approximately 10^{-7} torr. The CH_3I product from both reactions was detected at m/e=142 with a triply differentially pumped detector that rotates in the plane of the two beams.

The methyl radical beam was formed by bubbling ≈160 torr of helium through di-t-butyl peroxide (Pfaltz and Bauer) at -19°C (vapor pressure, v.p.≈2 torr) and expanding the mixture through a tapered quartz nozzle heated to ≈1000°C with a tantalum heater. The nozzle was fabricated by drawing a quartz tube (0.64 cm OD) to an inner diameter of ≈0.5 mm and then

grinding the tip to an angle of 60°. The heating element consisted of a small square block (≈9 mm^2) of 1mm thick Ta spot-welded to a 0.5 mm thick strip of Ta. The Ta strip was attached to two bent molybdenum strips which were affixed to water cooled electrodes and served as springs [23]. A 60° conical hole was drilled into the 1mm block to mate with the quartz nozzle which was painted with a graphite suspension. Figure 1 is a drawing of the source. Typically, 120 A at 1.2 VAC were passed through the heater. A conical stainless steel skimmer with an orifice diameter of 1.5 mm was positioned ≈1.3 cm from the nozzle.

In order to minimize radical recombination, it was necessary to heat the quartz nozzle at the tip only. However, within a few hours of operating the source, a black polymeric deposit accumulated inside the nozzle that blocked the gas flow. By monitoring the source foreline pressure and the product signal at a reference angle, it was possible to determine when this clogging began to affect the experiment seriously. A thin drill bit (0.4 mm diameter) attached to a long piece of stainless steel tubing and residing permanently in the gas feedline was used to unclog the nozzle in between experimental runs.

It was found that, over time, the Ta heater reduced the quartz nozzle to silicon. In addition, the beam gases oxidized the heater. As a result, the heating element and the quartz nozzle needed periodic replacement. After each

replacement the velocity of the methyl radical beam was remeasured and adjusted to agree with the earlier value.

The CF_3I beam was formed by expanding 170 torr of a mixture of 12% CF_3I (SCM) in neon through a 0.15 mm diameter nozzle at 30°C. The $(CH_3)_3CI$ (Aldrich) beam was generated by bubbling 170 torr of neon through the reagent held at 0°C (v.p.≈20 torr). The mixture expanded through a 0.20 mm diameter nozzle warmed to 70°C. A conical stainless steel skimmer with an orifice diameter of 1.0 mm was positioned ≈0.9 cm from the nozzle for both beams. A second defining aperture was placed between the skimmer and the differential wall for the t-butyl iodide beam in order to reduce the background arising from impurities in the beam at detector angles close to 0°.

Product angular distributions were measured by modulating the methyl radical beam with a 150 Hz tuning fork chopper. Data were collected for approximately 12 minutes per angle. θ = -20° was used as a reference angle for subsequent time-normalization of the data for both reactions. No data was collected within 8° of the R-I beam.

The velocities of the reagent beams were measured using the time-of-flight (TOF) technique. A multi-channel scaler [24] interfaced to an LSI 11/73 computer accumulated the data. The peak velocities (in units of 10^4 cm/s), v_{pk}, and speed-ratios, S, of the reagent beams were: CH_3: v_{pk}=27.0, S=7.0 (CF_3I experiment), v_{pk}=27.4, S=7.2 ($(CH_3)_3CI$ experi-

ment); CF_3I: v_{pk}=6.0, S=12.5; $(CH_3)_3CI$: v_{pk}=7.0, S=10.6. The collision energies, E_c, were 12.3 and 12.8 kcal/mol for the CF_3I and $(CH_3)_3CI$ reactions respectively. The spread in collision energy was approximately 30% fwhm.

Since one molecule of di-t-butyl peroxide decomposes into two methyl radicals and two acetone molecules, there was a significant contribution to the m/e=15 signal in methyl beam TOF from acetone cracking in the electron bombardment ionizer. Because of the spread in the electron energy of our ionizer, it was not possible to ionize the methyl radicals selectively by lowering the electron energy below the appearance potential for dissociative ionization of acetone (I.P.(CH_3) = 9.8 eV; A.P.($C_3H_6O \rightarrow CH_3 + CH_3CO$) = 13.2 eV [25]). In the early phase of this study, the presence of methyl radicals in the beam was determined by inspecting the width of the m/e=15 TOF peak. At low stagnation pressures, when the expansion from the nozzle was mild and slippage in the terminal velocities of different species was noticeable, one could observe a widening of the m/e=15 peak compared with those of heavier species in the beam. Upon increasing the stagnation pressure to achieve a more isentropic expansion, no widening was apparent and presumably the methyl radicals and acetone molecules had the same terminal velocity distribution. All of the reactions were studied under such conditions.

Product TOF spectra were measured using the cross-

correlation method [22]. A Cu-Be alloy disk photo-etched with a 255 channel pseudorandom sequence of open and closed slots was spun at 392 Hz giving 10 μs resolution in the TOF spectra. The resulting spectrum was deconvoluted by the on-line computer. The nominal flight-path from wheel to ionizer was 29.9 cm.

III. RESULTS AND ANALYSIS

A. $CH_3 + CF_3I \rightarrow CH_3I + CF_3$

The CH_3I (m/e=142) laboratory angular distribution from this reaction is shown in Fig. 2. The product is entirely backward scattered with respect to the incident CH_3 beam (the center-of-mass angle, θ_{CM}, is 19°). Elastic and inelastic scattering of impurities in the CF_3I beam by both He and acetone in the CH_3 beam contributed to a substantial modulated non-reactive m/e=142 signal at LAB angles from 0° to 15° and, to a lesser extent, from 0° to -5°. In order to subtract this background from the measured CH_3I angular distribution, we substituted a properly diluted beam of acetone in helium for the CH_3 in helium beam and measured the non-reactive scattering signal. The interpolated slope of the non-reactive scattering angular distribution from 8° to 20° was virtually identical to that of the reactive angular distribution suggesting that there is no reactive signal at 8°. In addition, the m/e=142 TOF spectrum at 8° did not

change when acetone was substituted for CH_3. Since both the reactive and non-reactive angular distributions go to zero at 20°, this angle provides a rigorous upper limit to the width of the product angular distribution. Two possible experimental angular distributions are given in Fig. 2; one has N(8°)=0 and the other N(20°)=0.

In addition to the modulated background from in/elastic scattering, there was angle dependent unmodulated background at angles up to 12° from the CF_3I beam resulting from molecules effusing from the differential region. The error bars for the points at -8° and -10° reflect the statistical noise associated with this unmodulated background.

Product TOF spectra were measured at three angles (Fig. 4). The signal-to-noise ratios are relatively low. The gradual drop in the CH_3 beam intensity caused by the decay of the heater and nozzle made it unprofitable to count for longer than about five hours at a given angle. Unmodulated background was subtracted from the TOF spectrum at -12° by measuring the m/e=142 TOF at this angle with CH_3 and with acetone. The -28° TOF spectrum has a long tail which is likely to be non-reactive in origin. The underlying shape of this tail is uncertain so it was not subtracted from the data.

The product angular distributions and TOF spectra were simultaneously fit using a forward convolution program [11] that starts with a separable form for the center-of-mass (CM)

reference frame product flux distribution,

$$I_{CM}(\theta,E') = T(\theta)P(E'),$$

and generates laboratory (LAB) frame angular distributions and TOF spectra suitably averaged over the spread in relative velocities. $T(\theta)$ is the CM frame product angular distribution. A three parameter functional form was used for $P(E')$, the CM frame product translational energy distribution: $P(E') = (E' - B)^p(E_{avl} - E')^q$, where B appears as a threshold in the distribution and is related to any barrier in the exit channel and $E_{avl} = (E_c - \Delta H^\circ_0)$. The calculated angular distributions and TOF spectra are scaled to agree with the experimental data.

We found that it was necessary to add ≈3 kcal/mol to the collision energy of 12.3 kcal/mol in order to fit the wide-angle part of the CH_3I angular distribution well. Thus, our data are in accord with an exoergicity of 2 kcal/mol. However, if the reaction is indeed thermoneutral, this could indicate that $v_{pk}(CH_3)$ is slightly higher than we infer from the peak m/e=15 flight time, t_{pk}. A decrease of 4 μsec in t_{pk} would increase $v_{pk}(CH_3)$ to 2.8×10^5 cm/s and raise the most-probable collision energy to 13.2 kcal/mol (the resolution was 1 μsec/channel for the beam TOF measurements). Some of this additional energy could also come from the out-of-plane vibrational mode (ν_2 = 606 cm^{-1} (1←0) and 681 cm^{-1} (2←1) [26]) of the methyl radical which is essentially directed along the reaction coordinate. Assuming that the ν_2

mode is unrelaxed in the expansion, ≈50% of the methyl radicals will have at least one quantum in ν_2 and ≈40% will be in v=1 at a nozzle temperature of 1000°C.

Attempts were made to fit the data using differently shaped CM flux distributions. Both the N(8°)=0 and N(20°)=0 angular distributions could be fit with P(E') distributions having B values in the range 0 - 3 kcal/mol. The mean translational energy of the P(E') distributions (at the most-probable collision energy) increases from 9.9 - 10.2 kcal/mol on increasing B from 0 - 3 kcal/mol. Thus, $\langle E'/E_{avl} \rangle \simeq 0.66$ over a range of B values. We present fits for B = 2 kcal/mol (Fig. 7a) in Figs. 2 and 4.

A $T(\theta)$ distribution with T(65°)=0 (Fig. 6) has been used to fit the N(8°)=0 laboratory angular distribution and one with T(90°)=0 was used for the N(20°)=0 fit. Since CH_3I product scattered backwards at angles up to ≈80° in the CM frame can contribute to the TOF spectra at all three LAB angles, the slow tails of the calculated TOF spectra are sensitive to the maximum angle of $T(\theta)$. However, because of the noise in the TOF data, both $T(\theta)$ distributions give acceptable fits to the spectra. Figs. 4 a,b show the fits generated using the two distributions. With an (unrealistic) isotropic $T(\theta)$, the tail of the calculated TOF spectrum at -28° was still too low to fit the data.

Decreasing the value for the speed ratio of the CH_3 beam by 30% had a negligible effect on the calculated angular

distribution. It did, however, broaden the calculated TOF spectra slightly, especially at -28° where it seemed to improve the fit. However, the poor signal-to-noise ratio at this angle makes it difficult to judge the quality of the fits.

One can try to account for the presence of a barrier to the forward exchange reaction in the analysis by assuming that the collision energy dependence of the reactive cross section has the line-of-centers form [27],

$$\sigma = \begin{cases} \sigma_o(1-E_{th}/E_c), & E_c > E_{th} \\ 0, & E_c \leq E_{th}, \end{cases}$$

where σ_o is the maximum cross section and E_{th} is the threshold energy for the reaction, and by weighting the different collision energies used in the analysis by this function. If we take E_{th} = 3 kcal/mol the resulting fit is identical to that with no assumed barrier. The most probable collision energy is still 12.3 kcal/mol and the center-of-mass angle is 19°.

Interestingly, we were unable to observe product from the reaction $CH_3 + CF_3Br \rightarrow CH_3Br + CF_3$ (ΔH°_{298} = 0 kcal/mol [28]) at a collision energy of 13 kcal/mol. This is presumably due to a higher potential energy barrier to this reaction. The activation energy for this reaction has been measured as 12.5 kcal/mol [15].

B. $\underline{CH_3 + (CH_3)_3CI \rightarrow CH_3I + (CH_3)_3C}$

Elastic/inelastic scattering of impurities at m/e=142 was even more of a problem with $(CH_3)_3CI$ than with CF_3I. At 20°, the modulated m/e=142 count rate was ≈40 Hz as compared to ≈15 Hz at -20°; the modulated m/e=142 count rate at 20° in the CF_3I experiment was essentially 0 Hz. As a result, it was not possible to subtract unambiguously the non-reactive contribution to the signal at $\theta > 0°$ for this reaction. Only data for $\theta \leq -8°$ are presented (Fig. 3) ($\theta_{CM} = 18°$). Again, substantial background signal from the unscattered $(CH_3)_3CI$ beam increased the statistical uncertainty at the angles closest to the beam. A TOF spectrum of CH_3I product at -20° is shown in Fig. 5 along with a m/e=142 TOF spectrum at -15° which includes both reactive and non-reactive components.

With only a small backward part of the laboratory angular distribution available, the low recoil energy section of the P(E') cannot be definitively determined. The TOF spectrum at -20° is not sensitive to this part of the translational energy distribution; the shape of the calculated TOF spectrum does not change on increasing the B parameter from 0 - 4 kcal/mol. A P(E') with B = 0 kcal/mol is used to obtain the fits presented in Figs. 3 and 5; we assume $\Delta H° = -2$ kcal/mol. For this P(E'), $\langle E' \rangle = 7.6$ kcal/mol and $\langle E'/E_{avl} \rangle = 0.51$; $\langle E'/E_{avl} \rangle$ changes only slightly to 0.53 for the B = 3 distribution.

Acceptable fits to the m/e=142 angular distribution and

TOF spectra are obtained with the T(90°)=0 and T(60°)=0 CM angular distributions shown in Fig. 6. The two fits are virtually identical for $\theta \leq -8°$. The calculated TOF spectra in Fig. 5a are derived using the distribution that extends to θ=90°. The effect of truncating T(θ) at 60° is shown in Fig. 5b. The TOF spectrum at $\theta = -20°$ could not be fit well with a T(50°)=0 distribution. The noise in the TOF data again prevents us from being able to determine conclusively the length of the slow tail and hence the maximum angle of T(θ). Indeed, T(θ) could extend beyond 90°. Even with the uncertainty in T(θ), however, it is clear that the product is predominantly backward scattered.

IV. DISCUSSION

As mentioned above, a positive value of B in the P(E') distribution could result from a barrier in the exit channel. Our results for $CH_3 + CF_3I \rightarrow CH_3I + CF_3$ would therefore be consistent with the aforementioned kinetic study that suggests an activation energy of ≈3 kcal/mol for the reverse reaction. Assuming that the reaction is thermoneutral and direct, the potential energy barrier in the forward direction will be of the same magnitude. The energy required to rehybridize the methyl carbon from sp^2 (radical) to sp^3 (CH_3I) may contribute to the barrier on the CH_3-I-CF_3 potential energy surface. If this were the case, out-of-plane vibra-

tional motion of the proper phase in the methyl radical would be particularly effective in overcoming the barrier to I atom exchange.

There is, however, no consensus in the literature on the effectiveness of the out-of-plane bend of CH_3 in promoting exchange reactions. Experiments by Ting and Weston [29] in which methyl radicals were generated by photolyzing CH_3Br suggest that energy in ν_2 can help to overcome the barrier to H atom transfer in the reaction $CH_3 + H_2 \rightarrow CH_4 + H$. In addition, Brown et al. [5] were unable to fit their data for $CH_3 + ICl \rightarrow CH_3I + Cl$ without including part of the vibrational energy of the methyl radical in the total energy available. The spread in translational energy of their effusive radical beam is quite substantial, however, so it is unclear to what extent vibrationally excited methyl radicals were contributing to reaction. Kovalenko and Leone [30] conclude from experiments with photolytically produced methyl radicals that reagent translational energy promotes the $CH_3 + Cl_2$ reaction but they were unable to assess the relative importance of translational energy against energy in the out-of-plane bend in driving the reaction. Finally, Chapman and Bunker [31] have found from trajectory calculations that depositing energy in ν_2 actually decreases the cross section for H atom transfer in $CH_3 + H_2$.

The sharp backwards scattering of the CH_3I product from both of the reactions that we have studied, considered along

with the relatively high average product translational energies, suggests that a roughly collinear C-I-C geometry is favored and that the dominant interaction between the products is repulsive.

For heuristic purposes, we may neglect the internal degrees of freedom of the methyl radical and the CX_3 group (X = F, CH_3) and categorize the present reactions as L + HH systems (L = light atom; H = heavy atom). Classical trajectory studies by Polanyi and co-workers [32,33] of exoergic L + HH reactions on late-barrier, repulsive potential energy surfaces show that very little of the reaction exoergicity is channeled into product vibration. This so-called "light atom anomaly" is due to the rapid motion of the light atom which allows the LH bond to approach its equilibrium length before the HH bond breaks. Trajectory calculations [34] also indicate that reagent translation is less effective than vibration in promoting reactions on thermoneutral surfaces with late barriers, implying product translation will be preferentially excited on such surfaces.

It is not entirely straightforward, however, to extrapolate from the observation of a large value of $\langle E'/E_{avl} \rangle$ to the location of the barrier on the PES. The slope of the surface along the reaction coordinate and up to the barrier crest has been shown to influence the energy dependence of reaction cross sections [35]. Similarly the slope of the surface along the retreat coordinate will affect the product

energy distributions. We will discuss this aspect more below. In addition, an effect analogous to the anomaly mentioned above favors conversion of reagent translational energy in excess of threshold into product translational energy. As the collision energy is raised in the A + BC → AB + C reaction, AB recoils from increasingly more compressed A-B-C intermediates, leading to enhanced product translation [33,36]. This effect should be even more pronounced when A is considerably lighter than B and C. Such "induced repulsive energy release" could be important in the present nearly thermoneutral reactions for which the barrier is probably no more than a few kcal/mol.

Our results for the CH_3 + CF_3I reaction are strikingly similar to those of Davidson et al. [37] for D + CF_3I → DI + CF_3 and of McDonald and Herschbach [38] for D + HI → DI + H. In both studies, the DI product was found to be entirely backward scattered with respect to the incident D atom beam, with $\langle E'/E_{avl} \rangle \approx 0.7$. This similarity recalls that between the CH_3 + XY and D + XY crossed beam results. Studies of the D + XY reactions [8,9] revealed that DCl from Cl_2 was predominantly backward scattered but that the peak of the DX angular distributions shifted progressively forward in the order Cl_2 → Br_2 → I_2. The DI CM angular distributions for I_2, ICl, and IBr peaked near 90° (D beam at 0°) with the DI from ICl somewhat more forward scattered than the DI from I_2; the DBr angular distributions for Br_2 and IBr were also similar to

each other, peaking near 120° [8]. $\langle E'/E_{avl} \rangle$ decreased from 0.44 for Cl_2 to 0.28 for I_2; for ICl, $\langle E'/E_{avl} \rangle = 0.24$. The maxima of the P(E') distributions followed the same trend [8].

Thus, the D + XY potential energy surfaces appear to be largely repulsive, becoming less so as the transferred halogen atom increases in size. Indeed, chemiluminescence experiments on the H + X_2 → HX + X (X = Cl, Br) reactions have shown that the fraction of available energy in product vibration is greater for X = Br than for X = Cl [39].

As alluded to above, when the product interaction is largely repulsive, one can correlate the angle at which the CM frame product angular distribution peaks with the energetically favored geometry of the reaction intermediate. Thus, the reactive scattering experiments indicate that D-Cl-Cl should be roughly collinear whereas D-I-Cl should be bent, in accord with a frontier orbital model which predicts that, as the ionization potential of HX decreases, the 3p orbital of Cl will interact predominantly with the highest occupied, π^* antibonding, MO of HX [41-43]. Since this MO has it electron density primarily off the internuclear axis, the resulting H-X-Cl structure will be bent [44]. Classical trajectory calculations on D + I_2 → DI + D [40] confirm the general validity of inferring the structure of the reaction intermediate from the product angular distribution for reactions on repulsive surfaces. However, trajectory calculations on

$H + Br_2 \rightarrow HBr + H$ suggest that it is not possible to correlate the anisotropy of the surface with the preferred scattering angle in a direct and simple manner [45].

It can also be argued that the enhanced sideways scattering observed for the $CH_3 + ICl \rightarrow CH_3I + Cl$ reaction is evidence for a bent CH_3-I-Cl intermediate [4b]. However, there are notable differences between the $CH_3 + XY$ and the $D + XY$ results. The maxima of the CH_3X CM angular distributions for the $CH_3 + X_2$ reactions barely shift on going from $Br_2 \rightarrow I_2$ [3,6b]. (The maximum of the CH_3Cl angular distribution cannot be determined from the available data [2b].) Unlike the DI angular distributions, the CH_3I distributions for I_2 and ICl peak at 180° [3,6]. Classical trajectory calculations on the $H + I_2$ and $CH_3 + I_2$ reactions by Polanyi and Schreiber [46] using a single lateral-approach PES and treating the methyl radical as a structureless particle of mass 15 show that CH_3I is more backward scattered than the HI, in accord with the experimental findings. It is therefore possible that the differences between the D atom and CH_3 scattering data for I_2 and ICl are kinematic in origin. However, McDonald found [40b] that substituting a particle of mass 15 for deuterium in his $D + I_2$ trajectory study had no effect on the calculated product angular and energy distributions.

It is instructive to compare our results for $CH_3 + CX_3I \rightarrow CH_3I + CX_3$ (X = F, CH_3) with those for $CH_3 + IY \rightarrow CH_3I + Y$.

The CH_3I CM frame angular distributions obtained by Hoffman et al. [5,6b] range from ≈10°-180° for I_2 and from 0°-180° for ICl. Since the X groups will block sideways attack of the I atom by the incoming methyl radical, we might expect to see enhanced backward scattering for these reactions. The narrow backward-peaked $T(\theta)$ distributions used to fit both possible CH_3I angular distributions for $CH_3 + CF_3I$ are consistent with such a steric effect. What is most remarkable, however, is that the fraction of available energy in product translation for the CX_3I reactions is approximately twice the fraction that was observed for the CH_3 + IY reactions. Apparently, the $CH_3 + CX_3I$ potential energy surfaces are even more repulsive than those for CH_3 + IY.

The "attractiveness" of the CH_3-I-Y surfaces along the I-Y coordinate should increase with the electronegativity of the Y group [6b]. Work by Farrar and Lee [47] has shown that, at a collision energy of 2.6 kcal/mol, the reaction F + $CH_3I \rightarrow CH_3$ + IF proceeds through a long-lived collision complex that is bound by approximately 25 kcal/mol with respect to reactants and in which all of the vibrational degrees of freedom are equilibrated. Likewise, $O(^3P)$ and CF_3I form a long-lived CF_3-I-O complex at E_c=2.2 kcal/mol [48]. Although it is likely that CH_3-I-Cl is bent, the CH_3 + ICl → CH_3I + Cl crossed beam results lead one to speculate that the CH_3-I-Cl surface has a shallow potential well that enables the intermediate to live long enough to rotate slightly and to undergo

partial vibrational energy redistribution [3,5,6]. Recent work on $Cl + CH_3I \rightarrow CH_3 + ICl$ [49] strongly suggests that a long-lived complex is formed at E_c=5.5 kcal/mol. The CH_3I angular distribution from $CH_3 + IBr$, E_c=7.6 kcal/mol [6] also shows substantial forward scattering.

It is therefore tempting to neglect the internal degrees of freedom of the CX_3 groups and to correlate the repulsive nature of the $CH_3 + CX_3I \rightarrow CH_3I + CX_3$ surfaces with the CX_3 electronegativities. Using the Mulliken method for calculating the electronegativity, χ, of an atom [50],

$$\chi = 1/2\ (IP + EA),$$

where IP is the ionization potential and EA is the electron affinity, we find that χ = 6.1 eV for CF_3, below the value of 6.76 eV for I (see Table 1). $(CH_3)_3C^-$ has never been observed experimentally but kinetic measurements on the reaction of hydroxide ion with $(CH_3)_3SiC(CH_3)_3$ indicate that this anion is unbound by 0.3 eV [52]. By this crude measure, the CH_3-I-Y potential energy surfaces should be less attractive along the I-Y coordinate for Y = CX_3 than for Y = halogen atom.

Qualitative molecular orbital arguments give added insight into the CH_3-I-Y potential energy surfaces. The sp^2 hybrid orbital of CF_3 should interact primarily with the lowest-unoccupied σ^*, antibonding orbital of CH_3I. Such an interaction will favor a collinear transition state and will induce substantial I-Y repulsion. As Y becomes more electro-

negative, the dominant CH_3I-Y interaction will be between the highest occupied, antibonding or nonbonding $p\pi$ orbital of CH_3I and the singly occupied orbital of Y. This will give rise to a bent transition structure (see above) and less I-Y repulsion since the π orbital lies lower in energy than the σ^* orbital [54].

Yet the above discussion does not address the question of why the vibrational modes of the CX_3 fragments absorb so little energy during bond fission. We can use an impulsive model to calculate the fraction of energy expected in translation in the "soft radical" limit. In this limit [55], C-I bond fission is considered to deliver an impulse to the carbon and iodine atoms only. The atoms are therefore treated as being independent of the groups to which they are bonded. Momentum is conserved between the C and I atoms; the momentum of each product is then taken to be equal to the momentum of its constituent recoiling atom. For both reactions, the translational energy of the product is considerably higher than what the "soft"-impulsive model predicts: $\langle E/E_{avl} \rangle$ = 0.24 and 0.27 for CF_3I and $(CH_3)_3CI$ respectively whereas the experimental values are $\approx$0.7 and $\approx$0.5.

In the "rigid radical" limit, all of the available energy would go into product translation and rotation. However, even for non-collinear reactive geometries, the rotational energy of the products will be very small. For an

impulsive CH_3 + CF_3I collision (E_c=12.3 kcal/mol, <E'> = 10 kcal/mol) with a C-I-C angle of 150°, the difference between the initial and final orbital angular momenta is only ≈15 $\hbar$. This amounts to less than 0.1 kcal/mol of rotational energy in CH_3I assuming no torque on the CF_3 fragment. Thus, our results fall somewhere in between the "soft" and "rigid" radical predictions.

The lack of vibrational excitation of the CF_3 fragment may be partly due to its having an equilibrium geometry that is almost identical to the geometry of the CF_3 group in CF_3I; the FCF bond angle in the radical is 111° [56] whereas in the molecule it is 108° [57]. Thus, there is no structural change to promote excitation of the out-of-plane bend which has a frequency of 701 cm^{-1} [58].

We must be careful in interpreting the modest difference in $\langle E'/E_{avl} \rangle$ between the two reactions, since we do not know how the potential energy surfaces differ. Let us assume, however, that the shape of the two surfaces along their reaction coordinates is the same. The simple fact that $(CH_3)_3C$ has more than four times the number of vibrational modes as CF_3 (neglecting the high frequency C-H stretching modes) can account for the greater amount of vibrational excitation in that fragment. The structure of $(CH_3)_3C$ has been the subject of considerable controversy [53] but it appears to be slightly bent with a barrier to inversion of ≈0.5 kcal/mol [58,59]. Its ν_2 frequency has been estimated to be <200 cm^{-1} [60],

more than three times lower than ν_2 in CF_3. Thus, excitation of ν_2 is more likely in $(CH_3)_3C$ than in CF_3.

It is worth comparing our reactive scattering results with data on the ultra-violet photofragmentation of iodoalkanes. In these systems, C-I bond cleavage is believed to occur via excitation of a nonbonding $p\pi$ electron on the I atom to the σ^* antibonding C-I orbital [54]. Recent experiments by Zhu [61] on the photofragmentation dynamics of a series of iodoalkanes ($R\text{-}I \xrightarrow{248\ nm} R + I$) show that, on going from CH_3I to $(CH_3)_3CI$, the fraction of energy released into product translation decreases from 0.85 to 0.28. His value of $\langle E'/E_{avl} \rangle$ for $(CH_3)_3CI$ is in rough accord with the prediction of the "soft"-impulsive model. In his work on the photodissociation of CF_3I [19] and CH_3I [18] at 248 nm, van Veen found significantly greater vibrational excitation of CF_3 than CH_3 ($\langle E'/E_{avl} \rangle$ = 0.89 for $CH_3I \rightarrow CH_3 + I^*$, 0.61 for $CF_3I \rightarrow CF_3 + I^*$) despite the large structural change that the CH_3 group undergoes upon C-I bond rupture. This difference was attributed to a steeper dissociative potential and a lower CX stretching frequency in CF_3I. Our value for $\langle E'/E_{avl} \rangle$ for $CH_3 + CF_3I \rightarrow CH_3I + CF_3$ is in close agreement with the $CF_3I \rightarrow CF_3 + I$ photodissociation value, suggesting that the repulsive interaction between the I and C atoms in CF_3I is similar on the reactive and dissociative surfaces. In the case of $(CH_3)_3CI$, however, the vibrational degrees of freedom of the t-butyl radical appear to be more efficiently

excited during C-I bond rupture on the excited state surface.

VI. CONCLUSIONS

Our observations for the I atom exchange reactions, $CH_3 + CX_3I \rightarrow CH_3I + CX_3$ (X = F, CH_3), are remarkably similar to those of the analogous D atom reaction, $D + CF_3I \rightarrow DI + CF_3$, in that the CH_3I product is sharply backward scattered with most of the available energy going into product translation. The degree of product repulsion is greater than that observed for the reactions $CH_3 + IY \rightarrow CH_3I + Y$ (Y = Cl, Br, I). This can be rationalized in terms of differences in the stabilities of the reaction intermediates. The average fraction of energy released into product translation is ≈15% lower for $CH_3 + (CH_3)_3CI$ than for $CH_3 + CF_3I$. A higher probability of exciting the out-of-plane vibration of $(CH_3)_3C$ as compared to CF_3 is likely to be responsible for this decrease.

REFERENCES

1. J. A. Kerr, in Comprehensive Chemical Kinetics, Vol. 18, "Selected Elementary Reactions", edited by C. H. Bamford and C. F. H. Tipper (Elsevier, Amsterdam, 1976), Ch. 2.
2. (a) D. L. McFadden, E. A. McCullough, Jr., F. Kalos, W. R. Gentry, and J. Ross, J. Chem. Phys. 57, 1351 (1972); (b) D. L. McFadden, E. A. McCullough, Jr., F. Kalos, and J. Ross, J. Chem. Phys. 59, 121 (1973).
3. J. A. Logan, C. A. Mims, G. W. Stewart, and J. Ross, J. Chem. Phys. 64, 1804 (1976).
4. (a) C. F. Carter, M. R. Levy, and R. Grice, Chem. Phys. Lett. 17, 414 (1972); (b) C. F. Carter, M. R. Levy, and R. Grice, Faraday Discuss. Chem. Soc. 55, 357 (1973).
5. L. C. Brown, J. C. Whitehead, and R. Grice, Mol. Phys. 31, 1069 (1976).
6. (a) S. M. A. Hoffman, D. J. Smith, J. H. Williams, and R. Grice, Chem. Phys. Lett. 113, 425 (1985); (b) S. M. A. Hoffman, D. J. Smith, N. Bradshaw, and R. Grice, Molec. Phys. 57, 1219 (1986).
7. P. Somssich, K. Strein and H. Schmiedel, Ber. Bunsenges. Phys. Chem. 85, 401 (1981).
8. J. D. McDonald, P. R. LeBreton, Y. T. Lee, and D. R. Herschbach, J. Chem. Phys. 56, 769 (1972).
9. J. Grosser and H. Haberland, Chem. Phys. 2, 342 (1973).
10. Chapters 2 and 3 of this thesis.

11. R. J. Buss, Ph. D. Thesis, University of California, Berkeley, 1979.

12. J. A. Kerr and M. J. Parsonage, Evaluated Kinetic Data on Gas Phase Addition Reactions (CRC, Cleveland, 1972).

13. S. W. Benson, Thermochemical Kinetics (Wiley, New York, 2nd ed., 1976).

14. G. B. Ellison, P. C. Engelking, and W. C. Lineberger, J. Am. Chem. Soc. 100, 2556 (1978).

15. D. M. Tomkinson and H. O. Pritchard, J. Phys. Chem. 70, 1579 (1966).

16. W. G. Alcock and E. Whittle, Trans. Faraday Soc. 61, 244 (1965).

17. R. K. Sparks, K. Shobatake, L. R. Carlson, and Y. T. Lee, J. Chem. Phys. 75, 3838 (1981).

18. G. N. A. van Veen, T. Baller, A. E. de Vries, and N. J. A. van Veen, Chem. Phys. 87, 405 (1984).

19. G. N. A. van Veen, T. Baller, A. E. de Vries, and M. Shapiro, Chem. Phys. 93, 277 (1985).

20. Q. Zhu, E. J. Hintsa, X. Zhao, and Y. T. Lee (unpublished results).

21. Y. T. Lee, J. D. McDonald, P. R. LeBreton, and D. R. Herschbach, Rev. Sci. Inst. 40, 1402 (1969).

22. R. K. Sparks, Ph. D. Thesis, University of California, Berkeley, 1979.

23. The electrode assembly was designed by Dr. T. K. Minton.

24. P. S. Weiss, Ph. D. Thesis, University of California,

Berkeley, 1986.

25. J. L. Franklin, J. G. Dillard, H. M. Rosenstock, J. T. Herron, and K. Draxl, Ionization Potentials, Appearance Potentials, and Heats of Formation of Gaseous Positive Ions (NSRDS-NBS 26, US Dept. of Commerce, Washington, DC, 1969).

26. C. Yamada, E. Hirota, and K. Kawaguchi, J. Phys. Chem. 75, 5256 (1981).

27. R. D. Levine and R. B. Bernstein, Molecular Reaction Dynamics (Oxford University Press, Oxford, 1974).

28. CRC Handbook of Chemistry and Physics (CRC, Cleveland, 67th ed., 1986).

29. C. T. Ting and R. E. Weston, Jr., J. Phys. Chem. 77, 2257 (1973).

30. L. V. Kovalenko and S. R. Leone, J. Chem. Phys. 80, 3656 (1984).

31. S. Chapman and D. L. Bunker, J. Chem. Phys. 62, 2890 (1975).

32. P. J. Kuntz, E. M. Nemeth, J. C. Polanyi, S. D. Rosner, and C. E. Young, J. Chem. Phys. 44, 1168 (1966).

33. J. C. Polanyi and J. L. Schreiber, in Physical Chemistry: an Advanced Treatise, Vol 6A, "Kinetics of Gas Reactions", edited by W. Jost (Academic, New York, 1974), Ch. 6.

34. J. C. Polanyi and W. H. Wong, J. Chem. Phys. 51, 1439 (1969).

35. J. C. Polanyi and N. Sathyamurthy, Chem. Phys. 37, 259 (1979).

36. A. M. G. Ding, L. J. Kirsch, D. S. Perry, J. C. Polanyi, and J. L. Schreiber, Faraday Discuss. Chem. Soc. 55, 252 (1973).

37. F. E. Davidson, G. L. Duncan, and R. Grice, Mol. Phys. 44, 1119 (1981).

38. J. D. McDonald and D. R. Herschbach, J. Chem. Phys. 62, 4740 (1975).

39. K. G. Anlauf, P. J. Kuntz, D. H. Maylotte, P. D. Pacey, and J. C. Polanyi, Faraday Discuss. Chem. Soc. 44, 183 (1967); K. G. Anlauf, P. E. Charters, D. S. Horne, R. G. Macdonald, D. H. Maylotte, J. C. Polanyi, W. J. Skrlac, D. C. Tardy, and K. B. Woodall, J. Chem. Phys. 53, 4091 (1970); K. G. Anlauf, D. S. Horne, R. G. Macdonald, J. C. Polanyi, and K. B. Woodall, J. Chem. Phys. 57, 1561 (1972).

40. (a) J. D. McDonald, Faraday Discuss. Chem. Soc. 55, 372 (1973); (b) J. Chem. Phys. 60, 2040 (1974).

41. L. M. Lowenstein and J. G. Anderson, J. Phys. Chem. 91, 2993 (1987).

42. For alternative, though related, explanations see refs. 4b and 8.

43. DIM calculations predict that HICl should be linear; I. Last and M. Baer, J. Chem. Phys. 80, 3246 (1984).

44. Ab initio calculations on H-I-F have shown that it has

two minimum energy bent configurations- one with a bond angle of 82° another with an angle of 137°; R. J. Bartlett, L. Kahn and G. D. Purvis, J. Chem. Phys. 76, 731 (1982); R. J. Bartlett (private communication).

45. N. C. Blais and D. G. Truhlar, J. Chem. Phys. 61, 4186 (1974).

46. J. C. Polanyi and J. L. Schreiber, Faraday Discuss. Chem. Soc. 55, 372 (1973).

47. J. M. Farrar and Y. T. Lee, J. Chem. Phys. 63, 3639 (1975).

48. R. J. Buss, S. J. Sibener, and Y. T. Lee, J. Phys. Chem. 87, 4840 (1983).

49. S. M. A. Hoffman, D. J. Smith, A. Gonzalez Ureña, and R. Grice, Chem. Phys. Lett. 107, 99 (1984); S. M. A. Hoffman, D. J. Smith, A. Gonzalez Ureña, T. A. Steele, and R. Grice, Mol. Phys. 53, 1067 (1984).

50. R. McWeeny, Coulson's Valence (Oxford University Press, Oxford, 3rd ed., 1979).

51. J. H. Richardson, L. M. Stephenson, and J. I. Brauman, Chem. Phys. Lett. 30, 17 (1975).

52. C. H. DePuy, V. M. Bierbaum, and R. Damrauer, J. Am. Chem. Soc. 106, 4051 (1984).

53. F. A. Houle and J. L. Beauchamp, J. Am. Chem. Soc. 101, 4067 (1979).

54. R. S. Mulliken, Phys. Rev. 47, 413 (1935); J. Chem. Phys. 8, 382 (1940).

55. K. E. Holdy, L. C. Klotz, and K. R. Wilson, J. Chem. Phys. 52, 4588 (1970).

56. C. Yamada and E. Hirota, J. Chem. Phys. 78, 1703 (1983).

57. C. H. Townes and A. L. Shawlow, Microwave Spectroscopy (Dover, New York, 1975).

58. D. Griller, K. U. Ingold, P. J. Krusic, and H. Fischer, J. Am. Chem. Soc. 100, 6750 (1978)

59. B. H. Lengsfield, III, P. E. M. Siegbahn, and B. Liu, J. Chem. Phys. 81, 710 (1984).

60. J. Pacansky, D. E. Horne, G. P. Gardini, and J. Bargon, J. Phys. Chem. 81, 2149 (1977).

61. Q. Zhu (unpublished results).

Table 1. Mulliken electronegativities, χ, for atoms and radicals.

Atom/Radical	χ(eV)	Ref.
H	7.18	28
F	10.41	28
O	7.54	28
Cl	8.29	28
Br	7.59	28
I	6.76	28
CF_3	6.1	25,51
CH_3	4.96	28,53
$(CH_3)_3C$	3.6	52,53

FIGURE CAPTIONS

Fig. 1: Assembly drawing of methyl radical source. Not to scale. (1) tantalum block, (2) molybdenum springs; (3) water cooled copper electrodes; (4) precision ground quartz tube; (5) alumina spacers.

Fig. 2: CH_3I (m/e=142) product angular distribution for the reaction $CH_3 + CF_3I \rightarrow CH_3I + CF_3$. Center-of-mass angle is 19°. ——— fit obtained with T(65°)=0 CM angular distribution in Fig. 6; — — fit obtained with T(90°)=0 distribution. Error bars represent 90% confidence limits.

Fig. 3: CH_3I (m/e=142) time-of-flight spectra at three laboratory angles from the reaction $CH_3 + CF_3I \rightarrow CH_3I + CF_3$: (a) Solid line fit obtained with T(90°)=0 CM angular distribution in Fig. 6; (b) Solid line fit was obtained with T(65°)=0 CM angular distribution.

Fig. 4: CH_3I (m/e=142) product angular distribution from the reaction $CH_3 + (CH_3)_3CI \rightarrow CH_3I + (CH_3)_3C$. Fit was obtained with the T(90°)=0 CM angular distribution in Fig. 6. Error bars represent 90% confidence limits.

Fig. 5: CH_3I (m/e=142) time-of-flight spectra at two laboratory angles from the reaction $CH_3 + (CH_3)_3CI \rightarrow CH_3I + (CH_3)_3C$. (a) and (b) same as Fig. 3. Non-reactive signal has not been subtracted from the $\theta = -15°$ spectrum.

Fig. 6: Center-of-mass frame CH_3I angular distributions for both reactions.

Fig. 7: Center-of-mass frame product translational energy distributions: (a) Distribution used to fit $CH_3 + CF_3I$ data; (b) Distribution used to fit $CH_3 + (CH_3)_3CI$ data.

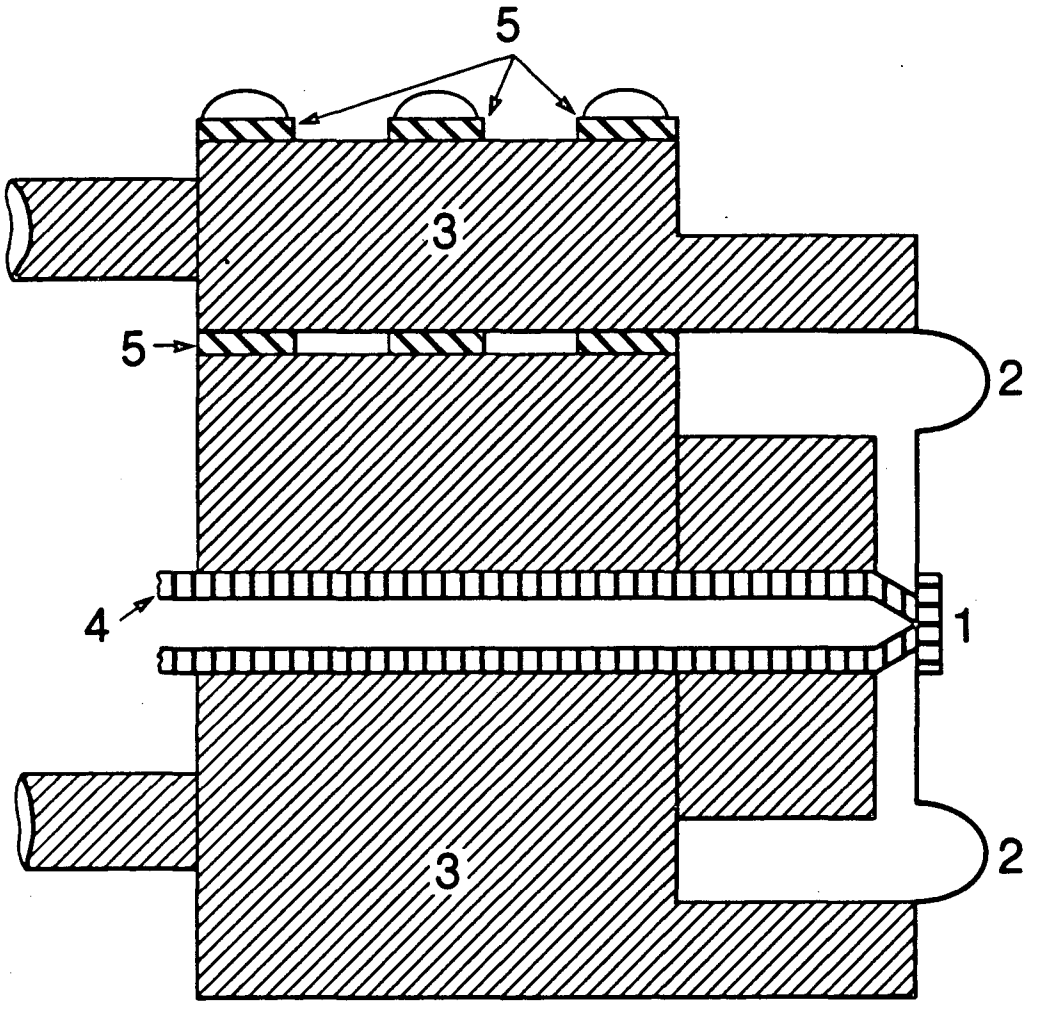

XBL 8712-5759

Figure 1

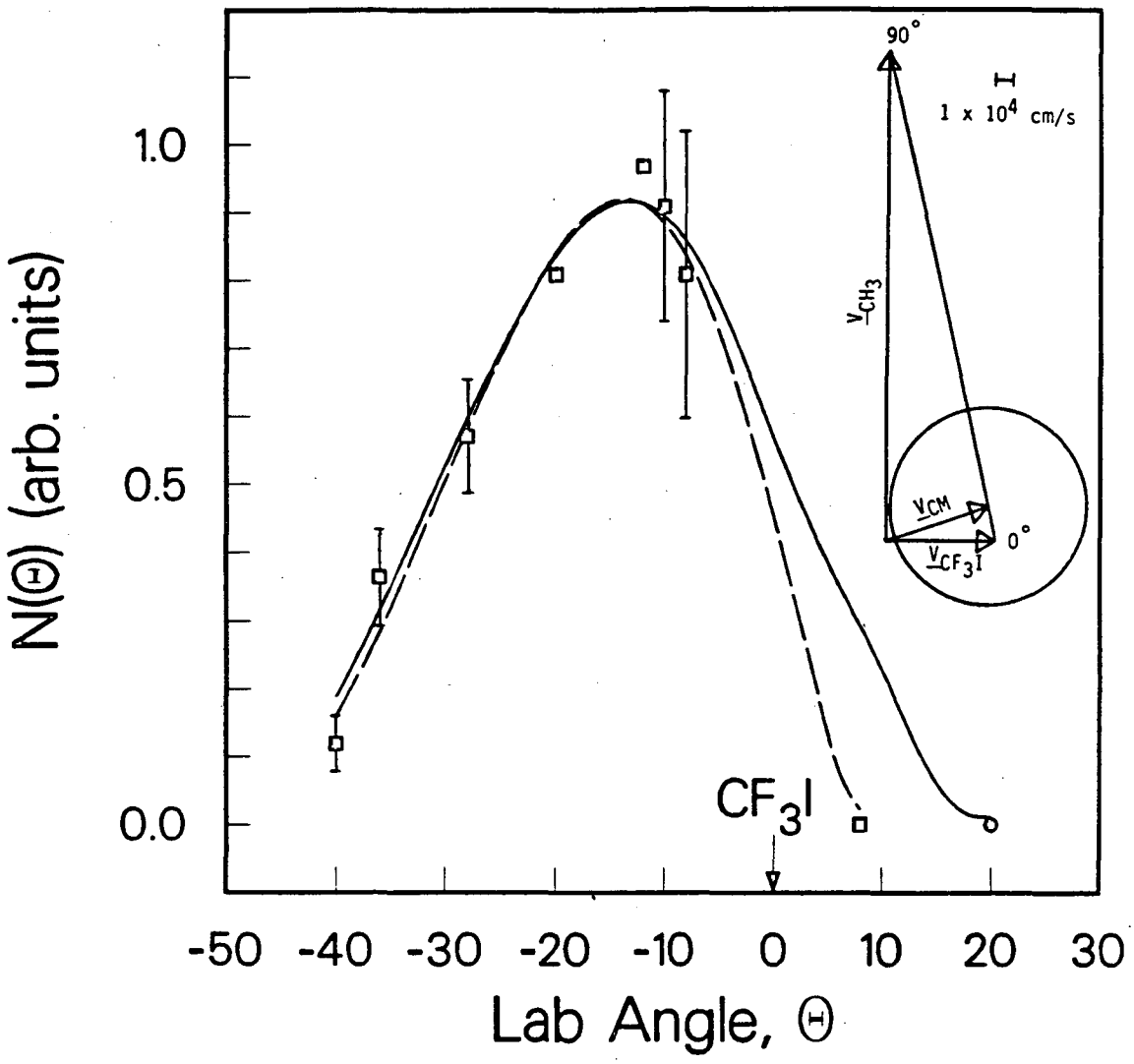
90°
1 x 10^4 cm/s
$\underline{v}_{CH_3}$
$\underline{v}_{CM}$
$\underline{v}_{CF_3I}$
0°
1.0
0.5
0.0
N(Θ) (arb. units)
CF_3I
-50 -40 -30 -20 -10 0 10 20 30
Lab Angle, Θ
XBL 8712-5280

Figure 2

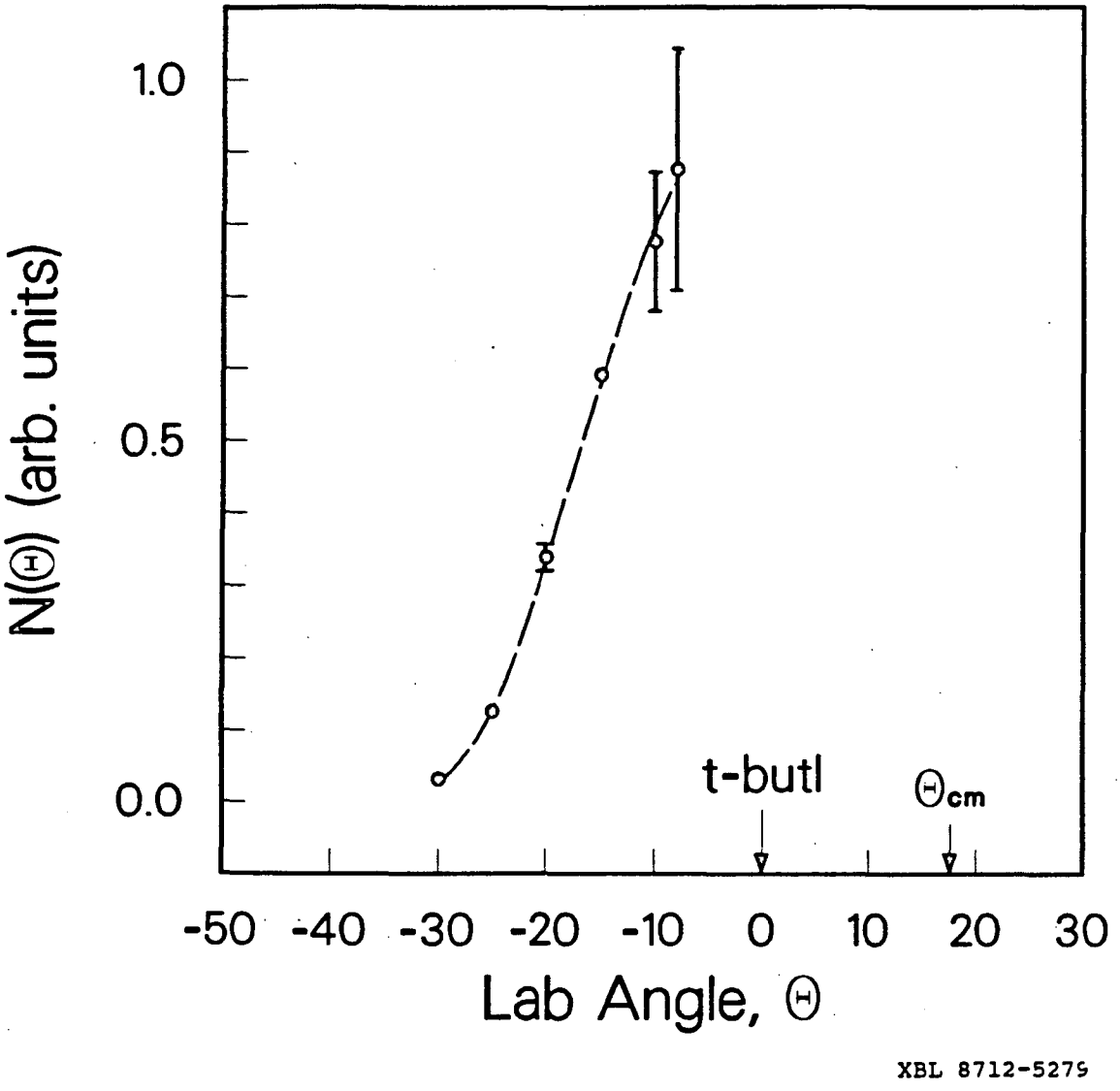
1.0
0.5
0.0
N(Θ) (arb. units)
t-butl
Θcm
-50 -40 -30 -20 -10 0 10 20 30
Lab Angle, Θ
XBL 8712-5279

Figure 3

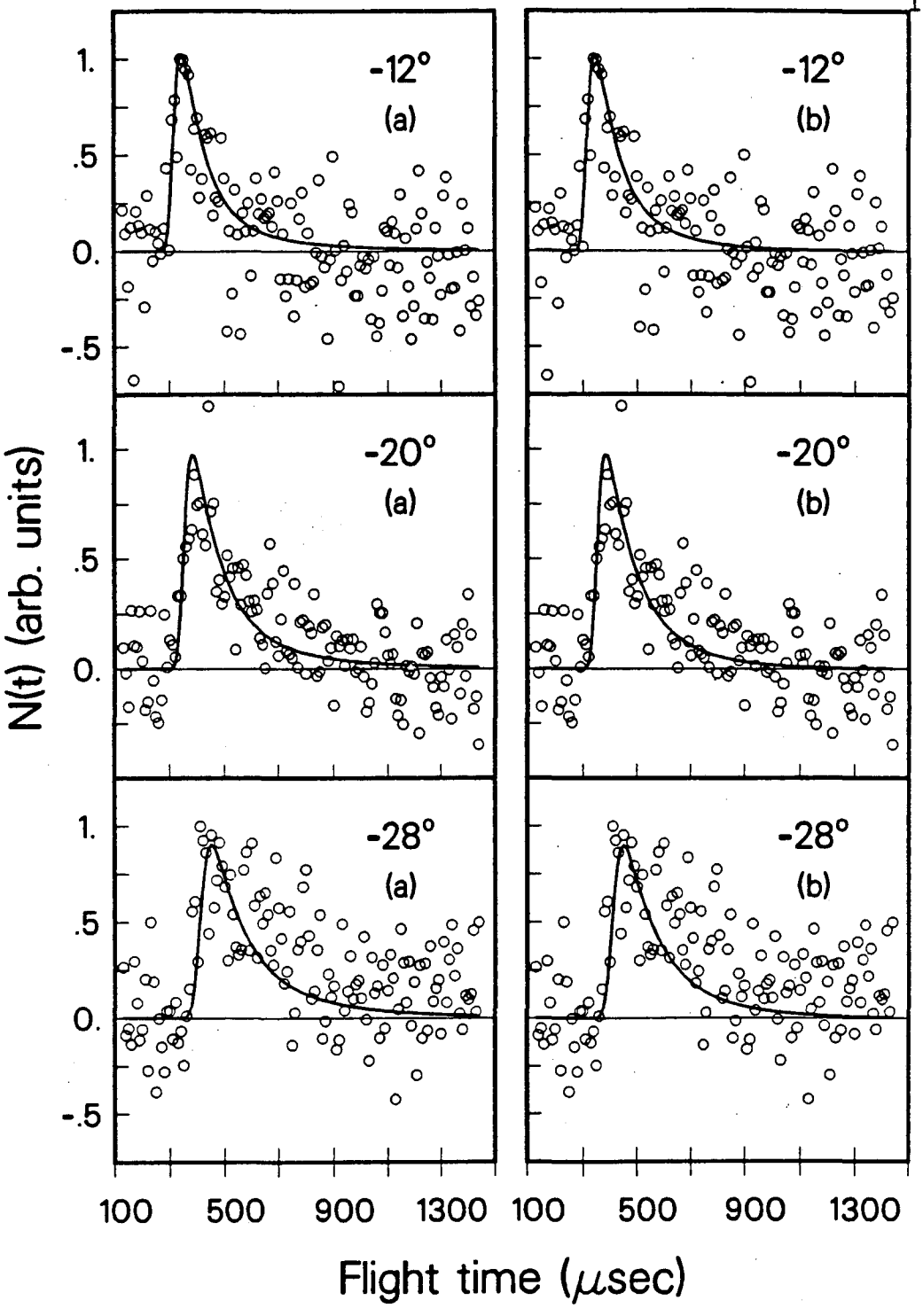
-12°
(a)
-12°
(b)
-20°
(a)
-20°
(b)
-28°
(a)
-28°
(b)
1.
.5
0.
-.5
N(t) (arb. units)
100
500
900
1300
Flight time (μsec)
XBL 8712-5144

Figure 4

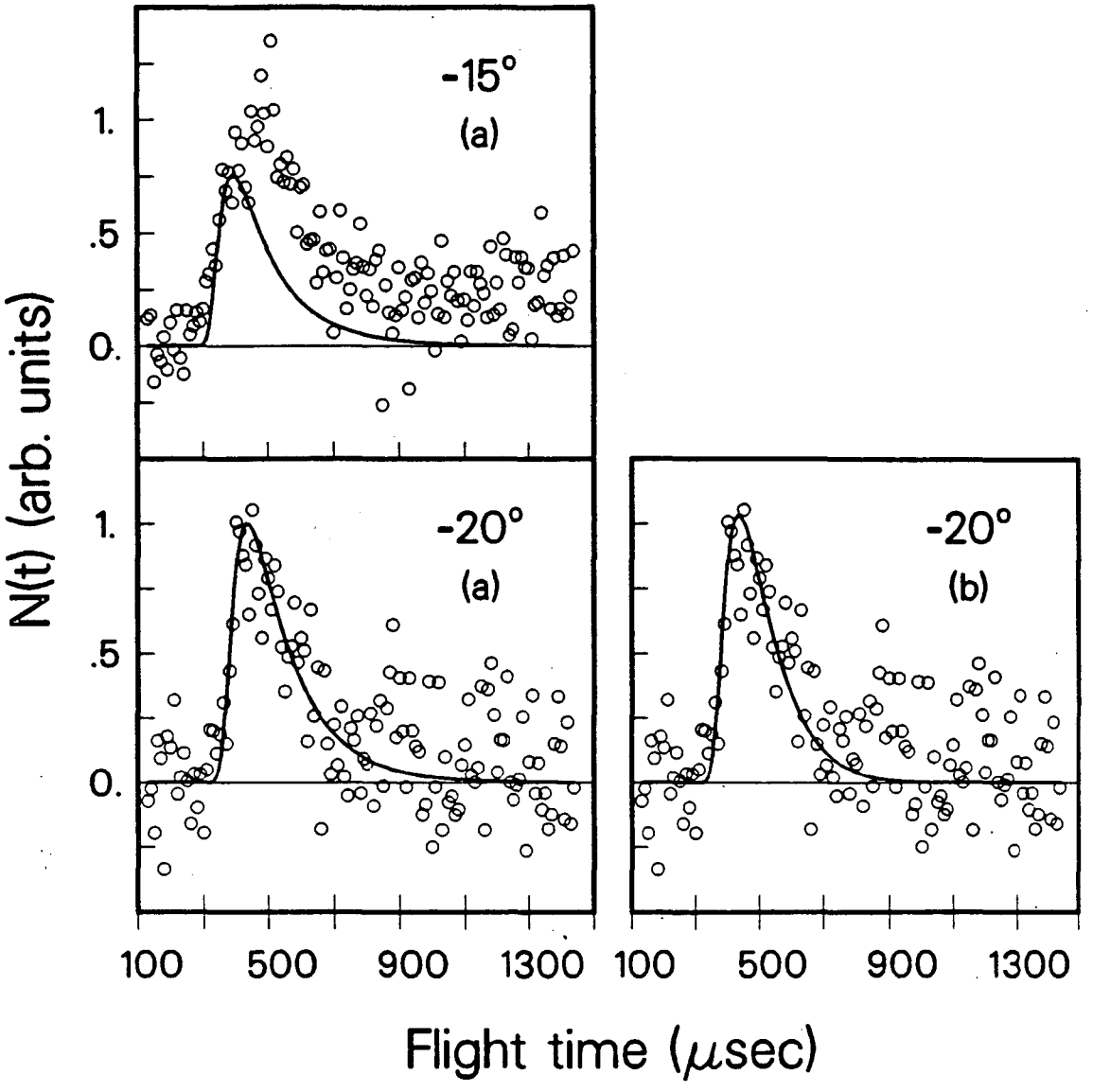
-15°
(a)
-20°
(a)
-20°
(b)
1.
.5
0.
N(t) (arb. units)
100
500
900
1300
Flight time (μsec)
XBL 8712-5143

Figure 5

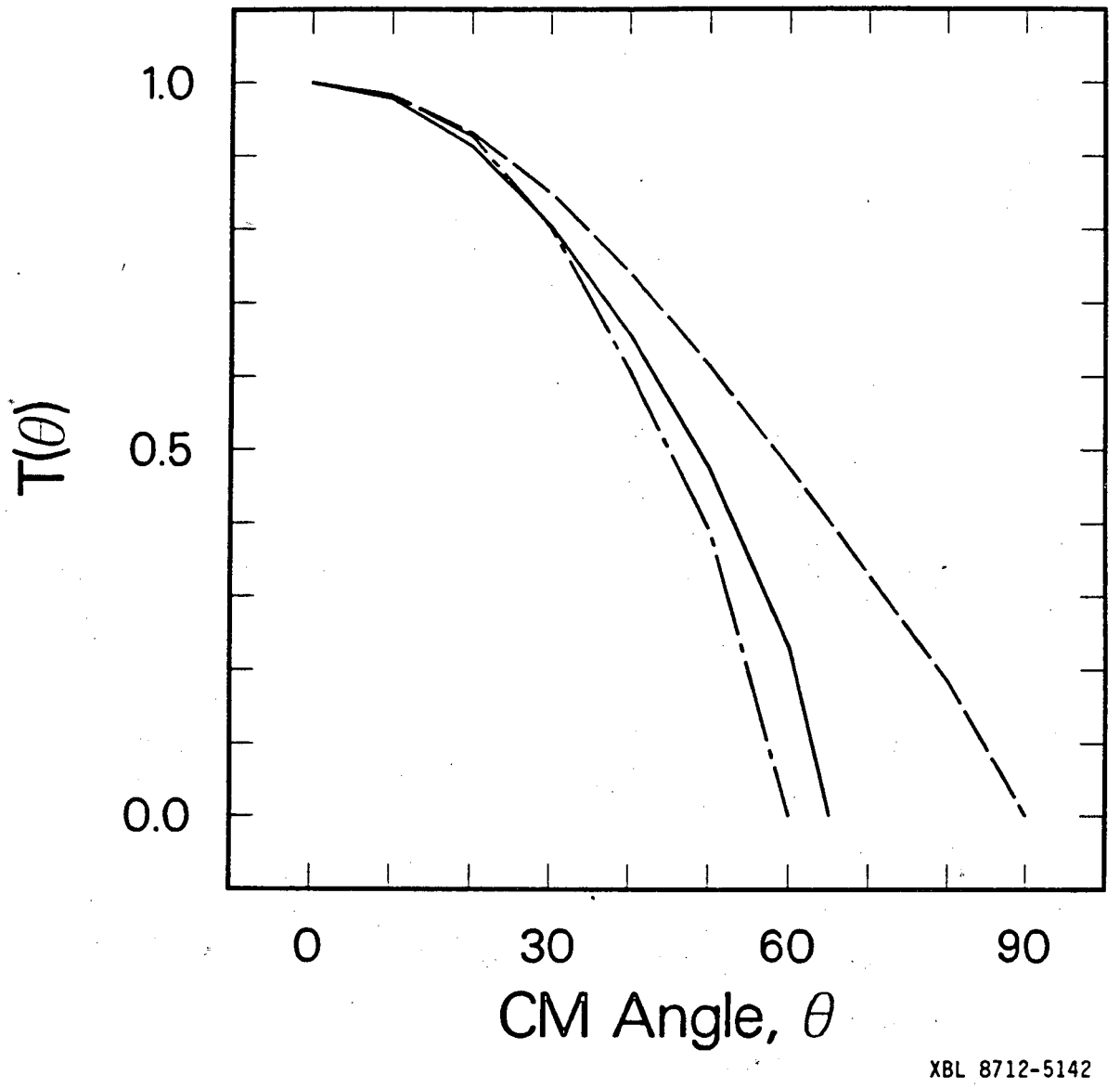

Figure 6

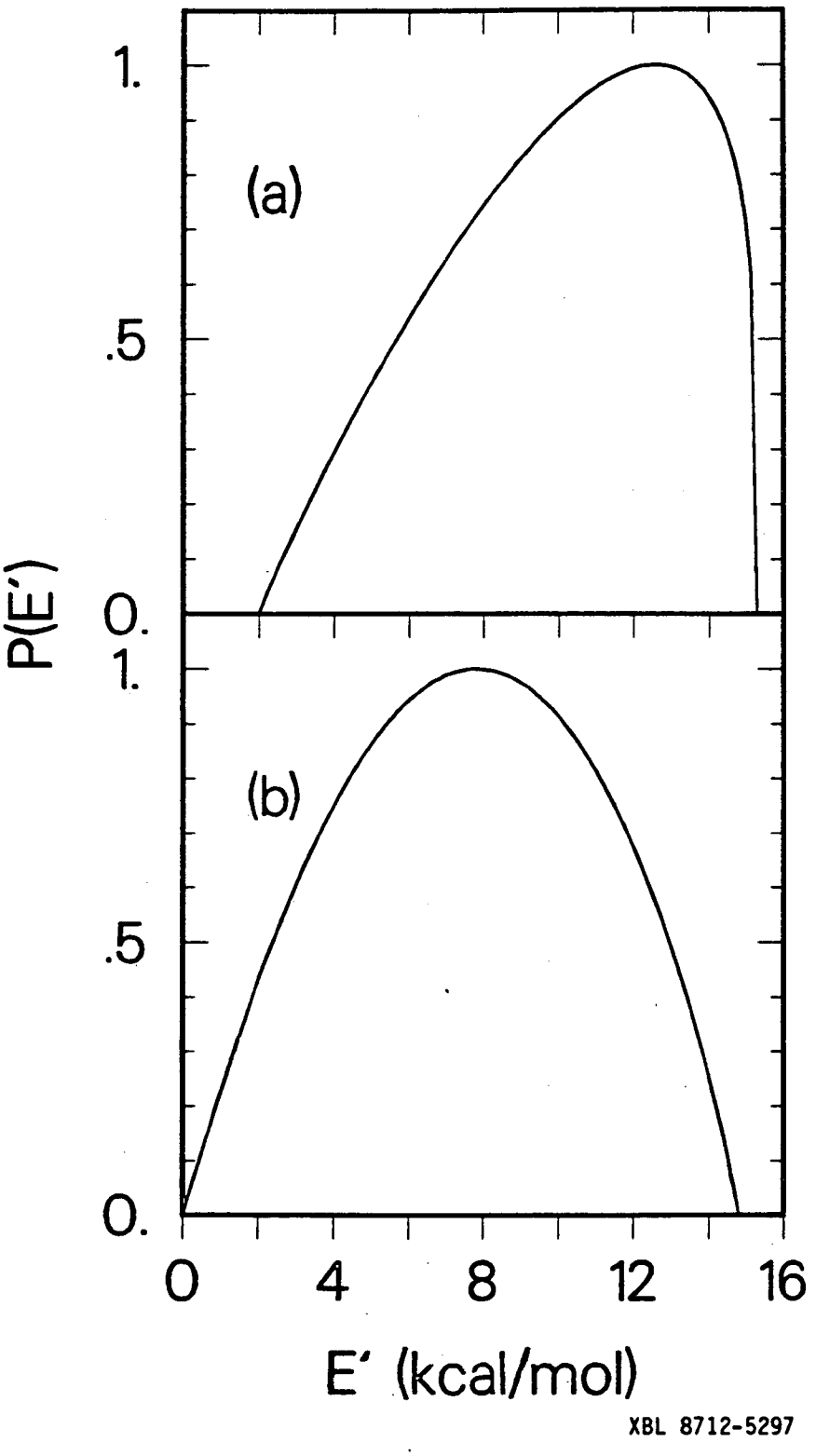

Figure 7

LAWRENCE BERKELEY LABORATORY
TECHNICAL INFORMATION DEPARTMENT
UNIVERSITY OF CALIFORNIA
BERKELEY, CALIFORNIA 94720